7926012

LESLIE, FRED WELDON
DYNAMIC BEHAVIOR OF SINGLE AND MULTIPLE VORTEX TORNADOES INFERRED FROM LABORATORY SIMULATION.

THE UNIVERSITY OF OKLAHOMA, PH.D., 1979

University Microfilms International 300 N. ZEEB ROAD, ANN ARBOR, MI 48106

DYNAMIC BEHAVIOR OF SINGLE AND MULTIPLE VORTEX TORNADOES

INFERRED FROM LABORATORY SIMULATION

APPROVED BY

Eugene M. Wilkins

Edward F. Blick

Martin C. Jischke

Bob Davies-Jones

DISSERTATION COMMITTEE

THE UNIVERSITY OF OKLAHOMA

GRADUATE COLLEGE

DYNAMIC BEHAVIOR OF SINGLE AND MULTIPLE VORTEX TORNADOES INFERRED FROM LABORATORY SIMULATION

A DISSERTATION

SUBMITTED TO THE GRADUATE FACULTY

in partial fulfillment of the requirements for the

degree of

DOCTOR OF PHILOSOPHY

BY

FRED W. LESLIE

Norman, Oklahoma

1979

ABSTRACT

A vortex generator is used to simulate tornado flows in the laboratory. Geometric and dynamic similitude are maintained to insure that the laboratory flow models the environment of natural tornadoes. The very small pressure drops are measured with a sensitive pressure transducer while the mean flow and the turbulent fluctuations are measured with a hot film anemometer. The influence of a rough surface on the vortex core and the multiple vortex transition phenomenon are also investigated.

The results indicate that the core radius over a given surface is determined predominantly by the swirl ratio parameter. When a lower rough surface is placed in the apparatus the core radius decreases significantly and the intensity of the turbulence increases. The increased drag also delays multiple vortex transition, requiring progressively higher swirl to initiate the process. The pressure profiles show that for a single vortex the central pressure decreases with increasing swirl ratio until multiple vortex transition. At that point a further increase in ambient swirl results in a central pressure increase with the pressure minimum shifting off the axis. The portion of the radial pressure gradient that drives the tangential flow also depends on the swirl ratio. It turns out that a higher tangential velocity at the core can be obtained with a higher swirl ratio for a given central pressure drop. This fact agrees with the

observation that multiple vortex tornadoes cause greater damage along their path than single cores. Measurements of the Reynolds stresses show that the eddies usually extract energy from the mean flow. However, in regions where the circulation profile shows peculiar increases toward the axis, the eddies appear to be adding momentum to the mean flow.

ACKNOWLEDGMENTS

I would like to express my appreciation to Dr. Eugene Wilkins, the Chairman of my committee, for sharing with me his time, knowledge, and experience. His insight and constant encouragement were largely responsible for the continuation and success of this research project. I would also like to extend my gratitude to the other members of my committee, Drs. Edward Blick, Robert Davies-Jones, Jay Fein, and Martin C. Jischke for their frequent comments and guidance.

A special thanks is in order to Dr. Masud Parang and Mr. Bruce Light for their stimulating conversations and assistance in the laboratory. I would also like to thank Ms. Nancy Masud for her diligent work in typing this dissertation.

Finally, I am grateful to the National Science Foundation for their financial support under Grant ATM77-20251.

TABLE OF CONTENTS

LIST OF FIGURES

FIGURE Page

FIGURE | Page

LIST OF TABLES

LIST OF SYMBOLS

a	aspect ratio (= h/r_0)
a_h	length of probe support
A_1, B_1	King's law constants at T_1
A_2, B_2	King's law constants at T_2
A', B'	generalized King's law constants
$\overline{AO}$	radius of the protractor
b	a measure of the horizontal convergence
c	efficiency factor
d	wire diameter
$d\vec{A}$	element of surface directed outward
D	Rankine-combined vortex exponent
D_a	an advection operator (= $\frac{\partial\hat{\psi}}{\partial\xi}\frac{\partial}{\partial\eta} - \frac{\partial\hat{\psi}}{\partial\eta}\frac{\partial}{\partial\xi}$)
D_h	horizontal divergence
$\hat{e}_r$, $\hat{e}_\phi$, $\hat{e}_z$	unit vectors in radial, azimuthal, and vertical directions, respectively.
E	voltage
E_c	voltage output for an invariant ambient temperature
F	scale factor
h	inflow depth
h_1	height of probe's leading edge
h_2	height of probe's trailing edge
H	roughness element height
k	thermal conductivity
l	wire length

l_p	projection length of the probe
l_t	distance from probe tip to support bracket (see Fig. 5)
L	height to probe support bolt
M	ambient circulation in apparatus
M_t	ambient atmospheric circulation
MV	multiple vortex
N	radial Reynolds number
N_0	number of observations
$\hat{p}$	nondimensionalized pressure $(= \frac{p}{\rho u_s^2})$
P	nonhydrostatic part of total pressure
P_1	ambient pressure
Q	volume flow rate
Q_t	atmospheric volume flow rate
r	radial distance
r_c	laboratory core radius
$\hat{r}_c$	nondimensionalized core radius $(= r_c/r_s)$
r_c'	tornado radius
r_c^*	core radius over a rough surface
r_h	radius of the honeycomb
r_0	radius of convection
r_{0t}	atmospheric updraft radius
r_{ps}	radius to the probe support
r_s	radius to the screen
$\hat{r}$	nondimensional radius $(= r/r_s)$
R_e	a Reynolds number

R_p	distance from vortex core to the protractor
R_w	wire resistance
s	silhouette area of roughness obstacle
S	swirl ratio ($= \Gamma_s r_0/2Q$)
S*	total surface area of roughness obstacles divided by total number of elements
SV	single vortex
t	time
T	average overall pressure-weighted temperature
T_1	average pressure-weighted temperature outside the core
T_2	average pressure-weighted temperature inside the core
T_a	ambient fluid temperature
T_w	wire temperature
u	radial velocity
u', v', w'	fluctuating velocities in the radial, azimuthal, and vertical directions, respectively
$\hat{u}$	nondimensionalized radial velocity ($= u/u_s$)
$\bar{u}_p$, $\bar{v}_p$	mean velocity in the streamline direction and perpendicular to it, respectively
u_p', v_p', w_p'	fluctuating velocities in the probe's reference frame
u_s	radial velocity at the screen
U	effective cooling velocity
v	tangential velocity
v_{max}	maximum tangential velocity
$\hat{v}$	nondimensionalized tangential velocity ($= v/v_s$)

$\bar{v}_h$	mean horizontal velocity
v_h'	fluctuating horizontal velocity
$\vec{V}$	velocity vector
V_t	total velocity
w	vertical velocity
y	observed values
y_{est}	estimated values
z	height
z_0	roughness length in the apparatus
z_0'	Lettau's roughness length
z_{0t}	atmospheric roughness length
α	geometric parameter ($= r_0^2/h^2$)
α_{ps}	inflow angle at r_{ps}
α_t	inflow angle at the probe tip
β	dip angle
β_0	a buoyancy parameter
Γ	circulation/2π ($=rv$)
$\hat{\Gamma}$	nondimensional circulation
Γ_∞	ambient circulation/2π
Γ_s	circulation at the screen
δ	length of support bracket
Δp	pressure drop
$\Delta\hat{p}$	nondimensionalized pressure drop
ε	temperature departure
ε'	swirl parameter
ζ	nondimensional radial coordinate

ζ_0	vertical vorticity
η	nondimensional radius $(= r^2/r_0^2)$
θ	inflow angle
θ'	overheat ratio
μ	dynamic viscosity
ν	molecular viscosity
ξ	nondimensionalized height $(= z/h)$
ρ	fluid density
σ	temperature ratio $(= \theta'-1)$
σ_{est}	standard error of estimate
τ	time scale
ϕ_c	angular diameter of the vortex core
ψ	stream function
$\hat{\psi}$	nondimensional stream function

DYNAMIC BEHAVIOR OF SINGLE AND MULTIPLE VORTEX TORNADOES INFERRED FROM LABORATORY SIMULATION

CHAPTER I

INTRODUCTION

Tornadoes are one of nature's most violent yet transient forces, taking about 113 lives annually and producing about 75 million dollars worth of damage (Davies-Jones and Kessler, 1974). Tornadoes represent the end result of how the atmosphere's dynamics can act to concentrate its energy and momentum locally for a short period of time. Although twisters have occurred all over the world, the United States leads the way in the frequency of tornadoes per unit area. In particular, the greatest threat lies in the Central Plains, probably because of its unique geography and the fact that its mid-latitude position lies in a favorable springtime storm track. While most of the tornadoes occur during the spring and early summer months when the air is often in its most unstable state, tornadoes have occurred during every month of the calendar. It is interesting to note that while the number of tornado sightings has increased over recent years the number of fatalities has diminished.

This can probably be attributed to the use of modern radars and more sophisticated spotter networks. Earlier warning and improved communication are responsible for reducing the annual death toll.

Operational meteorologists take two approaches to alerting the public of a possible tornado threat. One of these is by forecasting their occurrence. This involves analyzing the large scale meteorological parameters and determining whether the conditions are right for tornadogenesis. Although there are several parameters to look for, such as the air's instability and the vertical wind shear, the current technique for predicting tornadoes requires little knowledge of the formation process. Most of the important forecasting parameters have been taken from past experience (Miller, 1972). The significant tornado producing weather patterns involve a scale many times larger than the actual tornado scale (or microscale). It is therefore believed that the large scale pattern plays an important role in reinforcing the smaller scale atmospheric structures essential to tornadogenesis. Kaplan and Paine (1977) have recently demonstrated how this process might take place. Using a primitive equation model they demonstrated how the large scale flow can reinforce the potential instability of the smaller scales. The terms which dominate thus depend on the particular scale of interest. Only if this link between scales exists can we hope to be able to accurately forecast tornadoes with the sparse data base currently available.

Once the possibility of tornadoes has been established the forecaster's next task lies in the area of detection. Of the many thunderstorms that occur in the United States, only a few become severe (e.g., produce high winds and large hail) and fewer still generate tornadoes. The use of weather radar has greatly improved tornado detection. Conventional radar cannot replace the storm spotter for verifying tornadoes because it cannot actually resolve that scale. Furthermore, echo-producing material may not be present in the immediate vicinity. However, if the precipitation begins to wrap around the larger scale flow, i.e., the mesocyclone, a hook echo may appear on the radar screen which for many meteorologists justifies announcing a tornado warning in the threat area. Just recently it is believed that the actual tornado scale has been resolved crudely by Doppler radar (Brown and Lemon, 1976). The tornado vortex signature (or TVS) is detected as two adjacent volumes of air traveling in opposing directions at a high rate of speed (in the storm's reference frame). Observations show that the TVS is usually first apparent in the mid-levels of the storm and then spreads upward and downward in time. The fact that it has height and time continuity and is highly correlated with surface observations and damage supports the contention that the vortex itself is being resolved. Although presently the

Doppler radar is used primarily as a research tool, the capability of detecting the actual funnel aloft some 30 minutes before it propagates to the surface makes it an attractive aid to the operational forecaster.

The Nuclear Regulatory Commission has become interested not only in the geographic distribution of tornado frequency but also in the maximum wind speeds to be expected from tornadoes. With the anticipated increase in the number of nuclear power stations there is concern as to how strong these structures must be in order to survive tornadoes. Significant damage could result not only in radiation leaks but some of the radioactive material might also be carried up into the storm and be dispersed across a community downwind. A review of some of the techniques used in estimating the maximum velocity is given by Davies-Jones and Kessler (1974). In most cases it appears that tornadic winds rarely exceed 112 m s^{-1}, although the Atomic Energy Commission has used 161 m s^{-1} as its design criterion. With this in mind Jankov et al. (1976) propelled test projectiles such as pipes and utility poles into concrete walls to determine what strength would be necessary to insure that tornado-generated missiles would not consititute a threat to a building housing a nuclear reactor. For most cases they found that reinforced concrete 60 cm thick appears to be quite adequate.

All research efforts can be categorized by four different approaches; namely, analytical, numerical, observational, and experimental. The analytical approach involves obtaining explicit solutions of the equations which are believed to govern the flow. More precisely, these solutions come from a simplified set of equations, since a general solution to the governing equations lies outside the reach of contemporary mathematics. Typically, the Navier-Stokes momentum equations are used along with the continuity equation and a thermodynamic energy equation. A perturbation approach is commonly used which alters the equation to describe a mean flow with turbulent stresses. It is difficult to analytically determine these stresses in a straightforward manner. To simplify matters, the eddy processes are compared to molecular diffusion resulting in a series of terms involving the Laplacian of the mean flow and an effective eddy viscosity. Since this value is believed to be several orders of magnitude larger than the laminar value the effects of molecular diffusion can be ignored altogether. To further simplify the equations for analytical purposes, the eddy viscosity is often assumed to be a constant. A similar approach is used for the turbulent diffusion of scalar quantities. The assumptions necessary seem to be particularly suspect when there exists more than one length or time scale to the flow (Tennekes and Lumley, 1974) as is the case for tornadic flows. It is clear that the eddy diffusion process must certainly be important in modifying the flow significantly. Not only is it uncertain what the magnitude of the eddy viscosity might be (since it is a property of the flow and not the fluid) but it is unlikely that it is the same throughout the tornado flow field. It has been suggested (Lilly, 1969) that it may even be negative in some regions, meaning that the turbulent fluxes act to accelerate the mean flow locally. Aside from the simplifications used in modeling the effects of turbulence, some other common assumptions are: symmetry about the vertical axis, a steady flow field, adiabatic motion, and an incompressible atmosphere (or one in which density changes are important only in the buoyancy term, as in the Boussinesq approximation). Scale analysis justifies many of these assumptions.

Although the analytical models certainly give an insight into the flow behavior, not one is entirely satisfying, either because the boundary conditions are unreasonable or because the indicated solutions contradict some of the observations. For example, in the solutions of Burgers (1948) and Rott (1958) the radial inflow is the greatest in regions farthest from the tornado and the updraft is the strongest at extreme heights. Also, the updraft is independent of radius, and the core size is independent of the ambient circulation. Sullivan's (1959) solution, which possesses some similarity to Kuo's (1966) solution, offers some improvement since his vertical velocity has a realistic dependence upon radius, although it still increases linearly with height. However, his radial velocity also shows the largest inflow at large radius and is independent of height. Several other theoretical models are discussed in a review paper by Lewellen (1976) who concludes that, while no model completely describes a tornado, many are at least qualitatively accurate in certain regions of the flow.

When analytical solutions to the governing equations cannot be obtained, numerical integration has been used. One then has the flexibility to vary the experiment such as by changing the boundary conditions, the fluid viscosity, or density. Schlesinger (1977) numerically modeled the growth of a thunderstorm in an environment with directional wind shear. The model simulated many features that have been observed in nature, such as a tilting updraft and storm splitting into two oppositely rotating cells. Of course, few thunderstorms split, which leads one to ponder whether this behavior is an ever present result of his particular model or if it is dependent upon a strongly sheared wind field in the initial conditions. Davies-Jones and Vickers (1971) have succeeded in modeling vortex formation using the Boussinesq set of equations and a constant eddy viscosity. As they changed their lower boundary condition from no slip to free slip, the amplification of the tangential velocity increased, and the radius and height of the velocity maximum decreased. The time of maximum vortex intensity did not change significantly during this process. Wilkins *et al.* (1971) numerically simulated vortex formation by the release of successive thermals. They found that the vertical velocity of the thermal was suppressed by an ambient rotation field. In a later experiment Wilkins *et al.* (1974) added a friction layer to the numerical model and demonstrated how the enhanced convergence increased the vertical velocity in agreement with their laboratory observations.

One drawback for numerically modeling natural flows is that the appropriate boundary conditions are not obvious, although they are very important. In fact, it has been suggested that choosing the boundary conditions is equivalent to guessing much of the solution by solving for the interior flow that matches the boundary values. To sidestep this problem some investigators have chosen to numerically simulate laboratory models whose solid walls dictate more obvious boundary conditions. Harlow and Stein (1974) used the Navier-Stokes equations to model Ward's (1972) tornado simulator. They reproduced many of the features observed in the apparatus, such as a downward flow along the vortex axis and core expansion with increasing swirl. However, actual quantitative agreement is lacking. Rotunno (1977) also modeled the Ward simulator. His scheme used different boundary conditions from those of Harlow and Stein. In particular, he had the azimuthal vorticity equal to zero at the updraft radius instead of the vertical velocity equal to zero there. His core radii correspond very well to those observed by Ward. He also obtained flows which he interpreted as vortex breakdown. In addition his calculations showed that the core radius is mainly a function of the swirl ratio and is largely independent of the Reynolds number for high Reynolds numbers. Both these features are present in Ward's (1972) model.

Numerical models are certainly not without drawbacks. The importance of selecting suitable boundary conditions has been mentioned. In addition, it is a little discomforting to know that the numerical solution is somewhat dependent upon the finite difference scheme used. Some schemes selectively filter or damp waves at particular frequencies. Others may have higher order truncation error or may artificially simulate viscosity by smoothing the solution. As with analytical models, simulating the effects of turbulence is difficult and largely uncertain. Some use has been made of higher order closure models to predict the behavior of the Reynolds stresses, but this still involves some questionable assumptions at some point in the development. Finally, a more general drawback to numerical models is that even though they may produce what seems to be a tornadic flow, the numbers they grind out may not necessarily increase our understanding of the processes taking place. Only by scrutinizing the model to determine which terms are important in a given place and at a given stage of tornadogenesis can some useful information be obtained. Some models have been considered successful because they exhibit some behavior that is observed in nature such as storm motion to the right of the mean wind vector, or tornadogenesis, or storm splitting. However, these events do not occur invariably, even in very significant storms. This suggests that perhaps there is a stage in storm development when the presence or absence of some process or phenomenon (possibly somewhat random in its occurrence) is crucial in determining the storm's behavior during the remainder of its lifetime. Until these problems are overcome, numerical models may continue to simulate some particular storm traits, but will be lacking in detail.

The observational approach to tornado research has received much attention over the years, and justifiably so. The information from this approach must serve as a basis of comparison with all others. Only by this method can one witness tornado formation, maturity, and dissipation without truncation error or the enforcement of some simplifying assumptions. The prime difficulty, of course, is being in the right place at the right time. Because tornadoes are rather rare and short-lived, much of their useful photography is done by laymen. Some of the popularity in obtaining photographic evidence of tornado behavior comes from the success of Hoecker's (1960, 1961) photogrammetric analysis of the Dallas tornado of 1957. His research verified many of the existing ideas of tornado dynamics and provided the impetus for the further refinement of others. An organized attempt to intercept and photograph tornadoes (Golden and Morgan, 1972) has been successful in providing observational information. A result of such an effort was the documentation of the Union City tornado's lifespan (Brown, 1976). This tornado study is perhaps the most thorough to date because not only was the storm photographed but simultaneous Doppler radar data were taken and correlated with the physical phenomenon. This information can then be used in reverse to interpret radar images as physical characteristics of the thunderstorm. The tornado intercept idea not only advances storm analysis but also improves forecasting skills because early prediction of the areas of high tornado probability plays a decisive role in the success of the program. Using photogrammetric analysis of the Great Bend tornado of 1974, Golden and Purcell (1977) have observed the high inflow into the tornado through a thin layer near the surface. Such a flow had previously been presumed, and is present in many models. They also detected vertical accelerations of the order of 3 g's near the ground demonstrating that the flow in the lower levels of the tornado is far from hydrostatic balance.

There is little information about the structure of the tornado in the mid and upper levels of the storm because visual observations are obscured by cloud. Doppler radar has the capability of determining the flow within the thunderstorm. Data from Doppler radar indicate that the vortex maintains its continuity to very high levels in the storm although with diminishing intensity. The storm tops have been studied from satellite and aircraft. Fujita's (1972, 1973) observations suggest a correlation between the collapsing of overshooting tops and the occurrence of a tornado below. However, the cause and effect have not been resolved and these features are not always present for tornadogenesis.

Clearly the updraft in nature is a result of the convective and conditional instability resulting from the temperature and moisture structure of the environment. The updraft may be sustained longer if the air column is rotating, since it is then less diluted by the surrounding air. Also, the presence of the environmental wind shear tends to tilt the updraft column. This allows the precipitation shaft to lie outside the updraft. As a consequence, the falling precipitation does not quench the convection, but instead falls adjacent to the updraft and cools the air by evaporation. This process further enhances the instability.

Vonnegut (1960) suggested that lightning strikes may initiate or maintain a strong updraft. However, Wilkins' (1964) laboratory experiments indicate that lightning strikes would not significantly contribute to the updraft strength unless the flashes occurred successively in the same place. Wilkins (1968) later concluded that the vortex core is not a preferred region for multistroke lightning strikes. It now appears that the necessary updraft strengths can be obtained through atmospheric instability without the assistance of electrical heating.

The source of rotation for tornadic storms is not so clear. Looking at the equation for the vertical component of vorticity one can see several possible sources; namely, the concentration of pre-existing vorticity by horizontal convergence, the advection of vorticity, the tilting of horizontal vorticity into the vertical, production by pressure-density solenoids, and production by horizontal variations of the frictional forces. It is generally believed that the latter contributes little significant vorticity in most cases. From radar data Barnes (1968) concludes that the tilting term made important by the typically sheared environmental winds and strong storm updraft can make a significant contribution to the production of vertical vorticity. On the other hand, Lilly (1966) claims that the tilting term and the horizontal divergence term cancel each other when integrated over an area. He therefore maintains that the vorticity concentration in the tornado results from the horizontal convergence of pre-existing vorticity. From dual-Doppler observations of an intense thunderstorm, Ray (1976) estimated the magnitude of the terms in the vorticity equation. His results ruled out any significant contribution by the solenoidal term. Finally, Davies-Jones and Kessler (1974) show that sufficient vorticity for a tornado could be produced in 3 hours by the horizontal convergence of typical ambient values of circulation. Obviously, the rotation source or sources cannot be pinpointed. They may vary from storm to storm or depend on the particular stage of its development. In any case, it is likely that frictional and solenoidal contributions to the microscale can be ruled out.

The phenomenon of multiple vortices (MV) has received much interest since Fujita _et al._ (1970) and Fujita (1971) proposed their existence to account for the peculiar surface markings left by some tornadic storms. It has since been noted that MV may be more common to the very intense storms than first realized. In fact, Clare's (1976) observations indicate that their presence is highly correlated with greater than average intensity. Jischke and Parang (1974) interpreted MV transition as a torque reduction process whereby the new configuration resulted when the surface torque increased with swirl faster than the momentum supplied. Davies-Jones (1976) suggests that MV are analogous to the wrapping up of an unstable vortex sheet. Although the MV mode is not completely understood, Snow (1978) has succeeded in demonstrating conditions in which a rotating flow becomes unstable to nonaxisymmetric disturbances. In spite of the fact that his model is simplified and fails to predict explicitly the parameter values at which the instability begins, many of the phenomenon's characteristics can be argued in terms of the model. It is worth pointing out that his model indicates that vortex splitting can be explained in terms of inviscid processes.

Laboratory models have long been used to simulate atmospheric phenomena. Much can be learned from these models because the experimenter can control certain parameters and observe the results. Furthermore, the important parameters governing some event can be isolated while others may be found to be negligible. To insure that the model does represent the natural tornado, dynamic and geometric similitude must be maintained throughout the simulation. This is accomplished by forcing certain nondimensional parameters to be the same for both phenomena. These parameters may also distinguish which type of vortex is being simulated; tornado, hurricane, or dust devil. Generally, all of the parameters cannot be matched. Thus, it is advisable to single out the relevant parameters and attempt to keep these equivalent.

A review of tornado simulators has been given by Davies-Jones (1976). Despite the variety of the different models they all reproduce two ingredients necessary for tornado formation: namely, background rotation of the ambient fluid and a means of concentrating vorticity by convergence. The fact that tornadoes do not always form when these two are present in nature suggests that a critical ratio of the two may be necessary over a sufficient length of time. The initial swirl is usually created by a rotating screen, louvered windows, or by rotating the entire container of fluid. Louvered windows are less satisfactory because the volume flow rate is not independent of the inflow angle and the flow is choked at high swirl. The flow convergence is provided by an updraft (or downdraft) along the vertical axis. Usually an exhaust fan maintains this but a heated plate has also been used for producing convection currents. In liquids, the use of tiny bubbles or dyes of different densities is common.

The experimental approach has its own set of difficulties. For example, the experimenter faces problems with maintaining calibration of delicate instrumentation and with disturbances due to spurious fluctuations of voltage, air flow, pressure, and temperature in the laboratory. Vibration of the apparatus also causes difficulties.

All of the four approaches to tornado research have increased our understanding of this natural phenomenon. Each has its advantages and disadvantages. There seem to be two motivations which provide the impetus for the study of tornadoes; one is purely scientific and requires no immediate or practical justification and the other works to gain knowledge with a particular application in mind. If the end goal of the latter is to better forecast or even modify tornadoes, the necessary information must be extracted from the same pool of knowledge which resulted from the effort of the pure scientist. This basic information is still being accumulated and will continue to be as long as tornadoes remain either a direct or indirect threat to man. This work is an attempt to add to our present understanding of tornado behavior using the experimental approach. The apparatus as well as the measurement equipment and techniques are described in Chapter 2. The variation of the vortex core size with the experimental parameters has not been determined analytically with sufficient accuracy. Because this information aids in estimating other vortex properties such as pressure and velocity, an empirical formula was obtained from the laboratory observations. These data are presented and examined in Chapter 3. Both smooth and rough surface effects are discussed. With the core radius data, an estimate was made of the maximum tangential velocity obtained for a given pressure drop. A comparison of these pressure and velocity estimates with the measurements in the apparatus is given in Chapter 4. Of course, the mean flow is also affected by the turbulent stresses. To better understand their influence, the Reynolds stresses were measured and these data are presented in Chapter 5. The effect of the turbulence on the mean flow is then discussed. Finally, Chapter 6 provides the summary, conclusions, and suggestions for future research.

CHAPTER II

SIMULATOR AND INSTRUMENTATION

The tornado simulator used in this study is the one designed by Ward (1972) with a few modifications. Fig. 1 shows a schematic of the original apparatus. It is cylindrical in shape with a maximum diameter of about 2.4 m and a height of about 3 m. Vortex generation is accomplished by reproducing two basic ingredients necessary for tornado formation and maintenance; namely, ambient rotation of the air and a means of concentrating the vorticity by converging the flow with a central updraft. The updraft is created by an exhaust fan that provides a pressure deficit across the honeycomb and pulls air into the apparatus through a cylindrical screen which rotates about a vertical axis. When the screen is rotating it imparts angular momentum to the converging flow and the swirl is concentrated at the center of the convection zone to form one or more vortices. Both the fan speed and the screen rotation rate can be controlled. Typically, the volume flow rate can be varied between 0.05 to 2 m^3s^{-1} while the screen generally operates in the range of 0.5 to 7 rpm. Although the volume flow rate is dependent upon the convection radius r_0 it is insensitive to the screen speed (Jischke and Parang, 1975). This apparatus is believed to be one of the more realistic simulators to date. For a review of and a comparison with other machines see Davies-Jones (1976).

The unique geometry of this vortex chamber is very important in determining the flow pattern. Vertical motions in the confluent zone are constrained by a lower boundary representing the earth's surface and by an upper boundary which simulates a capping inversion that is typical in many atmospheric soundings near tornadoes (Miller, 1972). Once the air flows past r_0 it is exposed to the updraft and then continues out of the apparatus. A honeycomb separates the fan from the working section to eliminate fan-generated vorticity from influencing the vortex. The convection radius r_0 can be varied from 0.15 m to 0.61 m and the inflow depth h can range from 0 to 0.61 m. The screen radius is 121 cm. Although the distance between the floor and the honeycomb can be varied, it was held constant at 90 cm for all experiments.

Shortly after this study began it was discovered while the screen was stationary that the updraft was neither uniform across the honeycomb nor axially symmetric. The updraft was much stronger on the fan side. This initiated several modifications to the apparatus. Fig. 2 is a diagram of the simulator after the alterations. The major changes were concerned with the exhaust duct. The suction end of the duct, which had been located at the side of the plenum chamber, was moved to the center to assure updraft symmetry. The outlet end, which formerly passed through the wall to outdoors, was terminated inside the laboratory to avoid flow instabilities caused by turbulence in the winds flowing around the building. Hitherto, the wind gusts caused fluctuations in the volume flow rate and contributed to the meandering of the vortex away from the center of the chamber. Now the vortex wanders very little and is more stable at high volume flow rates than before.

Among the less significant changes are the following: an additional honeycomb section made of tubes 2.5 cm in diameter and 15.2 cm long was installed immediately upwind of the fan; a damping screen was placed at the top of the plenum chamber; flood lamps which were suspended inside the apparatus were moved outside to avoid disturbing the flow; an electrostatic air cleaner was installed downwind of the exhaust fan to filter out the smoke used for flow visualization, the screen was replaced and later fitted with snaps for easy removal; and the fan motor was set up to be D.C. operated to increase its efficiency and lifespan.

To insure that the apparatus is modeling tornadoes the laboratory flow must be dynamically and geometrically similar to its atmospheric counterpart. This can be accomplished by nondimensionalizing the equations of motion and determining the governing parameters. The procedure to be followed now is that used by Lewellen (1962) except that the nonsteady terms will be retained. The continuity equation and the radial, tangential, and vertical momentum equations for axisymmetric incompressible flow are, respectively,

$$\frac{\partial ru}{\partial r} + \frac{\partial rw}{\partial z} = 0 \tag{1}$$

$$\frac{\partial u}{\partial t} + u\,\frac{\partial u}{\partial r} + w\,\frac{\partial u}{\partial z} - \frac{v^2}{r} = -\frac{1}{\rho}\,\frac{\partial P}{\partial r} + K\,\left(\frac{\partial^2 u}{\partial r^2} + \frac{1}{r}\,\frac{\partial u}{\partial r} - \frac{u}{r^2} + \frac{\partial^2 u}{\partial z^2}\right) \tag{2}$$

$$\frac{\partial v}{\partial t} + u\,\frac{\partial v}{\partial r} + w\,\frac{\partial v}{\partial z} + \frac{uv}{r} = K\,\left(\frac{\partial^2 v}{\partial r^2} + \frac{1}{r}\,\frac{\partial v}{\partial r} - \frac{v}{r^2} + \frac{\partial^2 v}{\partial z^2}\right) \tag{3}$$

$$\frac{\partial w}{\partial t} + u\,\frac{\partial w}{\partial r} + w\,\frac{\partial w}{\partial z} = -\frac{1}{\rho}\,\frac{\partial P}{\partial z} + K\,\left(\frac{\partial^2 w}{\partial r^2} + \frac{1}{r}\,\frac{\partial w}{\partial r} + \frac{\partial^2 w}{\partial z^2}\right) \tag{4}$$

where ρ is the air density, K is an appropriate eddy viscosity, P is the nonhydrostatic component of the total pressure and u, v, w are the respective radial, tangential, and vertical velocities.

If we define the circulation as $\Gamma = rv$ and a stream-function such that $u = \frac{1}{r}\,\frac{\partial\psi}{\partial z}$ and $w = -\frac{1}{r}\,\frac{\partial\psi}{\partial r}$ then the continuity equation is satisfied identically. Eqn. (2) and Eqn. (4) can be combined to give

$$\begin{aligned} r\,\frac{\partial\Gamma^2}{\partial z} &= 3\,\frac{\partial\psi}{\partial z}\,\frac{\partial\psi}{\partial r} - 3r\,\frac{\partial\psi}{\partial z}\,\frac{\partial^2\psi}{\partial r^2} + r\,\frac{\partial\psi}{\partial r}\,\frac{\partial^2\psi}{\partial r\partial z} + r^2\,\frac{\partial\psi}{\partial z}\,\frac{\partial^3\psi}{\partial r^3} \\ &- r^2\,\frac{\partial\psi}{\partial r}\,\frac{\partial^3\psi}{\partial r^2\partial z} - 2r\,\frac{\partial^2\psi}{\partial z^2}\,\frac{\partial\psi}{\partial z} + r^2\,\frac{\partial\psi}{\partial z}\,\frac{\partial^3\psi}{\partial r\partial z^2} - r^2\,\frac{\partial\psi}{\partial r}\,\frac{\partial^3\psi}{\partial z^3} \\ &+ r^3\,\frac{\partial}{\partial t}\,\left(\frac{\partial^2\psi}{\partial z^2} + \frac{\partial^2\psi}{\partial r^2} - \frac{1}{r}\,\frac{\partial\psi}{\partial r}\right) - K\,\left(-2r^2\,\frac{\partial^3\psi}{\partial r\partial z^2} + 2r^3\,\frac{\partial^4\psi}{\partial r^2\partial z^2}\right. \\ &\left.+ r^3\,\frac{\partial^4\psi}{\partial z^4} - 3\,\frac{\partial\psi}{\partial r} + 3r\,\frac{\partial^2\psi}{\partial r^2} - 2r^2\,\frac{\partial^3\psi}{\partial r^3} + r^3\,\frac{\partial^4\psi}{\partial r^4}\right). \end{aligned} \tag{5}$$

The tangential equation becomes

$$r \frac{\partial \Gamma}{\partial t} + \frac{\partial \psi}{\partial z} \frac{\partial \Gamma}{\partial r} - \frac{\partial \psi}{\partial r} \frac{\partial \Gamma}{\partial z} = K \left(r \frac{\partial^2 \Gamma}{\partial r^2} - \frac{\partial \Gamma}{\partial r} + r \frac{\partial^2 \Gamma}{\partial z^2}\right) \tag{6}$$

Now all the quantities can be nondimensionalized by defining new variables as follows

$$\zeta = \frac{r^2}{r_0^{\,2}} \qquad \xi = \frac{z}{h} \qquad \hat{\Gamma} = \frac{\Gamma}{\Gamma_\infty} \qquad \hat{\psi} = \frac{\psi}{Q}$$

where Γ_∞ is the ambient circulation and Q is the volume flow rate. Furthermore, a time scale can be formed as

$$\tau = \frac{r_0}{u} = \frac{r_0}{\frac{1}{r}\frac{\partial \psi}{\partial z}}$$
$$\sim \frac{r_0^2 h}{Q}$$

Substituting these quantities into Eqn. (5) and Eqn. (6) yields the nondimensionalized equations of motion:

$$\frac{1}{2} \frac{\partial \hat{\Gamma}}{\partial t} + \frac{\partial \hat{\psi}}{\partial \xi} \frac{\partial \hat{\Gamma}}{\partial \zeta} - \frac{\partial \hat{\psi}}{\partial \zeta} \frac{\partial \hat{\Gamma}}{\partial \xi} = \frac{2\zeta}{R_e} \frac{\partial^2 \hat{\Gamma}}{\partial \zeta^2} + \frac{\alpha}{2R_e} \frac{\partial^2 \hat{\Gamma}}{\partial \xi^2} \tag{7}$$

$$\frac{\partial}{\partial \xi} \frac{1}{2} \hat{\Gamma}^2 = \varepsilon' \{4\zeta^2 [D_a - \frac{4}{R_e} \frac{\partial}{\partial \zeta} - \frac{\partial \zeta}{R_e} \frac{\partial^2}{\partial \zeta^2} + \frac{1}{2} \frac{\partial}{\partial t}) \frac{\partial^2 \psi}{\partial \zeta^2}$$

$$+ \alpha \; [(\zeta D_a - \frac{\partial \hat{\psi}}{\partial \zeta} - \frac{4\zeta^2}{R_e} \frac{\partial^2}{\partial \zeta^2} - \frac{\alpha \zeta}{\partial R_e} \frac{\partial^2}{\partial \xi^2} + \frac{\zeta}{2} \frac{\partial}{\partial t}) \frac{\partial^2 \hat{\psi}}{\partial \xi^2}]\} \tag{8}$$

where D_a is an advection operator equal to $\frac{\partial \hat{\psi}}{\partial \xi} \frac{\partial}{\partial \zeta} - \frac{\partial \hat{\psi}}{\partial \zeta} \frac{\partial}{\partial \xi}$, $\varepsilon' = (\frac{Q}{\Gamma_\infty r_0})^2$ is a swirl parameter, $R_e = \frac{Q}{h\nu}$ is a Reynolds number, and $\alpha = (\frac{r_0}{h})^2$ is a geometric parameter. The Froude number and Coriolis parameter are absent because buoyancy and the earth's rotation have been neglected. To be consistent with the parameters used in the recent work with the simulator a new set is adopted all of which are proportional to the above parameters. These are the aspect ratio $a = \frac{h}{r_0}$, the radial Reynolds number $N = \frac{u_s r_s}{\nu}$, and the swirl ratio $S = \frac{\Gamma_s r_0}{2Q}$ where r_s is the radius to the screen, u_s is the radial velocity at $r = r_s$, and Γ_s is the circulation at the screen. All of these parameters are related to the previous ones as

$$\varepsilon' = \frac{1}{4S^2} \qquad R_e = 2\pi N \qquad \text{and} \qquad \alpha = \frac{1}{a^2}.$$

In addition, for the slightly more complicated geometry of Ward's apparatus another parameter $\frac{r_0}{r_s}$ comes out of the Buckingham π-theorem. If the values of these parameters can be made to match those of the atmosphere then the two flows are said to be geometrically and dynamically similar. Generally the Reynolds number cannot be matched but as will be shown later this is not crucial. The typical parameter ranges used in the apparatus are presented in Table 1.

Flow visualization is often used in the apparatus to render the vortex visible. It also provides quick qualitative information on the flow's speed, its steadiness, and its turbulence level. Several methods of visualization were tried but all utilized the reflection or scattering of light by particles introduced into the flow. There were several criteria established in choosing a compound to be used. The substance must not significantly disturb the air flow as, for example, by forming deposits on the walls of the chamber and thereby altering the streamlines. The particles must be of sufficiently small mass so that they respond to any sudden accelerations of the fluid and do not settle out. They must be neutrally buoyant so as not to induce their own motion. The substance should have a high albedo so as to be easily visible. It should be an inert material so that it does not damage equipment or the confining walls, or create a hazard to persons nearby. Finally, the particles should be easily generated and relatively inexpensive.

Initially, titanium tetrachloride was used because it produces a dense white smoke by reacting with water vapor in the air and forming hydrochloric acid. One problem with this volatile compound is that it tends to sink at low flow velocities. The most serious drawback of this vapor is its extremely corrosive nature and its powdery deposit. Since the apparatus was modified to exhaust back into the laboratory, titanium tetrachloride was deemed a health hazard and ruled out. It should be mentioned that if this compound is to be used the gas can be rendered harmless by allowing the flow to pass through a porous material that has been treated with a neutralizing agent such as a weak ammonia solution. One must also be assured that the laboratory is well ventilated. Dry ice immersed in a warm water bath was also tried (see Hsu and Fattahi, 1975) as a smoke source. However, the turbulence levels near the vortex core were sufficiently high that diffusion quickly diluted the vapor and evaporation took place a few centimeters above the injection point. Additionally, the vapor tended to sink at low speeds.

The smoke system finally adopted is made commercially by Testing Machines Inc. and is shown in Fig. 3. It utilizes a pure mineral oil heated electrically to the point that it vaporizes. The smoke is forced out of the heating chamber by compressed carbon dioxide gas stored in a separate cylinder. The output can be varied up to 28 m^3 per minute. The smoke is composed of very tiny oil droplets not significantly affected by gravity and of such size and thermal conductivity that they rapidly adjust to the ambient temperature. This smoke is dry and has the desirable characteristics mentioned before. Its disadvantage is that in large concentrations some of the oil droplets coalesce and grow to such a size that they precipitate out leaving an oil deposit on the walls of the flow chamber. The smoke generator is mounted under the apparatus and the smoke enters the center of the chamber floor through a hose. It was found that oil condensation in the hose can be minimized by having the entrance end of the hose about 2 cm from the nozzle of the smoke generator. This allows air to enter the hose and prevent saturation. The output end of the hose has a small deflector plate lying horizontally over it to reduce the momentum of the outpouring smoke and allow it to spread along the floor of the apparatus.

Fluid velocity measurements were made with a hot film anemometer system manufactured by Thermo-Systems Inc. Three different probes were used for these measurements. The probe used for volume flow rate measurements has a sensing element 0.005 mm in diameter and 1 mm long. Velocity profiles and core measurements were made with a linear probe 0.4 mm in diameter. The third probe is similar to the first one except that there are two wires mounted at right angles to each other and used to measure turbulent fluctuations and two-dimensional mean flows. The sensors are electrically heated and the flowing air removes heat in proportion to the air velocity and the temperature difference between the sensor and the fluid. The heat conduction is measured by the amount of voltage necessary to maintain the sensor at a constant temperature (accomplished automatically by a feedback circuit). This voltage can be related to the fluid velocity by King's law of heat transfer:

$$E^2 = R_w \, lk(T_w - T_a)A' + R_w \, lk(T_w - T_a)B' \left(\frac{\rho U d}{\mu}\right)^{\frac{1}{2}} \tag{9}$$

where E is the output voltage, R_w is the wire resistance, l is the wire length, k is the thermal conductivity of the fluid, T_w is the wire temperature, T_a is the ambient fluid temperature, A' and B' are constants, ρ is the fluid density, U is the fluid velocity, d is the diameter of the wire, and μ is the viscosity of the fluid. Differentiation of Eqn. (9) with respect to velocity while holding the resistance constant shows that the greatest sensitivity is achieved for small velocities and a large difference in temperature between the film and the air.

It is important to remember when using hot film anemometry that heat transfer is the property of the flow that is actually being measured. King's law shows that this quantity depends upon the fluid temperature as well as the velocity. Thus, when interpreting anemometer output the two effects must be separated. Since velocity is generally the property of interest, the output must be corrected for temperature variations in the flow. Although temperature compensation circuitry is available it is unnecessary for flows with slowly varying temperatures. One could calibrate the flows for different temperatures but this is very time consuming. The approach adopted for the present research is a technique developed by Bearman (1970) for incompressible flows with slow temperature drifts. His correction formula is derived by writing Eqn. (9) for two flows; one at the calibration temperature T_{a1} and the other at the measurement temperature T_{a2}. For a constant temperature sensor we have

$$E_1{}^2 = A_1 + B_1\, U^{\frac{1}{2}} \tag{10}$$

$$E_2{}^2 = A_2 + B_2\, U^{\frac{1}{2}} \tag{11}$$

where $\dfrac{A_1}{A_2} = \dfrac{B_1}{B_2} = \dfrac{T_w - T_{a1}}{T_w - T_{a2}}$.

In terms of the overheat ratio $\theta' = \dfrac{T_w}{T_{a1}}$ and letting

$\varepsilon = \dfrac{T_{a1} - T_{a2}}{T_{a1}}$,

$$\frac{A_1}{A_2} \doteq \frac{B_1}{B_2} = \frac{\sigma}{\sigma+\varepsilon} \quad \text{where } \sigma = \theta' - 1.$$

Substituting the above result into Eqn. (11) gives

$$E_2{}^2 = A_1\left(\frac{\sigma+\varepsilon}{\sigma}\right) + B_1\left(\frac{\sigma+\varepsilon}{\sigma}\right) U^{\frac{1}{2}}. \tag{12}$$

A temperature change results in a voltage change δE given by

$$E_2 = E_c + \delta E \tag{13}$$

where E_c is the output if the temperature remains constant. Substituting Eqn. (13) into Eqn. (10) gives

$$(E_2 - \delta E)^2 = A_1 + B_1 U^{\frac{1}{2}} \tag{14}$$

Eqn. (12) and Eqn. (14) yield

$$E_2{}^2 = (1 + \tfrac{\varepsilon}{\sigma})(E_2 - \delta E)^2 \text{ or}$$

$$E_2 = (1 + \tfrac{\varepsilon}{\sigma})^{\frac{1}{2}} E_c. \tag{15}$$

If $\frac{\varepsilon}{\sigma}$ is small then Eqn. (15) may be approximated by

$$E_c \cong E_2(1 - \tfrac{\varepsilon}{2\sigma}).$$

Thus, A and B can be regarded as constants determined at the time of calibration and King's law now becomes

$$E_2{}^2 \;(1 - \tfrac{\varepsilon}{2\sigma}) = A_1 + B_1 U^{\frac{1}{2}} \tag{16}$$

So, U can be calculated knowing the ambient temperature and the output voltage.

Calibration of the sensors was accomplished in a windtunnel with a pitot tube (see Fig. 4). The pitot-static pressure difference was read from a Datametrics electronic manometer (also used for pressure measurements in the apparatus) and related to the air velocity by the equation

$$\Delta p = \frac{1}{2}\rho V_t^2$$

where V_t is the velocity, ρ is the air density and Δp is the difference between the static pressure measurement at the windtunnel wall and the stagnation pressure measured by the pitot tube. The air density was calculated from the air temperature and the atmospheric pressure as measured by a mercury-in-glass barometer. The probes were calibrated in the range of 1 ms^{-1} to 8 ms^{-1} and a least squares fit of the data to King's law was calculated to determine A and B in Eqn. (16). If the average absolute value of the deviations of the data from the least squares fit exceeds about 3.5 cm s^{-1} the calibration was repeated. Often a honeycomb was placed in front of the windtunnel to minimize the turbulence which contributed to this error.

The single most difficult aspect of measuring a three dimensional flow is aligning the sensor with the streamlines. The output voltage of the anemometer decreases as the cosine of the angle of alignment error. For steady flow the proper probe orientation can be obtained directly by maximizing the output. However, for a turbulent flow this is much more difficult to do unless a split film sensor or other special probe is used because changes in the output voltage are a result not only of flow direction changes but also spontaneous changes in the air speed. The alignment procedure used was as follows. Smoke tracer was introduced into the flow and crude alignment was accomplished visually using a mock probe so as not to contaminate an actual sensor. Then the smoke was turned off and a real probe was put into place. Next, the probe orientation was changed slightly until a maximum was reached in the average output. This optimization generally showed the first guess to be quite precise. Finally, the anemometer output was displayed on an oscilloscope so that the peak signal could be observed as well as the intensity of the fluctuations. The voltage averaging was done by circuitry simulating a first order response and with a choice of 2 sec, 10 sec, 50 sec, and 100 sec time constants. For velocity measurements away from the core a small wind vane was attached to the probe support. In this manner the probe could be aligned horizontally and then by rotating the wind vane 90° about the probe's axis the proper vertical orientation could be achieved. Afterward, minor displacements were made so as to optimize the output as before.

Once the total velocity V_t of the air was measured, the components were derived from the probe's orientation. Fig. 5 shows a sketch of the probe and its support. The following quantities were measured after each run: h_1 (see Fig.

5), h_2, L, r_{ps} (the radius to the probe support), and α_{ps} (the inflow angle at the radius r_{ps}). The vertical dip angle β was then calculated from $\sin\beta = \frac{h_2-h_1}{a_h}$ and used to determine the vertical velocity component. The actual coordinates of the probe tip are given by

$$z = L - l_t \sin\beta + \delta \cos\beta$$

$$r^2 = r_{ps}^2 + l_p^2 + 2r\, l_p \cos\alpha_{ps}$$

where l_t is the distance from the probe tip to the support bracket and l_p is the projection length of the probe calculated from

$$l_p = l_t \cos\beta + \delta \sin\beta.$$

The inflow angle at the probe α_t is given by $\sin\alpha_t = \frac{r_{ps}}{r} \sin\alpha_{ps}$. Finally, the velocity components in cylindrical coordinates are

$$u = V_t \cos\beta \cos\alpha_t$$

$$v = V_t \cos\beta \sin\alpha_t$$

$$w = V_t \sin\beta.$$

The volume flow rate was determined by $Q = \int_A \vec{V} \cdot d\vec{A}$ where $\vec{V}$ is the velocity vector and $d\vec{A}$ is an element of surface area. Since $\vec{V} = u\hat{e}_r + v\hat{e}_\phi + w\hat{e}_z$ and $d\vec{A} = -r\, d\phi\, dz\, \hat{e}_r$ at the screen then $Q = \int_0^{2\pi} \int_0^h u\, r\, d\phi dz$. In the region $r_s < r < r_0$ and $0 < z < h$, u is independent of height and the flow is axisymmetric. Consequently, $Q = -2\pi uhr$. For simplicity, since Q is independent of swirl (Jischke and Parang, 1975), u was measured in the absence of screen rotation so that the probe could be easily aligned with a local radial.

For measuring turbulent fluctuations, cross-film probes, an electronic correlator, and a true RMS meter were used. The probe has two wires mounted 90° to each other separated by a distance of 1 mm. This probe cannot be calibrated like the single sensor probes because when the inner probe was rotated perpendicular to the flow it lay in the wake of the outer probe's supports. So, to calibrate the cross-wire probe the anemometer was switched to the linearized mode. Both probes were zeroed for zero flow. The outer probe was then rotated perpendicular to the flow and calibrated as with the single sensor. The gain of this sensor was therefore determined. With the windtunnel fan left at some setting the probes were rotated so that both were oriented 45° to the mean flow. During this process the output of the outer probe would drop to 70.7% (= cos 45°) of its original value. In this position the inner probe was no longer in the path of the other's supports. Its gain was then adjusted to give the same value of the other sensor. In this manner, both probes had the same gain which greatly simplified the interpretation of the output.

With the probe calibrated as above, the output of the correlator gave the velocities in the plane of the two sensors and also the Reynolds stresses when an RMS voltmeter was used. One drawback was that the measured velocities were in the reference frame of the probe, not the simulator. Since no information was given about velocities perpendicular to the sensor plane a coordinate transformation was not possible unless the mean flow was two-dimensional with respect to the nonrotating cylindrical coordinate system of the machine. As a consequence, the turbulence measurements were made near the lower surface where the mean vertical velocity is near zero. The error associated with this approximation is proportional to $\frac{\bar{w}^2}{(\bar{u}^2+\bar{v}^2)}$ (Brunn, 1975) where $\bar{w}$ is the mean vertical velocity, $\bar{u}$ is the mean radial velocity, and $\bar{v}$ is the mean tangential velocity. The correlator output gives the mean flow in the streamline direction, $\bar{u}_p$, the mean flow perpendicular to that $\bar{v}_p$, the fluctuations in these directions u_p' and v_p', respectively, and the correlation $\overline{u_p' v_p'}$. Thus, the velocities in the machine's coordinate system are

$$\bar{u} = -\bar{u}_p \cos \alpha_{ps} + \bar{v}_p \sin \alpha_{ps}$$

$$\bar{v} = \bar{u}_p \sin \alpha_{ps} + \bar{v}_p \cos \alpha_{ps}$$

$$\overline{u'^2} = \overline{u_p'^2} \cos^2 \alpha_{ps} - 2\, \overline{u_p' v_p'} \cos \alpha_{ps} \sin \alpha_{ps} + \overline{v_p'^2} \sin^2 \alpha_{ps}$$

$$\overline{v'^2} = \overline{u_p'^2} \sin^2 \alpha_{ps} + 2\, \overline{u_p' v_p'} \sin \alpha_{ps} \cos \alpha_{ps} + \overline{v_p'^2} \cos^2 \alpha_{ps}$$

$$\overline{u'v'} = (\overline{v_p'^2} - \overline{u_p'^2}) \cos \alpha_{ps} \sin \alpha_{ps} + \overline{u_p' v_p'}\,(2 \sin^2 \alpha_{ps} - 1)$$

The core radius was measured visually using the protractor arrangement shown in Fig. 6. Smoke was introduced at the bottom center of the chamber and illuminated with flood lamps. The apparent angular diameter of the visible core was then measured at a height of about 15 cm to be consistent with Ward's (1972) data (although the core expands little outside the boundary layer). With the protractor aligned as shown in Fig. 6 the core radius is given by $r_c = (\overline{AO} + R_p)\tan(\phi_c/4)$ where $\overline{AO}$ is the radius of the protractor, R_p is the distance from the vortex to the protractor, and ϕ_c is the angular diameter of the vortex core. The error in the core radius measurements is estimated to be about ±1.4 cm.

To simulate the influence of a rough surface on a tornado, the atmospheric roughness length z_0' had to be scaled down to a laboratory value z_0. The core radius was chosen as the appropriate length scale because the tangential velocity changes significantly over that distance. Thus, the roughness length used in the apparatus is given by

$$z_0 = z_0' \frac{r_c}{r_c'}$$

where r_c is an average core radius in the apparatus (7.6 cm) and r_c' is an average tornado radius (taken as 70 m). Consequently, the scale was about 1:920. Since the aim of the rough surface was to model city houses in a dense array and having a roughness length of 125 cm (Lettau, 1969) the apparatus value was calculated to be z_0 = 0.14 cm. To design such a surface, use was made of Lettau's equation, which is

$$z_0' = \frac{1}{2} \frac{Hs}{S}$$

where H is the element height, s is the silhouette area of the obstacle and S* is the total surface area divided by the total number of elements. A constraint on this technique is that the elements must not be spaced so far apart that one is actually modeling flow around obstacles nor should they be packed so tightly together that a new continuous boundary layer forms at the height H. The surface was constructed of 626 elements distributed over the 4.6 m^2 of the apparatus in a hexagonal pattern to reduce directional bias. The effect of the surface appeared to be rougher than expected, although qualitatively in agreement with Rotunno's (1977) numerical model. The vortex appeared laminar in the lower portions with a stagnation bubble at midlevels and turbulent flow above (see Fig. 7). This flow pattern also occurred for small values of swirl ratio in Rotunno's (1979) numerical model when he incorporated a no-slip lower boundary condition. Since no amount of swirl could bring the stagnation point to the surface and produce a fully turbulent vortex core, experiments with this surface were abandoned.

Although the phenomenon of vortex breakdown is not well understood, the honeycomb in the apparatus probably plays a very important role in its formation by reducing the horizontal flow to zero. Evidence for vortex breakdown occurring in tornadoes has been given by Burggraf and Foster (1977). In the simulator the profile of w at the honeycomb is unknown but for an axisymmetric flow continuity requires $Q = 2\pi \int_0^{r_h} rwdr$ where r_h is the radius of the honeycomb. Breakdown then occurs at the honeycomb when w reverses sign at the axis and flows downward. For this to happen the axial pressure gradient force must act downward and be large enough not only to reduce w but also to reverse its direction. The axial pressure gradient force depends mainly on the decay of v_{max} with height. Near the lower surface the magnitude of v_{max} for a given volume flow rate is determined by the imposed swirl. At the honeycomb, v_{max} is zero. As the swirl ratio is increased, v_{max} near the surface increases and must therefore decay more rapidly with height. If the swirl ratio is increased the surface pressure drops until the axial pressure gradient is large enough to create a stagnation point at the honeycomb. A further increase in the swirl enhances the adverse axial pressure gradient and the stagnation point descends. This idea also agrees qualitatively with the observation that the axial downdraft is less likely with a small r_0. In this case continuity causes w to be much greater at z = h so that a stronger downward pressure would be necessary to reverse the direction. With a rough surface in place Dessens (1972) found that the surface pressure deficit is not as high, probably due to frictional convergence. Consequently, the axial pressure gradient is likely to be downward. Under the more favorable pressure gradient the vortex core is more likely to remain laminar.

A different approach was adopted to simulate natural ground roughness using a shag carpet (Hansen _et al._, 1975). Since the roughness length was difficult to calculate, the scaling was calculated using the average obstacle height. The carpet fibers were about 1.5 cm high corresponding to natural obstacle heights of about 14 m when scaled up by the core radius ratio. With this surface in place the axial stagnation point could be brought well below the core radius measurement height of 15 cm.

CHAPTER III

THE CORE RADIUS AND THE INFLUENCE OF SURFACE ROUGHNESS

Tornadoes have been observed to range in size from tens of meters to a few hundred meters in diameter. Generally, the larger tornadoes are most destructive not only because they may generate higher wind speeds but also because they occupy a wider space that sweeps out a greater damage path. As a consequence it is important to determine which parameters govern the tornado's size.

It is first necessary to clarify what is meant by the core of the tornado since it can be specified in a number of ways. Figure 8 is a conceptual sketch of how a typical vertical-radial streamline pattern might appear for a two-cell vortex. Notice that there is a weak downdraft in the center and that most of the inflow into the tornado is through the ground boundary layer. Some numerical models (e.g., Rotunno, 1977) then define the core radius as the distance from the central axis to the surface which separates the two meridional cells. This is consistent with how the core size is determined in the laboratory, where smoke is injected at the bottom center of the vortex and the visible core is measured. This approach is adopted to be consistent with the past studies of Ward (1972) and because of the ease in quickly identifying the core. Figure 9 is a photograph of a typical vortex core rendered visible in this manner.

Another way to define the core is in terms of the radius of maximum tangential velocity at a given level. This might be called the dynamic core. Laboratory measurements in Ward's apparatus and in that of Purdue University (Church, private communication) indicate that for a two-cell vortex this radius does not differ much from the previous one. In Sullivan's (1959) two-cell analytic solution the radius separating the two meridional cells is given by $r = 3.37\sqrt{\nu/b}$ where ν is the kinematic viscosity and b is a measure of the horizontal convergence. The radius of the velocity maximum is $r = 3.47\sqrt{\nu/b}$. In Kuo's (1966) analytic solution the two radii are given as $r = 1.59\sqrt{4\nu/\beta_0}$ and $r = 2.06\sqrt{4\nu/\beta_0}$, respectively, where β_0 is a buoyancy parameter. In any case, there seems to be little practical difference between these two radii in the laboratory model.

In nature, the tornado size can differ greatly from the dynamic core size, because the visible core is composed of moisture condensation as well as dust and debris. This can be illustrated with the aid of Figure 10 which shows a hypothetical pressure distribution for a tornado. As an air parcel approaches the tornado its pressure is lowered and it cools off adiabatically. Eventually it cools to the saturation point and forms the visible core. However, this core size depends a great deal on the environment and not just the flow dynamics. It can be seen that if the humidity of the air is such that the condensation pressure is P_4 then the core appears very large. If, however, the humidity were lower and the condensation pressure decreased to P_1, then the vortex would appear only as a funnel aloft. In either case the dynamic core could remain unchanged. Figure 11 shows a plot of condensation radius as a function of humidity for the Dallas tornado of 1957 from Hoecker's (1961) analysis. The condensation radius is very sensitive to moisture changes at low and high humidities. The actual humidity was 87% and a change of only 3% could result in a 12% change in the condensation radius. If the humidity had dropped below 73% the condensation radius would have gone to zero and broken contact with the ground. Figure 12 shows the condensation height versus humidity. Again there is high sensitivity to the relative humidity. In the midrange a 3% change in humidity results in about a 90% change in the condensation height. Clearly the environmental moisture can play a very significant role in the apparent tornado size.

The visible core is not only a function of the moisture field but also of the radial velocity component since the condensation process requires a finite amount of time and air parcels may be displaced inward during this period.

In fact, for the Dallas tornado the condensation pressure occurred at a radius of about 49 m but the visible core was only 17 m in radius. This could be explained if for a radial inflow velocity of 18 ms^{-1} (see Hoecker, 1960) the condensation process required 1.8 sec. The condensation time was estimated more quantitatively by Jischke and Parang (1975). Of course, the availability of cloud condensation nuclei would also determine where the condensation will form but nuclei should be rather abundant in the vicinity of most tornadoes over land. Often the condensation core is totally obscured by the debris stirred up from the surface. In this case, the particles approximately follow the streamlines and outline the core in much the same manner as the smoke injection technique used in the laboratory simulator.

Using the Buckingham π-theorem, Davies-Jones (1973) has shown that the core radius and other properties of the flows in Ward's apparatus are governed by the following set of parameters: h/r_0 (=a), $Q/2\pi\nu h$ (=N), $r_0\Gamma_s/2Q$ (=S), and r_0/r_s where a is the aspect ratio, Q is the volume flow rate, ν is the kinematic viscosity, N is a Reynolds number, Γ_s is the circulation at the screen, r_0 is the radius of convection, h is the inflow depth, and r_s is the radius of the cylindrical screen. The first three quantities are proportional to those derived from the Navier-Stokes equations by Lewellen (1962) for a similar flow arrangement. One is assured that if the values of these parameters in the apparatus are the same as those in nature then the flows are dynamically and geometrically similar. Typically, it is not easy to match all of these parameters. For tornado cyclones the swirl ratio is of the order of one and the aspect ratio is about one half (Davies-Jones, 1973). It is difficult to estimate the parameter r_0/r_s in nature because r_s is not clearly defined. The Reynolds number for tornadoes is of the order to 10^9 while the apparatus works in the range of 10^4. At first this might suggest that the apparatus is not simulating tornadoes, but it will be shown that the flow is practically independent of the Reynolds number. Furthermore, the above Reynolds numbers were calculated using the kinematic value of viscosity. This may not be appropriate since both the laboratory model and natural tornadoes are turbulent. If one could estimate the value of the effective eddy viscosity for each, the two eddy Reynolds numbers would be much closer because the eddy viscosity of the natural tornado would be much larger than that for the laboratory model.

The variation of the core radius with the inflow angle was examined theoretically by Ward (1972) and by Jischke and Parang (1974). Each obtained an expression that was similar for small inflow angles. Davies-Jones (1973) pointed out that the geometry of the vortex cage must be taken into account and showed empirically that the core radius was predominantly a function of the swirl ratio alone. However, since the Reynolds number was not available in

Ward's data, the effect of this parameter was not established but thought to be small since the core radius was highly correlated with the swirl ratio alone. This dependence (or independence) of the core radius is important in establishing the credibility of the laboratory model because its Reynolds number can never match that of its atmospheric counterpart.

The first series of experiments discussed involves core radius measurements as a function of the swirl ratio, the aspect ratio, and the Reynolds number. The core radius measurements were made at a height of 15 cm to be consistent with Ward (1972), but the core radius does not change considerably above the boundary layer. Later, the influence of the parameter r_0/r_s was investigated since this quantity was not changed in Ward's experiments. Another experiment describes how the variation of the core radius with the flow parameter was altered by the addition of a new quantity, the roughness length. Laboratory experiments with surface friction effects on vortices have been carried out in air by Dessens (1972) and in water by Wilkins et al. (1975). In both investigations it was seen that the friction caused an increase in vortex diameter and a decrease in maximum tangential velocity if all other parameters were held constant. It is clear that surface drag can have a pronounced effect. Finally, the influence of surface roughness on multiple vortex transition was examined and related to atmospheric observations.

In Ward's apparatus eight cases were examined over a smooth surface in which r_0/r_s was left constant at 0.5. Since the swirl ratio is believed to be the most important parameter it was varied over a greater range for a given aspect ratio and Reynolds number. The other parameter values for all eight cases are listed in Table II. Once the core radius was measured it was nondimensionalized with r_0. Figure 13 shows a plot of the data for cases I through IV. It is clear that the core radius is strongly dependent on the swirl ratio and much less on the Reynolds number. Figure 14 shows a plot for cases V through VIII. Aside from a little more scatter, the data appear much like that in the previous graph. A least squares analysis of the data was performed and gave

$$\frac{r_c}{r_0} = 0.537\ a^{-0.073}\ S^{0.78}\ N^{-0.038} \tag{17}$$

The standard error of estimate $\sigma_{est} = \sqrt{\frac{\Sigma(y-y_{est})^2}{N_0}}$ is 0.015 where y represents the observed values, y_{est} is the estimate given by Eqn. (17) and N_0 is the total number of observations. The overall correlation coefficient of the log of the left hand side of Eqn. (17) with the log of the right hand side is 0.951. The correlation with just the log of the swirl ratio is 0.950. Obviously, the core radius is determined almost entirely by the swirl ratio, and is largely independent of the Reynolds number for the limited range available.

From Ward's (1972) data Davies-Jones (1976) found that the core radius was a function of $S^{1.14}$. The difference in curvature results in Ward's core radii being somewhat smaller than those presented in this work. It is not clear why Ward's observations differ slightly from those described by Eqn. (17), but the modification of the apparatus may have contributed. In particular, the exhaust fan was centered over the convection zone. Previously, the fan was located on the side of the plenum chamber resulting in a less intense pressure drop at the center of the honeycomb. In the present configuration the vortex central pressure may be lower, and lower pressures are correlated with larger vortices (over a smooth surface). Differences in the core measurement and visualization techniques may also have contributed.

The experiment was repeated over a rough surface simulating obstacles about 13 m high. The aspect ratios and Reynolds numbers used are in Table III. The results are plotted in Figures 15 and 16. Again the core radius has a strong dependence on the swirl ratio alone but the data points have shifted to the right implying that more swirl is necessary to obtain a vortex of the same size. Fitting a least squares power law to all of the rough surface data and denoting this series of core measurements by r_c^* gives

$$\frac{r_c^*}{r_0} = 0.184a^{0.25}\ S^{1.05}\ N^{0.078} \qquad (18)$$

with a standard error of estimate of 0.011. As before, the

Reynolds number is not a critical parameter. The overall nonlinear correlation coefficient is 0.967. For the swirl ratio alone, the value is 0.954.

One might ask (for the same conditions) which core is larger - the one over the smooth surface or the one over the rough surface? If we divide Eqn. (18) by Eqn. (17) and extract the aspect ratio from the swirl ratio we obtain the ratio of the two core sizes,

$$\frac{r_c^*}{r_c} = 0.284\ a^{0.05}\ (\tan\theta)^{0.27}\ N^{0.12}.$$

The ratio of the two core sizes depends mainly on θ and not S. This is consistent with the fact that θ determines the path length taken by an air parcel from the screen to the vortex. As θ increases, the path length increases and the effect of the rough surface is more pronounced. For typical values of θ and N the core over the rough surface is always smaller than over a smooth surface. For example, taking an average Reynolds number of 3.57×10^4 and an average aspect ratio of 0.635, the rough surface core is larger than the smooth surface only when $\theta < 47°$. However, no measurements of the core radius can be taken at such high inflow angles to verify this trend because the single vortex undergoes transition to two vortices.

Comparing the above results with the work of others it was found that both Dessens (1972) and Wilkins et al. (1975) observed vortices over a rough surface to be larger than those over a smooth surface. However, their vortices were driven by different mechanisms than Ward's and their measurements may have been made in different regions of parameter space. The fact that neither experimenter measured the swirl ratio or inflow angle further hampers direct comparison of their results with Eqn. (18), but by illustrating this expression in another manner some general relationships can be seen. Figure 17 shows a plot of the swirl ratio versus the aspect ratio for which the core radius over the rough surface is a given fraction of the core radius over a smooth surface. At various points along each line the corresponding inflow angle is given. The middle line indicates the conditions for which $r_c^* = r_c$. Above this line $r_c^* > r_c$. The data presented thus far are all in the range of $0.036 < S < 0.78$ and $0.478 < a < 0.797$ corresponding to a rough surface core which is always smaller than the smooth surface core. However, if one extrapolates the graph to the higher aspect ratios at which Dessens and Wilkins worked it can be seen that large inflow angles would result in the smooth surface core being smaller than the rough case. Thus, if Dessens' apparatus was operating at inflow angles larger than 32° or if Wilkins' rotating tank was operating at angles larger than 9° then their observations would be consistent with Eqn. (18). Of course, it should be pointed out that no data was taken on Ward's apparatus at very large aspect ratios so it cannot be assumed that Eqn. (18) remains valid in that region.

One other difference that makes a comparison difficult is that the surface chosen for the rough case varied. For instance, the author used a shag carpet with fibers 1.5 cm long corresponding to natural obstacle heights of about 1.4 m when scaled up (based on the core radius). Dessens used pebbles 6 mm high and distributed so as to produce a roughness length, as described by Lettau (1969), of 0.2 cm while Wilkins used plexiglass rods 3.18 cm high and 1.59 cm in diameter corresponding to a roughness length of 0.39 cm. Each apparatus is constructed to a different scale and the roughness length used is meaningful only when compared to this scale. For artificial surfaces in the apparatus to truly simulate natural roughness, it must be scaled up with some appropriate length in the chamber that is relevant to the flow. Since the fibers making up the carpet are very close together the roughness length cannot be properly computed using Lettau's approach.* Instead, the roughness was parameterized by taking an average height of the roughness elements and normalizing that by a typical core radius. Using this method, Dessens' obstacles would correspond to natural

---

*A rough surface was constructed that had a roughness length of 0.14 cm according to Lettau's formula (and a scaled up value of about 1 m). The surface was composed of cylinders 4 cm high, 1.27 cm in diameter and spaced one per 74.6 cm^2. However, the surface caused the vortex to become laminar at the surface with a stagnation point aloft and turbulent flow immediately above it. The laminar core radius appears to be independent of the swirl ratio.

structures about 42 m high and those of Wilkins to 127 m high.

In a final series of experiments the convection radius was changed to determine the core's dependence upon it. All of Ward's data were taken with the convection radius fixed at 0.61 m, and so the effect of the parameter r_0/r_s could not be established. The updraft radius was reduced from 0.61 m to 0.305 m and the other parameters shown in Table IV.

Figures 18 and 19 show a plot of the 122 observations. Again the data show a strong dependence of the swirl ratio but also slightly more dependence on the Reynolds number than before. Qualitatively the data are not significantly different from the previous smooth surface data. When this last set of observations was combined with cases I to VIII the least squares fit gave for the smooth surface the following relationship:

$$\frac{r_c}{r_0} = 0.198a^{0.076}\ S^{0.81}\ N^{0.085}\ \left(\frac{r_0}{r_s}\right)^{0.15}$$

with a standard error of estimate of 0.021. The overall non-linear correlation coefficient is 0.948. For the swirl ratio alone the value is 0.947. The correlation coefficients for a, N, and r_0/r_s are 0.105, 0.248, and -0.386, respectively. For typical parameter values in the apparatus the core radius can be estimated from the swirl ratio alone as $r_c/r_0 = 0.42\ S^{0.81}$. Of course these expressions cannot hold for all S since r_c/r_0 cannot exceed one.

The above results and conclusions can be summarized as follows. The flows in the laboratory apparatus are similar to natural flows only if certain nondimensional ratios are the same for the two. For Ward's apparatus these parameters are the aspect ratio, the normalized updraft radius, the swirl ratio, and the Reynolds number. For simulating a tornado over a rough surface, the roughness parameter must also be included. While the first few parameters can generally be matched with the atmosphere the Reynolds number of the apparatus based on molecular viscosity can never equal that of the atmosphere. However, the above experiments showed that the dynamics governing the tornado core size remain largely independent of the Reynolds number. This result also agrees with Rotunno's (1977) numerical model which was insensitive to Reynolds numbers greater than about 10^3. The variation of the core radius with the other parameters was examined and the results indicate that over a particular surface the vortex size can be closely determined solely by the swirl ratio, which also contains the geometry of the flow.

The influence of the rough surface was to reduce the size of the vortex core. Although this result differs from that found by Dessens and Wilkins <u>et al.</u>, it is attributed to the fact that their simulators were very different from Ward's, and they worked in a different region of the parameter space from that examined by the author. Furthermore, each investigator used different magnitudes of relative roughness. In the absence of roughness the core is largely established at the radius where the centripetal acceleration and the pressure gradient force balance. When an air parcel enters the apparatus it is given angular momentum by the screen. As the pressure gradient accelerates the parcel toward the center of the chamber it approximately conserves its angular momentum and consequently its tangential velocity increases inversely with the radius. The air parcel will continue to approach the axis of the chamber until its tangential velocity is so large that the resulting centripetal acceleration balances the radial pressure thrust. At this point the radial forces are in balance and continuity forces the parcel upward. When the rough surface is in place it provides a partial sink for the angular momentum. Thus the parcel must converge to a smaller radius before it can generate enough centrifugal force to balance the pressure gradient.

The pressure distribution on the lower surface depends mainly on the flow velocity above the boundary layer and the radial inflow. Although the pressure deficit may not be as intense with the rough surface in place, the radial inflow is larger because the tangential flow has been reduced by the increased drag. Consequently, the air flows closer to the axis establishing a smaller core. It should be pointed out that this simple physical argument is not always valid.

In a numerical study by Bode _et al_. (1975), the simulated vortex expanded when the surface drag was increased, even though the axial velocity increased and the tangential velocity decreased. On the other hand, Rotunno (1979) states that the maximum tangential velocity can increase by as much as 50% when the lower boundary condition is changed from free slip to no slip. In addition, his vortex core contracted during this change.

Effects of Surface Friction on Multiple Vortex Transition

The existence of "suction vortices" was proposed by Fujita (1971) to explain the cycloidal surface markings along the paths of some tornadoes. Eyewitness accounts and photographic evidence now clearly prove the existence of a configuration in which two or more vortices rotate around a common axis while translating with the parent storm. Furtheremore, the phenomenon may not be as rare as it was once thought to be.

Ward (1972) showed that the MV phenomenon can be modeled in the laboratory. He hypothesized that a single vortex (SV) transition occurs as a result of vortex flow instability associated with a critical inflow angle for fixed a (≤ 0.5). He demonstrated that further stepwise increases in the number of vortices, up to four, at least, could be brought about by increasing the inflow angle.

Jischke and Parang (1974) also studied the SV-MV transition by experimenting with the tornado simulator built by Ward. They viewed the transition as a torque reduction process, wherein the torque of the vortex system against the ground is reduced by increasing the number of vortices. Their data indicated that the transition occurred at critical values of the swirl ratio. However, Davies-Jones (1976) pointed out several difficulties with the torque reduction concept. The swirl ratio was shown by Davies-Jones (1973, 1976) to be the key parameter governing vortex size as well as SV-MV transition and number of suction vortices. He showed also that the range of swirl ratios available to the Ward simulator is compatible with that which logically could be calculated for real tornadoes. For these reasons the swirl ratio has been selected as the parameter against which all vortex phenomena are compared in these experiments. Davies-Jones (1973) offered an alternative explanation for the transition in terms of a non-axisymmetric instability, wherein a vorticity maximum develops (due to shear) away from the core. Snow (1978) examined theoretically the inertial stability of a two cell vortex. His model predicted the destabilization of progressively higher wave numbers and the hysteresis effect showing qualitative agreement with the laboratory observations.

For the following experiments the volume flow rate was held constant at $Q = 0.123\ m^3\ sec^{-1}$, with $a = 0.48$, and a smooth surface was used for the first series of transition experiments. Starting with a swirl ratio of 0.127, a SV existed in the apparatus. The first indication of transition occurred at a swirl ratio of 0.277, as two tightly wound vortices appeared, translating around a common center. A further increase in S caused the two vortices to unwrap and move farther apart, until the transition to three vortices occurred at S = 0.898. This third transition was characterized by the vortex pair losing its identity in a rotating turbulent flow. The three vortices emerged as the flow pattern gradually reorganized from the chaotic state. In other words, the transition does not occur by simply adding another vortex to the ensemble. The transition to four vortices occurred in the same manner, as the swirl ratio was increased to 1.79.

Roughness effects were introduced by covering the floor of the tornado simulator with a shag carpet of one-inch fibers. This kind of surface was chosen because it produces a boundary layer in wind tunnels that is similar to that of the atmospheric boundary layer (Hansen *et al.*, 1975). The experiment was then repeated with the "rough" surface in place, and the critical swirl ratios observed for each transition are tabulated in Table V for comparison with the smooth surface transitions.

In the rough surface experiments the vortices had an irregular appearance characteristic of turbulent flow. As a result, individual vortices in the MV configurations were not as well defined, making the identification of transitions more difficult. However, the critical swirl ratios are believed to be accurate and the increased magnitudes due to roughness are certainly real. Table V shows the following:

(1) Increasing surface roughness causes MV transitions to occur at higher swirl ratios.

(2) Transition from even to odd numbers of vortices (e.g., MV_2 to MV_3) require larger percentage increases in swirl ratio than odd-even transitions. This is the case for both smooth and rough surfaces.

(3) The critical swirl ratio is about 40 percent larger on the average for the transitions over the rough surface used in these experiments.

The rather impressive response of the experimental parameters and vortex appearance to the rough surface suggests that the effective roughness length z_0 of the carpet is "large" in the aerodynamic sense. For future experiments it would be highly desirable to evaluate z_0 quantitatively, and also to scale the roughness parameter to real atmospheric flow.

Any scale factor relating model dimensions to the atmospheric counterpart must show that z_0 was indeed large for the experiment. Ideally such a factor should be based on the ratio of the two boundary layer thicknesses, but these are not defined. If based on the assumption of swirl ratio similarity, then a scale factor F is given by

$$F = \frac{r_{0_t}}{r_0} = \frac{Q_t M}{Q M_t}$$

where M is the ambient circulation and the subscript t refers to tornado cyclone parameters. Davies-Jones (1973) pointed out that the swirl ratios must be similar for a relevant experiment, and in demonstrating similarity for the tornado simulator, used the values $Q_t \approx 10^8$ to 10^9 m^3 sec^{-1} and $M_t \approx 2.5 \times 10^4$ to 10^5 m^2 sec^{-1}. With this range of parameters the value of F could be anywhere between about 10^3:1 and 10^5:1. Roughness lengths are typically about 1/30 of the height of individual roughness elements; this would give $z_0 = 0.085$ cm for the model (or a little less since the carpet fibers are tilted by the flow somewhat), corresponding to $z_{0_t} \approx 0.85$ m to 85 m for the real atmosphere. The smallest of these numbers represents a fairly rough surface analogous to an area of tall trees, for example, but it is not unreasonable.

It is natural to suspect that the increased radial velocity component induced by surface friction is responsible for the increase in the critical swirl ratio. Near the surface, at least, a parcel of air entering the convergence zone must traverse a longer path to reach the vortex region as the swirl ratio is increased. This gives the parcel more time to be acted upon by surface friction. In the surface layer, then, a parcel of air must enter the convergence zone with a larger tangential component in order to possess the critical amount of swirl by the time it reaches the zone of maximum vorticity.

Thus, the experiments indicate that one effect of surface friction is to increase the magnitude of the critical swirl ratio for any given type of transition. This result has an important implication for the transition theory of Jischke and Parang (1974). They hypothesized that since the flux of angular momentum into the apparatus varies directly as the circulation, while the torque exerted by the surface on the flow varies as the circulation to the 9/5 power, then increasing the circulation will increase the ground torque much more rapidly than the influx of momentum necessary to drive the flow. Consequently, the flow must undergo a transition to a configuration of lower torque. They then claim that the MV mode is such a configuration. If, however, for a given angular momentum flux the ground torque is increased by a rougher surface then the transition should occur at a lower circulation (or swirl ratio). The experiments in this paper indicate that the opposite occurs. Also transitions from even to odd numbers of vortices require greater increases in swirl ratio (by a factor of two) than odd-even transitions. Experiments should be repeated over a greater range of aspect ratios to determine if this phenomenon is persistent. If it is, this would suggest that odd wave numbers are less stable, although no such analogy is observed in rotating dishpan simulations of the atmosphere's general circulation. Predicting changes in swirl ratio of a tornado system would be very difficult, but observing whether its path leads to smoother or rougher terrain may be possible in some circumstances. Blechman (1975) reported on a situation (the Oshkosh tornado) in which a multiple vortex tornado traveling over a relatively flat field transformed into a single vortex system as it moved onto the rougher terrain of a city. It follows that the more serious transition from SV to MV could be triggered by a change from rough to smooth terrain if the swirl ratio is sufficiently near critical and the other dynamic mechanisms remain unchanged. Experimentally at least there is a hysteresis effect such that transitions to smaller numbers occur at smaller swirl ratios than the corresponding transitions upscale (Ward, 1972).

With the empirical formula (Eqn. 17) for the core radius, estimates of the tangential velocity and the pressure profile can be made. In the next chapter, a simplified form of Eqn. 17 is used in an analytic expression to determine the greatest tangential velocity attainable with a given pressure deficit.

CHAPTER IV

PRESSURE AND VELOCITY MEASUREMENTS

The relative magnitudes of the pressure and velocities surrounding tornadoes are of great practical importance. When designing structures to withstand tornadic winds and the missiles they generate, engineers often rely upon simple models to determine the wind velocity profiles and magnitudes. Typically, a Rankine-combined vortex is assumed, i.e.,

$$v(r) = v_{max} \left(\frac{r}{r_c}\right)^D \qquad \text{with } D = +1 \quad 0 \leq r \leq r_c$$
$$D = -1 \quad r \geq r_c$$

where r is the radius, v is the tangential velocity, v_{max} is the maximum tangential velocity located at $r = r_c$. When this profile is combined with the cyclostrophic equation a relation between the pressure drop and v_{max} can be obtained. The radial momentum balance is

$$\frac{1}{\rho}\frac{\partial p}{\partial r} = \frac{v^2}{r}$$

where p is the pressure and ρ is the air density assumed constant. Then,

$$\frac{\partial p}{\partial r} = \rho v_{max}^2 \; r^{2D-1} \; r_c^{-2D} .$$

Upon integrating from 0 to ∞ we get

$$\Delta p = \rho v_{max}^2$$

where Δp is the deviation of the central pressure from the ambient value. More sophisticated analytical models change this relationship slightly. For instance, in Kuo's (1966) solution $\Delta p = c\rho v_{max}^2$ where $c = 1.74$ for his one celled vortex and $c = 1.14$ for his two celled vortex. The solution of Burgers (1948) and Rott (1958) gives $c = 1.68$. The reciprocal of c can be thought of as a measure of vortex efficiency, since it relates the maximum velocity obtained for a given pressure deficit. It is worth noting that each of the above models claims that c is a constant and independent of the background circulation. Plugging in typical values of Δp measured in the laboratory apparatus indicated velocities much different from those observed. As a consequence it was decided to measure the central pressure as well as the velocity maximum for several laboratory vortices in an attempt to determine experimentally the proper relationship of the pressure deficit to the velocity maximum. The data for these experiments were difficult to obtain because the vortex tends to wander around the probes and also because the turbulent core itself undergoes continuous changes. The two effects are almost indistinguishable on the sensor output because a sudden change in the output could result from either an instantaneous change in alignment of the vortex with the sensor or as a turbulent fluctuation that could occur even with a stationary vortex or both. Generally, however, the magnitude and the time scale of the turbulent fluctuations are smaller than those due to vortex meandering and a reasonable interpretation of the data is possible.

In order to determine the value of c for the laboratory flows, first the central pressure of the vortex was measured using a pressure port located in the center of the chamber. Although the vortex meandered about that point slightly (more so at lower swirl ratios) it was visually observed to center itself there frequently. So, the pressure transducer output was traced on an oscilloscope and the average minimum was taken as the central pressure. Figure 20 shows the results of these measurements for $a = 0.472$, $N = 5.4 \times 10^4$, and $r_0/r_s = 1/2$. The scatter in the data suggests the degree of uncertainty as well as the level of difficulty in obtaining the data. The vortex tends to wander away from the center of the chamber more at small swirl ratios than at larger values. This accompanied with the fact that the core is much smaller at small swirl values makes core pressure measurements difficult using a single port. A better estimate of the central pressure can be had by measuring the time-averaged radial profile and extrapolating the results to center (say, by employing the axial boundary condition $\frac{\partial p}{\partial r} = 0$) where the unsteadiness is very high. These profiles will be shown later and it will be more obvious that the central pressure for a single vortex decreases with increasing swirl ratio.

Perhaps the single most difficult measurement was in placing the hot film probe in the location of the velocity maximum and aligning it with the proper streamline. This was accomplished initially by orienting the probe along a streamline in the vicinity of the apparent velocity maximum and then changing its position so as to optimize the time-averaged output. As a general rule the location of the velocity maximum was at the radius of the visible core just above the boundary layer (see Figure 21). Once the proper position was determined the output of the anemometer was recorded from the oscilloscope and the average maximum was taken as the velocity maximum. These data nondimensionalized with Γ_S/r_0 are shown in Figure 22. It is not surprising to see that the velocity maximum increases with the swirl ratio. The analytical model of Kuo predicts this behavior. However, his solution indicates a linear relation between the ambient circulation and the maximum tangential velocity while the data suggest a higher order correspondence.

With these two data sets the value of c can be determined. The asterisks in Figure 23 show the results of the computations. It turns out that c is not a constant but in fact is a function of the swirl ratio. The fact that c decreases with increasing swirl implies that for a given pressure drop the vortex produces a higher tangential velocity at higher values of swirl ratio than at lower values of swirl ratio. As will be shown later this tendency is maintained even in the multiple vortex stage.

Another estimate of c which also is not constant but depends upon the swirl ratio can be obtained by approximating the velocity profiles. Let the horizontal velocity components be given by

$$\begin{aligned} u &= \frac{u_s r_s}{r} && \text{for} \quad r_0 \le r \le r_s \\ &= \frac{u_s r_s}{r_0^2}\, r && \text{for} \quad 0 \le r \le r_0 \\ v &= \frac{v_s r_s}{r} && \text{for } r_c \le r \le r_s \quad \text{and} \\ &= \frac{v_s r_s}{r_c^2}\, r && \text{for } 0 \le r \le r_c \end{aligned} \tag{19}$$

where u and v are the radial and tangential velocities, and u_s and v_s are the respective values at the screen. The radial equation of motion is

$$u \frac{\partial u}{\partial r} - \frac{v^2}{r} = -\frac{1}{\rho} \frac{\partial p}{\partial r}. \tag{20}$$

In nondimensional form Eqn. (20) becomes

$$\frac{\partial \hat{p}}{\partial \hat{r}} = -\frac{\partial \hat{u}^2}{\partial \hat{r}} + \frac{2v_s^2}{u_s{}^2} \frac{\hat{v}^2}{\hat{r}} \tag{21}$$

where $\hat{u} = \frac{u}{u_s}$, $\hat{v} = \frac{v}{v_s}$, $\hat{r} = \frac{r}{r_s}$, and $\hat{p} = \frac{p}{\frac{1}{2}\rho u_s^2}$.

Using Eqn. (19) with Eqn. (21) and integrating from the axis to the screen gives the magnitude of the pressure deficit as

$$\Delta p = 4a^2 S^2 (\frac{2\, r_s^2}{r_c^2} - 1) - 1.$$

Now c can be determined as

$$c = \frac{\Delta p}{\rho\, v_{max}^2} = \frac{1}{2} \frac{u_s^2}{v_s^2} \frac{\Delta \hat{p}}{v_{max}^2} \qquad \text{or}$$

$$c = 1 - \frac{r_c^2}{2r_s^2}\left(1 + \frac{1}{4a^2S^2}\right). \tag{22}$$

The core radius data of the previous chapter can be used to determine r_c which is predominantly a function of S. The measured values of c along with a plot of the above equation is shown in Figure 23. Eqn. (22) is almost linear in the range of swirl ratios used. The agreement with the data appears good only for large values of the swirl ratio. Elsewhere, the measured values are much larger. This suggests that the estimated pressure drop is smaller than actually observed and/or the estimated maximum velocity is larger than that observed for small swirl ratios. In an effort to clarify this, the pressure profiles measured in the apparatus were compared with those obtained from Eqn. (21). Solving for the pressure drop gives

$$\begin{aligned}
\hat{p}(\hat{r}) - \hat{p}(1) &= \left(1 - \frac{1}{\hat{r}^2}\right)(1 + 4a^2S^2) && \text{for } \hat{r}_0 \le \hat{r} \le 1 \\
&= \left(1 - \frac{\hat{r}^2}{\hat{r}_0^4}\right) + 4a^2S^2\left(1 - \frac{1}{\hat{r}^2}\right) && \text{for } \hat{r}_c \le \hat{r} \le \hat{r}_0 \\
&= \left(1 - \frac{\hat{r}^2}{\hat{r}_0^4}\right) + 4a^2S^2\left(1 + \frac{\hat{r}^2}{\hat{r}_c^4} - \frac{2}{\hat{r}_c^2}\right) && \text{for } 0 \le \hat{r} \le \hat{r}_c
\end{aligned} \tag{23}$$

where $\hat{r}_c = r_c/r_s$, and $\hat{r}_0 = r_0/r_s$.

The Burgers-Rott pressure profile is also to be compared with the data. This solution at z = 0 in dimensional form is

$$p(r) - p(r_s) = \rho \int_{r_s}^{r} \frac{v^2}{r}\,dr + \frac{1}{2}\rho a^2 (r_s^2 - r^2) \tag{24}$$

where $v = \frac{v_s r_s}{r} [1 - \exp(-\frac{ar^2}{2\nu})]$ and $a = \frac{u_s}{r_s}$. Because the flow is turbulent it would not be appropriate to choose the molecular value of viscosity for ν. Instead its value was calculated so that the theoretical core radius would be the same as the observed value. This is given by

$$\nu = \frac{u_s}{2r_s} \left(\frac{r_c}{1.12}\right)^2 .$$

It is a shortcoming of the Burgers-Rott solution that the core size is independent of the ambient swirl. Generally, the values from the above equation were between one and two orders of magnitude larger than the molecular value.

The radial pressure profiles were measured along the floor of the chamber through ports which were spaced at intervals of one every cm up to 40 cm, then one every 2.5 cm up to 100 cm and finally one every 3 cm out to the screen at 121 cm. The transducer output signal was time averaged with a first order filter. Typically, a time constant of 50 sec was required near the core and sometimes even 100 sec was used for highly unsteady vortices. In the outer region a 10 sec time constant was sufficient to do the filtering. The observed pressure fluctuations were about 10% of the mean value.

Figure 24 shows the pressure profiles for $S = 0.25$, $a = 0.472$, $N = 5.4 \times 10^4$, $Q = 0.413$ m^3 s^{-1}, and $r_0/r_s = 1/2$. The asterisks are the actual measurements while the solid line is the Burgers-Rott solution and the dashed line is Eqn.

(23). The data show only a slight pressure gradient in the region greater than about $\hat{r}$ = .19 and are in good agreement with Eqn. (23). The Burgers-Rott solution actually shows an outwardly directed pressure gradient force in the region $\hat{r}$ >.22. This is due to the fact that the integral in Eqn. (24) is small for large r and small swirl, and because the radial flow is decelerating inward (the u solution is u = −ar). Figure 25 shows the pressure profiles for S = 0.80. Here the central pressure deficit has increased significantly and the pressure gradient in the outer region is more obvious. The Burgers-Rott solution still exhibits an outwardly directed pressure gradient for $\hat{r}$ >.73. Inward from there the tangential velocity has increased to such a magnitude that the gradient is positive. Eqn. (23) describes the pressure fairly well except at small radii. Figure 26 is for S = 1.1 and on this run a vortex family of three now exists in the chamber. The central pressure is not quite as low as for S = 0.8 but the region of low pressure extends to a larger radius and even suggests the possibility of an off-axis pressure minimum. The Burgers-Rott solution continues to approximate the data poorly since the assumptions involved in its derivation are especially suspect in the case of multiple vortices. The discrepancy between Eqn. (23) and the data is larger now except in the far field. Finally, Figure 27 shows the profiles for S = 2.0 at which four vortices are now revolving in the apparatus. Here the pressure falls off much more rapidly at first and the pressure minimum is much lower than before occurring at $\hat{r} = .18$. It must be pointed out that the multiple vortices were revolving at a radius of about $\hat{r} = 0.25$ but because the pressure between the vortices is relatively high and the pressure transducer output was time averaged the profile did not exhibit a pressure minimum at $\hat{r} = .25$. Instead, the average minimum was closer to the axis. The Burgers-Rott profiles consistently overestimated the pressure drop in the apparatus, particularly near the core. This is due in part to the fact that the model overestimates the magnitude of the tangential velocity at small radii allowing v^2/r to be large. Eqn. (23) agrees well with the data in the outer regions where the assumptions used in its derivation are particularly accurate. At smaller radii, Eqn. (23) fails to describe the data because it predicts that the pressure drop has only a weak dependence on swirl ratio for the values used (recall $\hat{r}_c \propto S^{0.81}$). The fact that Eqn. (23) underestimates the pressure drop for small values of S contributes to Eqn. (22) underestimating the value of c.

The simultaneous measurement of the pressure and velocity of a satellite vortex was also completed in order to estimate the value of c for it. The tubing length from the pressure port to the transducer was minimized so as to eliminate any damping or time lag. Initially it was considered that the tubing might be eliminated altogether by mounting the transducer directly to the pressure port. However, it is believed that the vibrations of the table would be relayed to the transducer's membrane, thus generating signal noise. The tubing length finally used was about 25 cm. The frequency response of the transducer and 35 cm of tubing was very good up to about 20 Hz (Bruce Light, private communication). Since the frequency of the multiple vortices over the pressure port is of the order to 1 or 2 Hz the output of the transducer is believed to be accurate. Because the bottom of a satellite vortex tends to lead the upper portions the velocity probe was placed a little behind the pressure port. The output trace of the velocity and pressure is shown in Figure 28 for S = 1.98, a = 0.472, Q = 0.413 m^3 s^{-1}, and N = 5.4 x 10^4. It can be seen that the high velocity is associated with the very low pressure. The two effects in combination certainly work together to cause explosive effects accounting for the observed extensive damage from multiple vortices. The pulsing of these effects must also contribute to greater structural failure.

From these measurements the value of c was computed for comparison with Figure 23. Using the central pressure of the satellite vortex the value of c was 0.056. If the curve in Figure 23 is extended to the swirl ratio of 2.0 the value of c is computed to be 0.6, much larger than the observed value. Of course, the measured velocity is the sum of the rotational velocity plus the translational speed. If the translational speed is deducted from the measured velocity and c recomputed, the value becomes 0.074.

Using Figure 23 it might be possible to estimate the tornado intensity to be expected from a given storm. Since c is very dependent upon the swirl ratio it must first be necessary to estimate this parameter for a given mesocyclone. Barnes (1978) gives a technique for doing this from data typically measured by radar. His formula is $S = -\frac{r_0 \zeta_0}{(2hD_h)}$ where r_0 is the updraft radius inferred from the reflectivity pattern, ζ_0 is the vertical vorticity, h is the depth of the inflow, and D_h is the horizontal divergence (usually negative). Once the swirl ratio is known c can be determined from the graph. The air density as a function of pressure can easily be found by vertically averaging temperature over the lower portion of a nearby sounding. Finally, in order to calculate v_{max}, Δp must be estimated. This could also be done with the aid of a nearby temperature sounding. Kessler (1970) gives a formula for estimating the pressure drop by assuming an average hydrostatic balance in the tornado core as well as the environment and integrating vertically the difference between the temperature inside and outside the core. The outside temperature can be taken from the nearby sounding while the inside temperature can be determined by a dry adiabatic ascent up to the level of condensation and then moist adiabatically upward until the temperature equals that of the environment. Kessler's formula gives

$$\Delta p = P_1 [\exp\{\frac{gH}{RT^2} (T_1 - T_2)\} - 1]$$

where P_1 is the ambient pressure, g is the gravitational acceleration, H is the height where the pressure is horizontally uniform, R is the gas constant for air, T is an average overall pressure-weighted temperature, and T_1 and T_2 are the average pressure-weighted temperatures outside and inside the core, respectively.

Lilly (1969) proposes a similar technique for calculating Δp which additionally allows frictional heating in the lower layer and adiabatic ascent in the vortex core. Although downward flow is suspected to be present in many tornadoes and all the turbulent laboratory vortices, the additional heating from compression in his calculations tends to raise the temperature dramatically thereby causing large pressure falls. It is likely that frictional convergence in the boundary layer and turbulent mixing of the core air with the air in the adjacent walls tends to reduce the pressure drop resulting in his approach overestimating the pressure drop. Lilly's other approach, which allows only adiabatic ascent, does produce reasonable values of the core temperature and could be used to estimate v_{max}. Of course, in order to obtain the total velocity effect, the translational velocity due to the storm's motion would have to be added to the tangential velocity. Furthermore, the influence of surface roughness would be difficult to incorporate. A major effect of surface roughness is to reduce the local swirl ratio. Perhaps an effective swirl ratio could be used based on the ground roughness.

It turns out that the maximum velocity is related more strongly to the value of the swirl ratio than to the pressure deficit. For instance, Barnes (1978) calculated S for the storm he studied as S = 0.4. However, the uncertainty could be as high as ± 0.2. With this in mind and taking three different pressure deficits typical of significant tornadoes the value of v_{max} was calculated from $\Delta p = c \rho v_{max}^2$ where c is taken from Figure 23. These values are shown in Table VI. Clearly, changes in the swirl ratio affect the velocity much more than changes in the pressure drop. Once again the importance of the swirl ratio to the flow is reconfirmed.

Another experiment was designed to compare the maximum velocity of the SV with those occurring in the MV system where translation and rotation speeds combine. The volume flow rate was held constant in each case. The fan speed was adjusted to give a flow rate of $Q = 0.123 \ m^2 \ sec^{-1}$, and the aspect ratio was fixed at 0.48.

The most intense single vortex for this flow rate is obtained with a screen rotation rate of 0.06 rad sec^{-1} (0.57 rpm) corresponding to a swirl ratio S = 0.127. The visible vortex radius (also the radius of maximum tangential velocity) is 2.7 cm. The probe is placed at that radius and at a height of 2 cm. The peak velocity was measured at 3.12 m sec^{-1}.

To produce MV's the screen speed was increased to 0.63 rad sec^{-1} (6 rpm) while the flow rate was held constant. With the swirl ratio now at 3.18 (an increase by a factor of 25) four vortices formed, translating around the center of the simulator with a speed of 0.65 m sec^{-1}. The probe was repositioned to the radius of peak response (in this case 29.5 cm) and the response was also maximized by alignment with the streamlines present at the time of vortex passage. The velocity trace is shown in Figure 30. The peak velocity for the passage of the four suction vortices was 3.54 m s^{-1}, somewhat larger than for the SV. The velocity suddenly increased by an order of magnitude (between minimum and maximum) in less than half the time required for a complete cycle. Smoke tracers indicate that the direction of flow does not change appreciably from one vortex to the next at time of passage. The similarity of the velocity cycles in Figure 30. also indicates this to be the case.

A peculiar feature of the trace is the existence of a secondary maximum after 1.3 sec. This was observed to occur on a number of occasions and is believed to have resulted for the following reason. Although the MV generally rotated about the apparatus at a fixed radius there sometimes are slight departures. This means that for a stationary probe the vortex core will either be penetrated by the probe or miss it altogether. The former is responsible for the secondary maximum because if the probe passes through the core, it will experience two velocity maxima - one upon entering the core and another upon exiting. The second maximum is not as large as the first because of the probe's misalignment with the flow while exiting the core.

The peak velocity of 3.54 m sec^{-1} can be resolved into its components given the probe's orientation. When this is done and the translation speed is subtracted off of the tangential component, the suction vortices were found to have components as follows: radial velocity $u = -1.0$ m sec^{-1}, tangential velocity $v = 2.7$ m sec^{-1}, and vertical velocity $w = 0.4$ m sec^{-1}. These are only approximate, owing to the sensitivity of the components to the probe's proper orientation with the streamlines.

Laboratory observations also indicate that multiple vortices are highly concentrated near the ground and decay rapidly with height. Typically, the SV velocity reaches a maximum just above the boundary layer, and then diminishes gradually with height while the MV velocity decreases more rapidly with height. Since in the MV system the available energy must be distributed among more vortices, the peak velocities would be smaller for vortices of the same size unless the energy tends to concentrate in the lower portion.

When oil smoke was used for flow visualization in the MV configuration, a streamline pattern was revealed and is depicted in Figure 30. Air at the axis of the system spirals slowly downward and diverges near the surface. As the air approaches the annular ring around which the MV travel, it decelerates until a MV passes nearby. At that time the air is pulled into the vortex and spirals rapidly upward out of the system. As noted by Ward (1972) the convergence from the periphery of the apparatus concentrates vorticity into the annular region, creating a zone of large vorticity away from the center of rotation. This off-axis concentration of vorticity is important in the formation and maintenance of MV.

The above results indicate that wind speeds associated with MV systems are at least as high as in the SV for the same volume flow rate and updraft radius, although the ambient circulations were different. The MV system is thus likely to be far more destructive because of the abrupt accelerations and pressure changes due to passage of individual "suction vortices". In addition, the MV system sweeps out an area many times greater than the SV. Near the surface, at least, the tangential component is dominant with an inflow angle of about 70° at the radius of the MV. This combines with the translational speed to give peak velocities in a four-vortex system as large as the maximum in a single vortex system having the same flow rate and updraft radius (but much smaller circulation). The pressure drop is thus very sharp in these small vortices, and this may explain the presence of "suction spots" noted by Fujita (1971).

The mean flow velocity structure is also affected by the turbulence distribution. Generally, the eddies act to diffuse energy and momentum, but there are examples (Starr, 1968) of countergradient transports of these quantities. In the next chapter, profiles of the turbulent fluctuations are presented, and their influence on the mean flow discussed.

CHAPTER V

TURBULENCE MEASUREMENTS

The role of turbulence on vortex structure has long been debated. Often it was assumed that turbulence acted to diffuse energy and angular momentum, and that a balance existed between the advection of mean angular momentum and outward turbulent diffusion. Although the relative turbulence intensity has been measured for some laboratory vortices the direct measurement of the Reynolds stresses has not. It is important to investigate the effect of the turbulence on the mean flow. The values of the turbulent stresses have been inferred from the behavior of the mean flow with the use of the balance equation

$$\frac{\partial}{\partial r}\left(r^2\ \bar{\rho}\bar{u}\bar{v}\right) + \frac{\partial}{\partial z}\left(r^2\ \bar{\rho}\bar{w}\bar{v}\right) + \frac{\partial}{\partial r}\left(r^2\ \overline{\rho u'v'}\right) + \frac{\partial}{\partial z}\left(r^2\ \overline{\rho w'v'}\right) = 0.$$

Using this equation Lilly (1969) has examined Hoecker's (1960) data in an effort to explain the distribution of angular momentum in the Dallas tornado of 1957. Figures 31a and b show a plot of circulation versus radius for this tornado at heights of 150 ft. and 300 ft., respectively. Also, Figures 32a, b, c, and d show similar plots for the laboratory data of Jischke and Parang (1975). In all cases there are regions toward the axis where the circulation increases abruptly. This is noteworthy for two reasons: (1) angular momentum is not decreasing inward as might be expected because of the torque exerted by the surface on the flow, but actually increases in some regions, and (2) Rayleigh's (1916) criterion for inertial stability is violated if $\frac{\partial \Gamma}{\partial r} < 0$ (with Γ positive). Of course, the local persistence of this instability is feasible but one should expect to see some kind of an adjustment to the profile downstream. A similar peak also exists in Rotunno's (1979) steady state numerical solution for $S = 0.105$.

Calculating an angular momentum budget for the Dallas tornado, Lilly concludes that the turbulent stresses must be acting so as to add angular momentum to the mean flow near the core. This is analogous to the manner in which the upper atmospheric jet stream feeds from the angular momentum of the large eddies embedded in the prevailing westerlies (Starr, 1968). Thus, the turbulent eddies may have become a source rather than a sink for mean angular momentum locally.

Using data collected from dust devils, Sinclair _et al_. (unpublished manuscript) found slight eddy flux convergence occurring near the core in the lower layers but not extending upwards as Lilly found. Sinclair _et al_. are skeptical of Lilly's conclusions and state that the circulation values can be adjusted within Hoecker's error bounds to yield a distribution which is everywhere stable, viz. a Rankine-combined vortex.

This conjecture was the impetus for obtaining direct measurements of the Reynolds stresses. Using cross-wire probes and a signal correlator the turbulent fluctuations and cross-correlations were measured. In order to make a comparison of the mean flow with the data of Jischke and Parang (1975) the apparatus was operated so as to duplicate their case II (see Figure 32b and c), i.e., the volume flow rate was 1.33 $m^3\ s^{-1}$, the inflow angle was 5°, h = 30.5 cm and r_0 = 61 cm. This is equivalent to a swirl ratio of 0.09. Measurements of u, v, $\overline{u'v'}$, $\overline{u'^2}$, and $\overline{v'^2}$ were made at radii from 30 cm to 112 cm at a height of 1.4 cm. These measurements were made near the lower surface because the output signals can be more easily interpreted if the mean flow is quasi-horizontal (see Chapter II). At z = 1.4 cm the mean vertical velocity is very small. The associated output error is approximately given by $\frac{\bar{w}^2}{\bar{v}_h^2}$ where $\bar{w}$ is the mean vertical velocity and $\bar{v}_h$ is the mean horizontal velocity. From Jischke and Parang's data this error would be about 3% at r = 30 cm where $\bar{w}$ would have the largest value in the measurement region.

The circulation from the tangential profile is given in Figure 33. Although the profile is unlike Figure 32b and c (not surprising since the profiles are at different heights) the distribution does show a definite peak at r = 60 cm. It should be noted that Jischke and Parang's data show a distinct minimum in the circulation at that radius at higher levels. This suggests that vertical fluxes may be carrying angular momentum away from this region and into a lower level. The vertical flux will be shown later.

The distribution of $\overline{u'^2}$ is given in Figure 34. The values are large in the outer regions. This is probably due in part to the proximity of the rotating screen. The turbulence produced there does damp out as the flow accelerates inward under a favorable pressure gradient, i.e., radial stretching reduces the eddy size to a scale where viscous dissipation can become effective. Once the air flows past the convection radius of 60 cm the radial flow decelerates and the turbulence level starts to increase until about 45 cm. Then the radial turbulent kinetic energy begins to decrease as the flow accelerates toward the core. Fluctuations in the anemometer output indicate that errors in the measurements may be as high as $\pm$ 9 x 10^{-4} m^2 s^{-2}. Figure 35 shows the profile of $\overline{v'^2}$. Again the values are high near the screen and decrease inward thereafter. As the core is approached dramatic increases take place. Since $\overline{v'^2}$ is a measure of the turbulent kinetic energy associated with the tangential flow it would not be surprising to see the circulation respond to variations of $\overline{v'^2}$. Comparing Figure 35 with Figure 33, it is interesting to notice that $\overline{v'^2}$ decreases inward and reaches a minimum near 81 cm while the circulation is increasing and reaches a local maximum just immediately downstream of 81 cm. Then a rise in $\overline{v'^2}$ occurs as Γ decreases again. Another minimum in $\overline{v'^2}$ occurs at about 66 cm while a second peak in Γ takes place just downstream at about 61 cm. Next $\overline{v'^2}$ begins to increase until 46 cm while Γ drops until 41 cm. Finally, the value of $\overline{v'^2}$ drops then rises as Γ does just the opposite lagging about 5 cm downstream. Errors in these values may be as high as $\pm$ 3 x 10^{-4} m^2 s^{-2}. Figure 36 shows the distribution of $\overline{u'v'}$. Once more there are high values near the screen with a sudden decrease inward. At 65 cm an increase begins, reaching a peak at about 45 cm with a decline thereafter. The lack of a large time constant on the RMS voltmeter gives results with an uncertainty of about $\pm$ 5 x 10^{-4} m^2 s^{-2} for these values.

With this information we can now evaluate the third term in Eqn. (34) to see how it affects the mean flow. Figure 37 is a plot of this term using the turbulence data. Positive values indicate turbulent flux divergence which results in momentum flux convergence in the mean flow. Negative values indicate that the mean flow is losing its momentum to the eddies. The plot clearly shows that the turbulence is adding momentum to the mean flow at 60 cm and 76 cm, the positions of the two circulation peaks. However, because the measurement uncertainty is about $\pm$ 2.2 x 10^{-3} m^2 s^{-2} the minor peak may not be significant. This data supports the idea that turbulent energy is feeding the mean flow locally to account for higher than expected tangential velocities. It is unfortunate that the measurements could not be extended inward to see if this same process is taking place in the immediate vicinity of the core.

The effect of the vertical fluxes could not be determined so readily. The x-wire probes must be aligned so that the mean flow vector lies in the plane formed by the wires, and makes a 45° angle with the wires. The probe then measures only the velocities in this plane. This is not a problem in a two-dimensional mean flow (with three-dimensional turbulence, of course). However, if the mean flow is three-dimensional, the velocity components in the probe's reference frame may not be converted to the laboratory reference frame, because the velocity normal to the probe plane is not available. Consequently, the quantity $\overline{v'w'}$ could not be measured directly. Instead, the quantity $\overline{v_h'w'}$ could be determined where $v_h' = \sqrt{v'^2 + u'^2}$. Although this is not the quantity of interest it is close for high local swirl values and some qualitative conclusions can be drawn. The design of the probe support prevents the sensor from being placed closer than 2 cm from the surface, so values of $\overline{v_h'w'}$ were measured at 2 cm and 3 cm to approximate the flux at z = 2.5 cm. At a radius of 60 cm these quantities were measured as -1.1×10^{-4} m^2 s^{-2} and -1.6×10^{-4} m^2 s^{-2}, respectively. Thus the vertical flux was -1.6×10^{-3} m^3 s^{-2}. The sign indicates that angular momentum is being vertically transported away from the mean flow but the magnitude shows that this effect is smaller than the radial fluxes. One can conclude that mean flow momentum is being carried upward out of this region by the eddies but the radial flux more than compensates. This results in a net convergence of mean flow momentum in this region of the vortex.

Although it is difficult to draw general conclusions from a single experiment it appears that the eddies do add angular momentum to the flow in some regions. This results in a circulation profile which is inertially unstable. The growing instability must adjust the profile, but, because the process takes a finite amount of time, the adjustment is completed downstream of the point of instability. Thus the behavior of the eddies can maintain the unstable profile.

CHAPTER VI

SUMMARY, CONCLUSIONS, AND RECOMMENDATIONS FOR FUTURE RESEARCH

In Chapter II the parameters governing the unsteady flows in the apparatus were derived. These are the swirl ratio, the aspect ratio, the nondimensionalized convection radius, and the Reynolds number. Davies-Jones (1973) showed that the laboratory flows are dynamically and geometrically similar to actual tornado flows by estimating the parameter values in nature. Although the Reynolds number of the laboratory flow does not match the atmospheric value, several experiments indicated that the behavior of the laboratory flow was largely independent of the Reynolds number for the values examined. This result is further verified in Rotunno's (1977) numerical simulation of the apparatus. With the governing parameters clearly identified, future experiments can be more realistic.

Several machine improvements proved to be beneficial. Centering the updraft inlet made the pressure distribution across the honeycomb more axisymmetric and reduced vortex wander that previously occurred at high volume flow rates. Exhausting back into the laboratory decoupled outside influences from the behavior of the vortex. As a result overall vortex wander was decreased significantly. Operating the exhaust fan with direct current increased its efficiency and its lifespan.

Chapter III examined the sensitivity of the core radius to the flow parameters, including surface roughness. With more than 400 core radius data points taken it is clear that the core radius is governed predominantly by the swirl ratio. Of least importance is the Reynolds number. In fact, as an approximation the core radius can be estimated from the swirl ratio alone as

$$\frac{r_c}{r_0} = 0.42\ S^{0.81}$$

over a smooth surface.

When a rough surface was introduced the flow behavior was altered considerably. Initially several kinds of surfaces were experimented with. One of these was constructed in accordance with Lettau's formula for estimating the roughness length using a description of the surface elements. However, with this surface in place the turbulent core was above the standard measurement height. The technique finally adopted was to distribute the roughness elements uniformly and scale their height with the core radius. The influence of the surface roughness alone is to reduce the core radius. Because of the reduced centrifugal forces in the boundary layer air parcels can penetrate closer to the axis establishing a smaller core radius.

The rough surface also delayed multiple vortex transition. Progressively larger swirl ratios were required in order to initiate the transition to a larger number of vortices. The rough surface also increases the level of turbulence as well as the diffusion of momentum and vorticity. Thus, more swirl must be added in order for the transition to multiple vortices to take place. The implication is that a tornado on the verge of multiple vortex transition may be triggered into that mode if it travels over a smoother terrain.

The pressure and velocity measurements of Chapter IV show that these two quantities are not simply related. The maximum tangential velocity increases with increasing swirl ratio. The behavior of the pressure profile is as follows. For a single vortex the central pressure drops as the swirl ratio increases. When multiple vortex transition occurs the central pressure rises somewhat and the pressure minimum is displaced off-axis. The time-averaged pressure minimum, however, is not at the same radius as the multiple vortices. This is because the higher pressure between the vortices is large enough to compensate for the instantaneous pressure minimum that exists during the vortex passage. Simultaneous measurement of the total velocity and pressure show that the maximum of the former occurs during the minimum of the latter. This certainly results in the explosive effects of the multiple vortex mode. A further increase in the swirl ratio causes the pressure minimum to intensify and move farther away from the axis.

The maximum velocity in a multiple vortex system was measured to be slightly higher than for a single vortex at the same volume flow rate for the one case examined. Laboratory observations indicate that the multiple vortices are most concentrated near the surface and rapidly become diffuse with height. From direct measurement the region of maximum velocity for a single or multiple vortex system appears to be at the edge of the visible core and at a height where the lower laminar core transforms into a turbulent one. The relation of the maximum tangential velocity to the central pressure drop is not a constant as some analytical models suggest but depends on the swirl ratio. The implication is that vortices embedded in a higher ambient swirl are more efficient in using the central pressure drop to drive the tangential flow.

The influence of the turbulence on the mean flow was investigated in Chapter V. Although the entire flow field could not be mapped, some conclusions can be drawn about certain regions of the flow. The mean circulation profile showed regions where angular momentum was increasing inward locally. This is significant not only because one would expect the boundary layer to be a sink for angular momentum but also because such a profile is inertially unstable. The mean flow equation points to the Reynolds stress as a possible influence. Direct measurement of these stresses showed some interesting behavior. The profile of $\overline{v'^2}$, which is related to the turbulent energy of the tangential velocity fluctuations, showed a local minimum (maximum) immediately upstream of regions where the mean circulation showed a local maximum (minimum). The profile of $\overline{u'v'}$ indicated that in the regions where the circulation peaked, the eddies were adding angular momentum to the flow. Measurement of the vertical eddy flux was less conclusive because of the measurement constraints. However, the indications are that the vertical eddy flux extracted energy from the mean flow near the circulation peak, but the magnitude of this flux was smaller than the radial eddy flux at the same height. The eddies appear to pump angular momentum into the mean flow at the region of the circulation peaks and sustain the locally unstable profile. This suggests that the resulting instability must adjust the unstable profile downstream to a stable one.

There is still much work to be done with the tornado simulator. In order to make data collection easier and to insure greater accuracy several additional modifications to the apparatus should be incorporated. The lower surface of the apparatus has many holes drilled in it for measuring instruments. When these holes are not in use they are generally covered with duct tape. So much tape is present, in fact, that the table could be considered rough in some locations.

Replacing the lower surface with a new one containing an instrument slot would reduce the roughness and allow more versatile data collection. The slot should extend radially inward a little past the geometric center of the apparatus and have railing underneath to support probes (Snow, private communication). Also, the present table does not make continuous contact with the screen allowing some air to enter without receiving swirl. The gap varies with table height. Adding horizontal panels underneath the table that could be adjusted radially could tighten the fit and would greatly reduce this problem. The present table is also slightly warped making the inflow depth azimuthally variable. A new table should be supported by a threaded shaft so that its height can be controlled more continuously.

The screen rotation rate is very unsteady because the ring is also warped and the rope drive slips. A new ring assembly would greatly reduce the drag. A more direct drive could be implemented by using a roller attached to the motor and in contact with the ring. Another roller on the opposite side of the ring would be necessary to adjust the grip on the ring sufficiently. If the mass of the ring were increased its inertia would enhance a more uniform rotation rate. Of course, a new suspension would have to be made.

The electrostatic precipitator used to filter out the smoke is not very efficient. Many of the charged oil droplets pass through the electrified grid without being collected. This is due to the high volume flow rates used and the large concentration of smoke in the flow. A new filter could easily be made to be more effective simply by increasing its length and intensifying the electric field. In this manner each droplet would receive a greater charge and have more time to be collected by the oppositely-charged grid.

In future experiments the role of the turbulence and its influence on the mean flow should be investigated further. Because of equipment limitations the measurement of the turbulence field could only be accomplished in the outer regions. Evaluating these quantities close to the core will be most difficult but is needed to determine the dominant forces in balance there. In fact, a complete angular momentum balance of the entire flow field would be very informative on how the flow is maintained. It would also be of great interest to determine if the eddies supply angular momentum to the mean flow for a variety of flow configurations (swirl ratios) and at many heights and radii.

Measurements should also be made of v_{max} as a function of height for low swirl ratio flows. Rotunno's (1979) model indicates that for low swirl ratios the boundary layer separates close to the axis inducing a recirculating flow. This prevents incoming air from reaching a small radius near the surface. Instead, the air is diverted upward and approaches the axis aloft. If the swirl ratio is increased, the thickness of the recirculating cell decreases and the region of v_{max} descends. It is suggested that this behavior may account for the observation that the tornado vortex first forms at midlevels, then propagates downward. The height of v_{max} should be measured in the apparatus to verify this process for small values of swirl ratio increasing from zero.

The effects of surface roughness are still not completely known. Although it was established that the core size decreases with increasing surface drag, the roughness length z_0 should be varied over a large range to produce an empirical formula for the core radius as a function of z_0. In addition, profiles of pressure and velocity should be measured to determine how the roughness affects the angular momentum balance and resolve the conflicting results of some numerical models. The relation of Δp to v_{max} could be determined for a rough surface in the manner used in Chapter IV for a smooth surface.

Finally, there is much to be learned about vortex breakdown phenomena. It appears that the vertical velocity and axial pressure gradient play a major role in this event. Measurements of the pressure profile and vertical velocity at the surface as well as at the honeycomb could be used with the vertical equation of motion to predict the occurrence and location of the breakdown bubble and then compared with the observations. Repetition of the breakdown experiment over a rough surface may offer an opportunity to explain the observation that the presence of an extremely rough lower surface tends to raise the axial stagnation point off the surface. The effect is similar to decreasing the swirl ratio.

BIBLIOGRAPHY

Barnes, S. L., 1968: On the source of thunderstorm rotation. NOAA Tech. Memo. ERL NSSL-38, Nat. Severe Storms Lab., Norman, Oklahoma, 28 pp.

________, 1978: Oklahoma thunderstorms on 29-30 April 1970. Part II: Radar observed merger of twin hook echoes. Mon. Wea. Rev., 106, 685-696.

Bearman, P. W., 1970: Corrections for the effect of ambient temperature drift on hot-wire measurements in incompressible flow. Disa Information, 11, 25-30.

Blechman, J. B., 1975: The Wisconsin tornado event of April 21, 1974: Observations and theory of secondary vortices. Ninth Conf. on Severe Local Storms, Norman, Oklahoma. Amer. Meteor. Soc., 344-349.

Bode, L., L. M. Leslie, and R. K. Smith, 1975: A numerical study of boundary effects on concentrated vortices with application to tornadoes and waterspouts. Quart. J. R. Met. Soc., 101, 313-324.

Brown, R. A. (ed.), 1976: The Union City, Oklahoma Tornado of 24 May 1973, NOAA Tech. Memo, ERL NSSL-80, Norman, Okla., Nat. Severe Storms Lab., 167-175.

________, and L. R. Lemon, 1976: Evolution of the Doppler radar tornadic vortex signature in the Union City storm. Chapter 15, The Union City, Oklahoma Tornado of 24 May 1973, R. A. Brown, Editor. NOAA Tech. Memo. ERL NSSL-80, Norman, Oklahoma, Nat. Severe Storms Lab., 167-175.

Brunn, H. H., 1975: Interpretation of x-hot-wire signals. Disa Information, 18, 5-10.

Burgers, J. M., 1948: A mathematical model illustrating the theory of turbulence. Adv. Appl. Mech., 1, 197-199.

Burggraf, O. R., and M. R. Foster, 1977: Continuation on breakdown in tornado-like vortices. J. Fluid Mech., 80, 685-703.

Clare, P. R., 1976: Observational studies of hail and multiple vortex features associated with the 3 April tornado outbreak. M.S. Thesis, Purdue University, 175 pp.

Davies-Jones, R. P., 1973: The dependence of core radius on swirl ratio in a tornado simulator. J. Atmos. Sci., 30, 1427-1430.

________, 1976: Laboratory simulations of tornadoes. A Symposium on Tornadoes: Assessment of Knowledge and Implications for Man, Amer. Meteor. Soc., Lubbock, Texas, June 22-24, 1976, 151-174.

________, and E. Kessler, 1974: Tornadoes, Chapter 16, Weather and Climate Modification, W. N. Hess, Editor. John Wiley and Sons, New York, 552-595.

________, and G. T. Vickers, 1971: Numerical simulation of convective vortices. NOAA Tech. Memo. ERL NSSL-57, Nat. Severe Storms Lab., Norman, Oklahoma, 27 pp.

Dessens, Jeans, 1972: Influence of ground roughness on tornadoes: A laboratory simulation. J. Appl. Met., 11, 72-75.

Fujita, T. T., 1971: Proposed mechanism of suction spots accompanied by tornadoes. Prep. 7th Conf. on Severe Local Storms, Kansas City, Missouri, Amer. Meteor. Soc., 208-213.

________, 1972: Tornado occurrences related to overshooting cloud-top heights as determined from ATS pictures. SMRP Research Paper 97, 32 pp.

________, 1973: Proposed mechanism of tornado formation from rotating thunderstorm. Prep. 8th Conf. on Severe Local Storms, Denver, Colorado, Amer. Meteor. Soc., 191-196.

________, D. L. Bradbury, and C. F. Van Thullenar, 1970: Palm Sunday tornadoes of April 11, 1965. Mon. Wea. Rev., 98, 29-69.

Golden, J. H., 1976: An assessment of windspeeds in tornadoes. Proc. of the Symposium on Tornadoes: Assessment of Knowledge and Implications for Man, Texas Tech. University, Lubbock, Texas, 5-42.

________, and B. J. Morgan, 1972: The NSSL-Notre Dame tornado intercept program, Spring 1972. Bull. Amer. Meteor. Soc., 53, 1178-1180.

Golden, J. H., and D. Purcell, 1977: Photogrammetric velocities for the Great Bend, Kansas, tornado of 30 August 1974: Accelerations and asymmetries. Mon. Wea. Rev., 105, 485-492.

Hansen, A. C., J. A. Peterka, and J. E. Cermak, 1975: Wind-tunnel measurements in the wake of a simple structure in a simulated atmospheric flow. NASA CR-2540, Colorado State University, 45 pp. [NTIS No. N75-20658/1GI].

Harlow, T. H., and L. R. Stein, 1974: Structural analysis of tornado-like vortices. J. Atmos. Sci., 31, 2081-2098.

Hinze, J. O., 1975: Turbulence. 2nd Ed., McGraw Hill, New York, 790 pp.

Hoecker, W. H., 1960: Wind speed and air flow patterns in the Dallas tornado of April 2, 1957. Mon. Wea. Rev., 88, 167-180.

________, 1961: Three-dimensional pressure pattern of the Dallas tornado and some resultant implications. Mon. Wea. Rev., 89, 533-542.

Hsu, C. T., and B. Fattahi, 1975: Tornado funnel formation from a tornado cyclone. Prep. 9th Conf. on Severe Local Storms, Norman, Oklahoma, Amer. Meteor. Soc., 358-363.

Jankov, Z. D., J. A. Shanahan, and M. P. White, 1976: Missile tests of quarter-scale reinforced concrete barriers. Proc. of the Symposium on Tornadoes: Assessment of Knowledge and Implications for Man, Texas Tech. University, Lubbock, Texas, 605-622.

Jischke, M. C., and M. Parang, 1974: Properties of simulated tornado-like vortices. J. Atmos. Sci., 31, 506-512.

________, and ________, 1975: Fluid dynamics of a tornadic-like vortex flow. Unpublished manuscript, Dept. of Aerospace, Mechanical and Nuclear Engineering, The University of Oklahoma, 198 pp.

Kaplan, M. L., and D. A. Paine, 1977: A multiscale synoptic-dynamical model of tornadogenesis. Prep. 10th Conf. on Severe Local Storms, Omaha, Nebraska, Amer. Met. Soc., 307-314.

Kessler, E., 1970: Tornadoes. Bull. Amer. Meteor. Soc., 51, 926-936.

Kuo, H. L., 1966: On the dynamics of convective atmospheric vortices. J. Atmos. Sci., 23, 25-42.

Lettau, H., 1969: Note on aerodynamic roughness-parameter estimation on the basis of roughness-element description. J. Appl. Meteor., 8, 828-832.

Lewellen, W.S., 1962: A solution for three-dimensional vortex flows with strong circulation. J. Fluid Mech., 14, 420-432.

________, 1976: Theoretical models of the tornado vortex. Proc. of the Symposium on Tornadoes: Assessment of Knowledge and Implications for Man, Texas Tech. University, Lubbock, Texas, 145-150.

Lilly, D. K., 1969: Tornado dynamics. NCAR manuscript 69-117, National Center for Atmospheric Research, Boulder, Colorado, 55 pp.

________, 1977: Sources of rotation and energy in the tornado. Proc. of the Symposium on Tornadoes: Assessment of Knowledge and Implications for Man, Texas Tech. University, Lubbock, Texas, 145-150.

Miller, R. C., 1972: Notes on analysis and severe-storm forecasting procedures of the Air Force Weather Central. U. S. Dept. of Commerce, AD-744 042.

Purcell, D., 1976: History of the Union City tornado. Chapter 11, The Union City, Oklahoma Tornado of 24 May 1973, R. A. Brown, Editor. NOAA Tech. Memo. ERL-NSSL-80, Norman, Oklahoma, Nat. Severe Storms Lab., 123-133.

Ray, P. S., 1976: Vorticity and divergence fields within tornadic storms from dual-Doppler observations. J. Appl. Meteor., 15, 879-890.

Rayleigh, J. W. S., 1916: On the dynamics of revolving fluids. Proc. Roy. Soc. London, A 93, 148-154.

Rott, N., 1958: On the viscous core of a line vortex. ZAMP, 9, 543-553.

Rotunno, R., 1977: Numerical simulation of a laboratory vortex. J. Atmos. Sci., 34, 1942-1956.

________, 1979: A study in tornado-like vortex dynamics. J. Atmos. Sci., 36, 140-155.

Schlesinger, R. C., 1977: A three-dimensional numerical model of an isolated large-diameter thunderstorm: results of an experiment with directional ambient wind shear. Prep. 10th Conf. on Severe Local Storms, Omaha, Nebraska, Amer. Met. Soc., 255-262.

Sinclair, P. C., V. H. Leverson, and R. T. Abbey, Jr., The vortex structure of dust devils, waterspouts, and tornadoes. Unpublished manuscript, 22 pp.

Snow, J. T., 1978: On inertial instability as related to the multiple-vortex phenomenon. J. Atmos. Sci., 35, 1660-1677.

Starr, V. P., 1968: Physics of Negative Viscosity Phenomenon. McGraw Hill, New York, 256 pp.

Sullivan, R. D., 1959: A two-cell vortex solution of the Navier-Stokes equations. J. Aerospace Sci., 26, 767-768.

Tennekes, H., and J. L. Lumley, 1974: A First Course in Turbulence. MIT Press, Cambridge, Massachusetts, 300 pp.

Vonnegut, B., 1960: Electrical theory of tornadoes. J. Geophy. Res., 65, 203-212.

Ward, N. B., 1972: The exploration of certain features of tornado dynamics using a laboratory model. J. Atmos. Sci., 29, 1194-1204.

Wilkins, E. M., 1964: The role of electrical phenomena associated with tornadoes. J. Geophy. Res., 69, 2435-2447.

________, 1968: Threshold conditions for vortex-stabilized electrical discharge in the atmosphere. J. Geophy. Res., 73, 2559-2568.

________, Y. Sasaki, R. L. Inman, and L. L. Terrell, 1974: Surface friction effects on thermal convection in a rotating fluid: A numerical simulation. Mon. Wea. Rev., 102, 4472-4486.

________, Y. K. Sasaki, and H. L. Johnson, 1975: Surface friction effects on thermal convection in a rotating fluid: A laboratory simulation. Mon. Wea. Rev., 103, 305-317.

________, Y. Sasaki, and R. H. Schauss, 1971: Vortex formation by successive thermals: A numerical simulation. Mon. Wea. Rev., 99, 577-592.

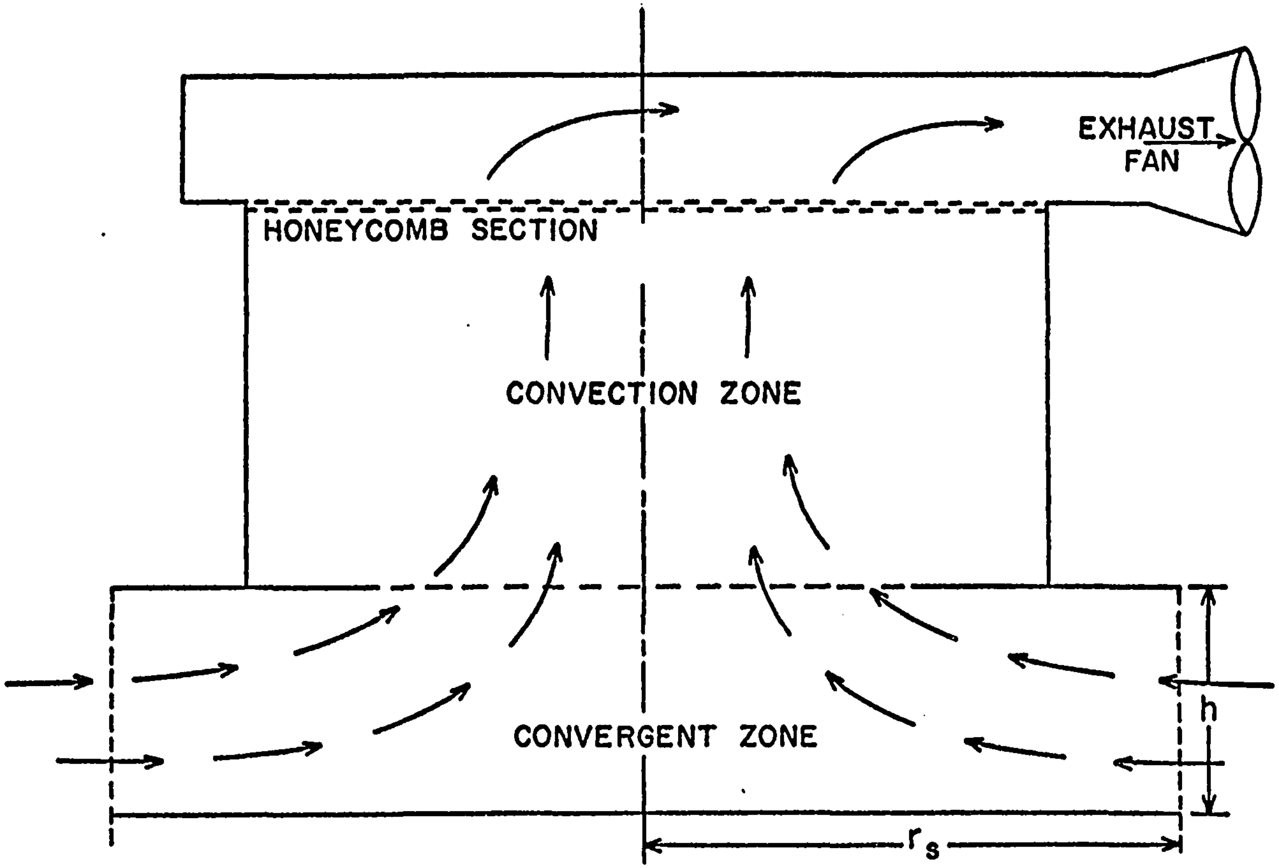

Figure 1. A schematic of Ward's original apparatus.

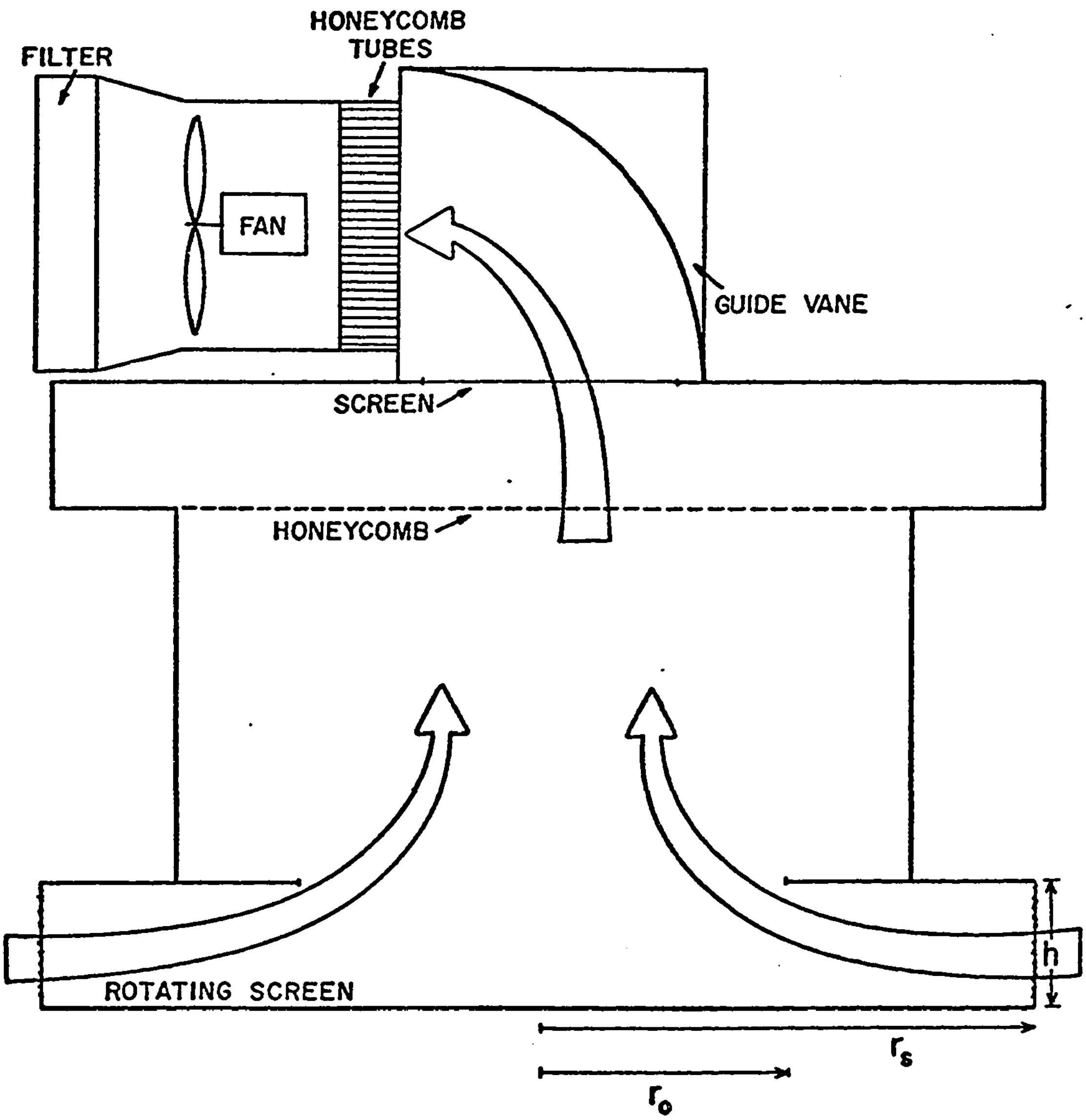

Figure 2. The modified tornado simulator.

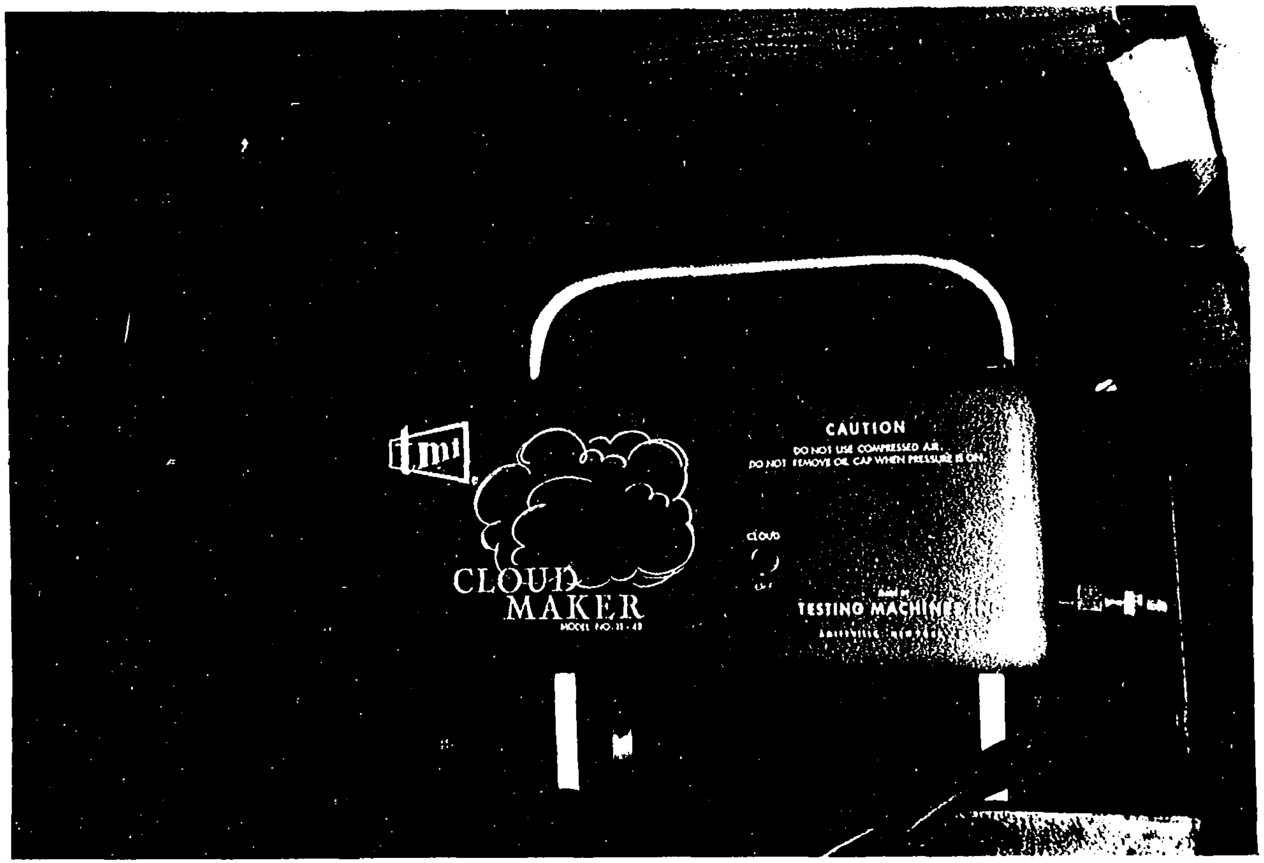

Figure 3. The smoke generator used for flow visualization.

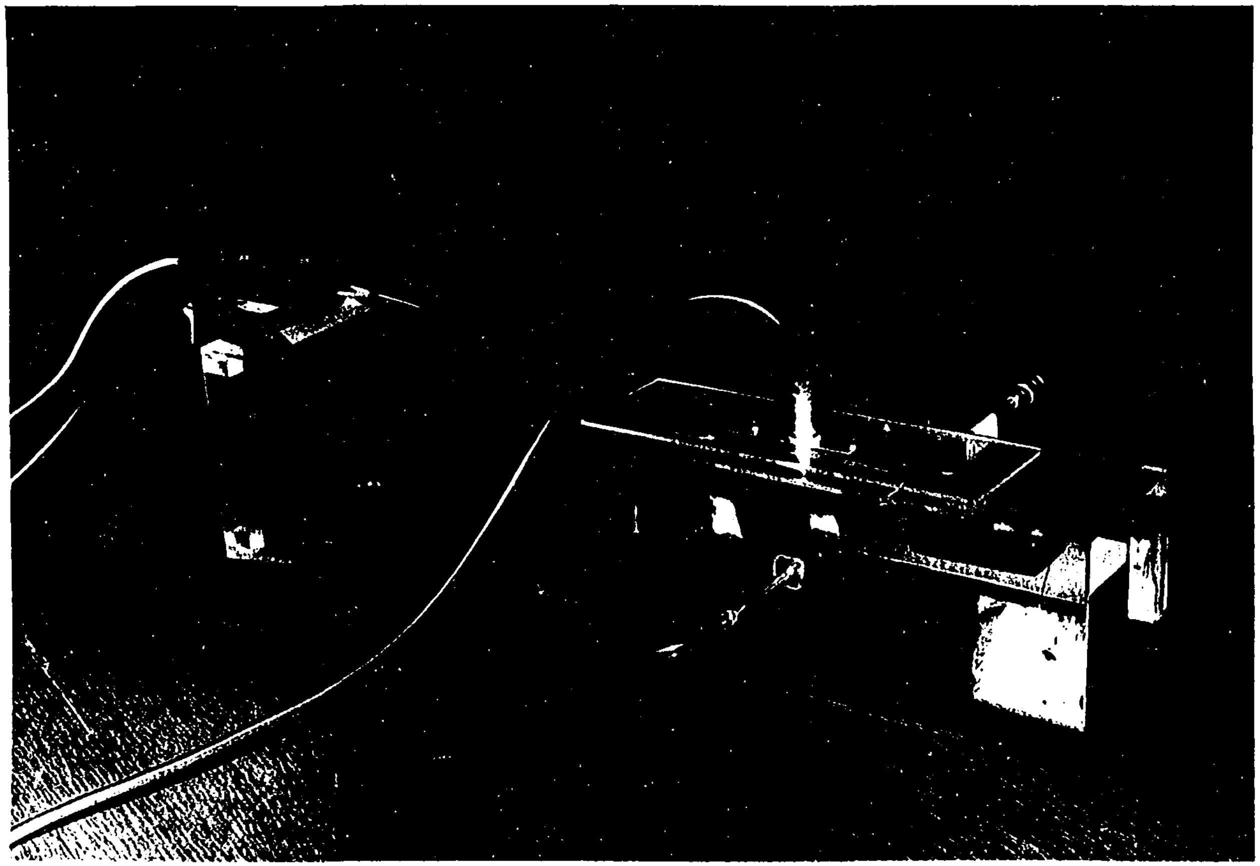

Figure 4. The calibration wind tunnel.

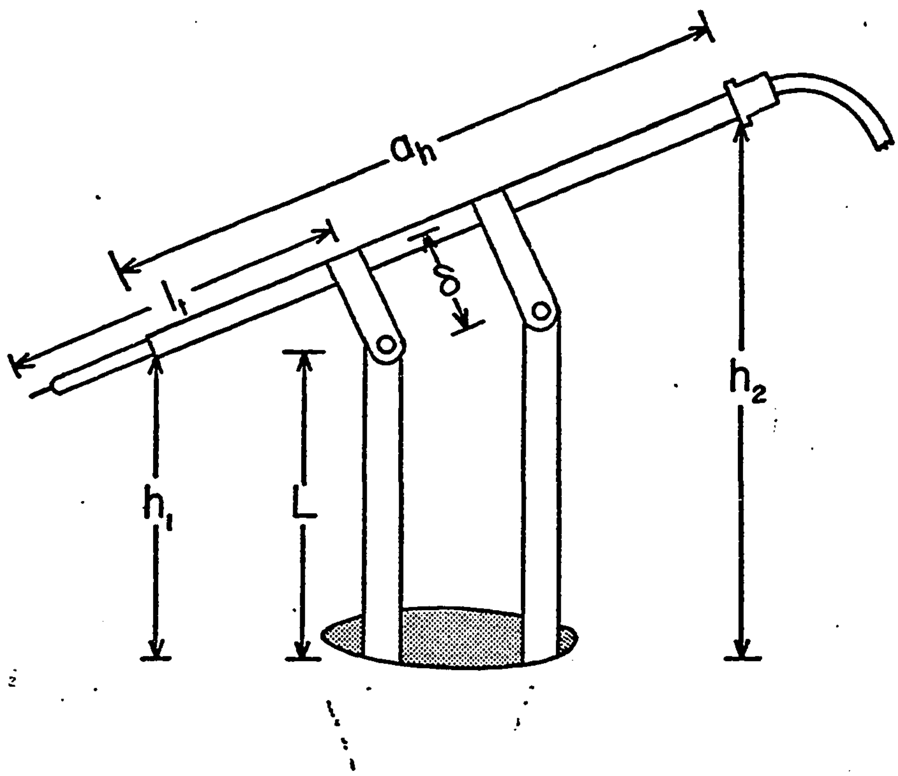

Figure 5. The velocity probe support.

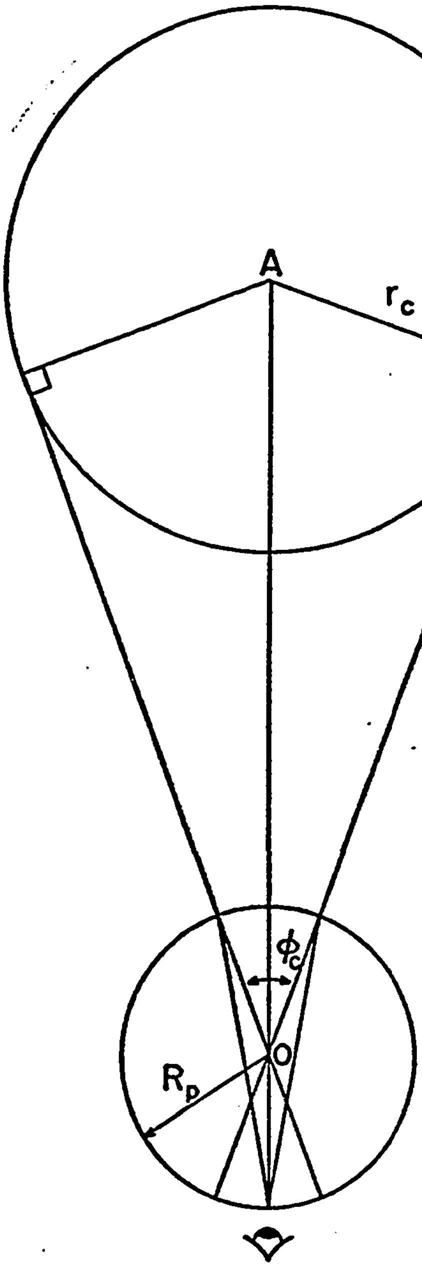

Figure 6. Protractor arrangement used for measuring the core radius.

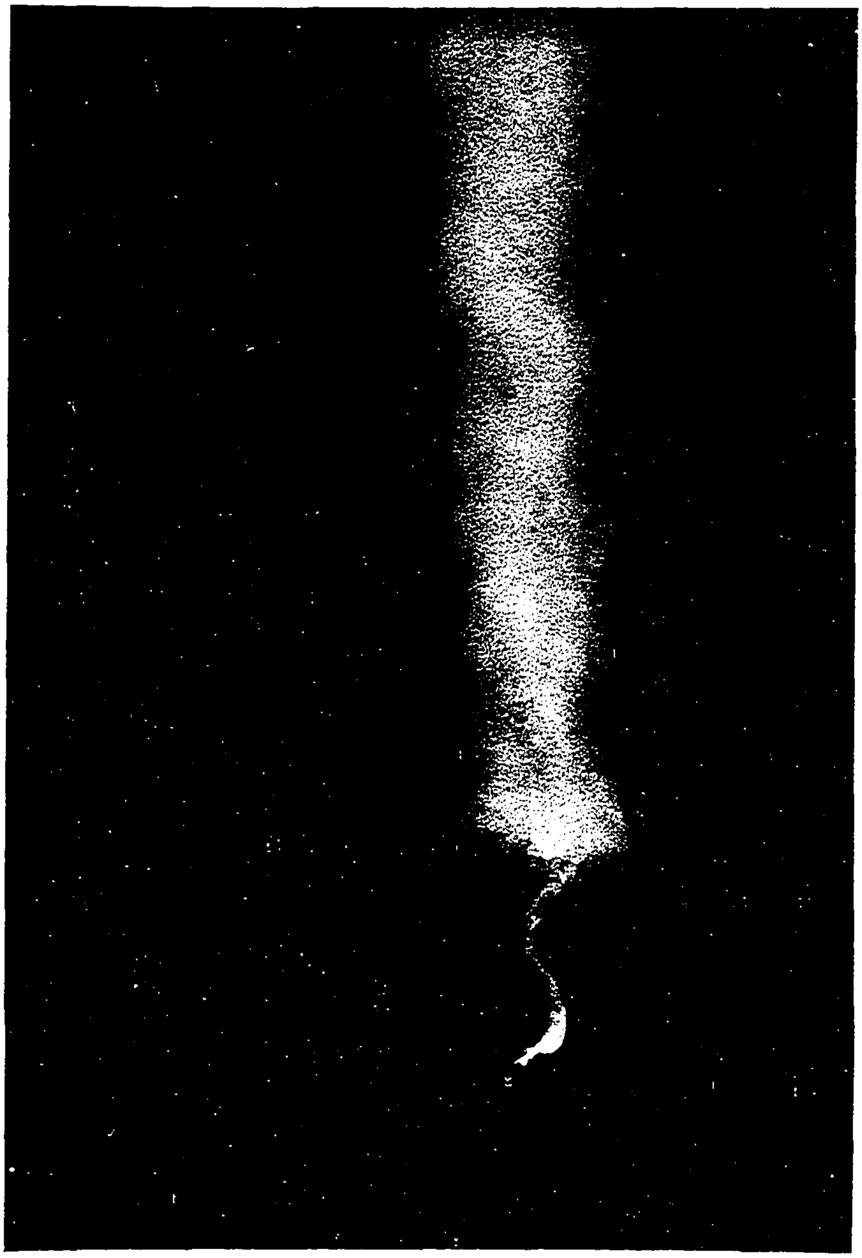

Figure 7. Vortex breakdown, typical of high aspect ratio and low swirl.

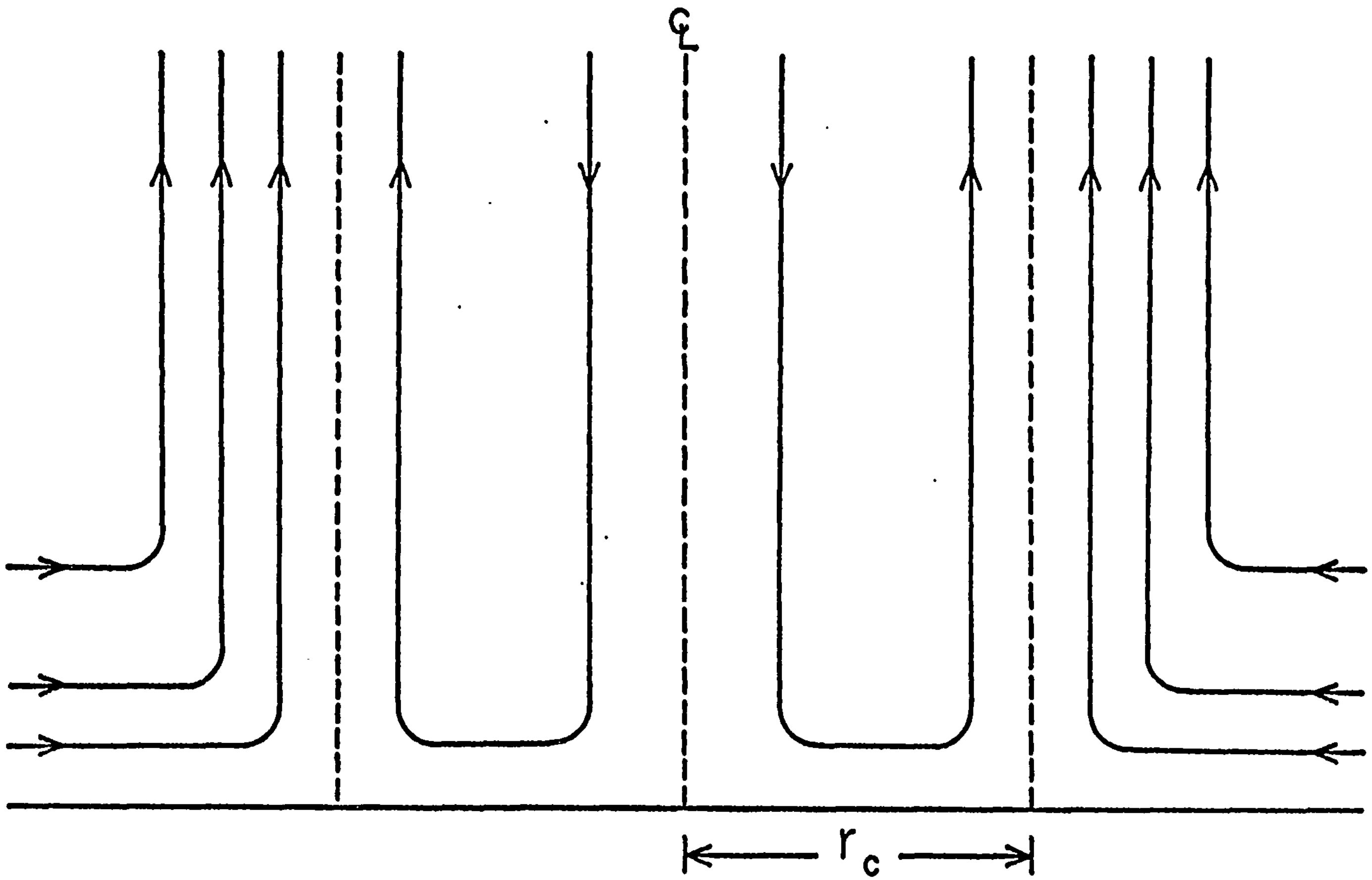

Figure 8. An idealized streamline pattern for a two-celled vortex.

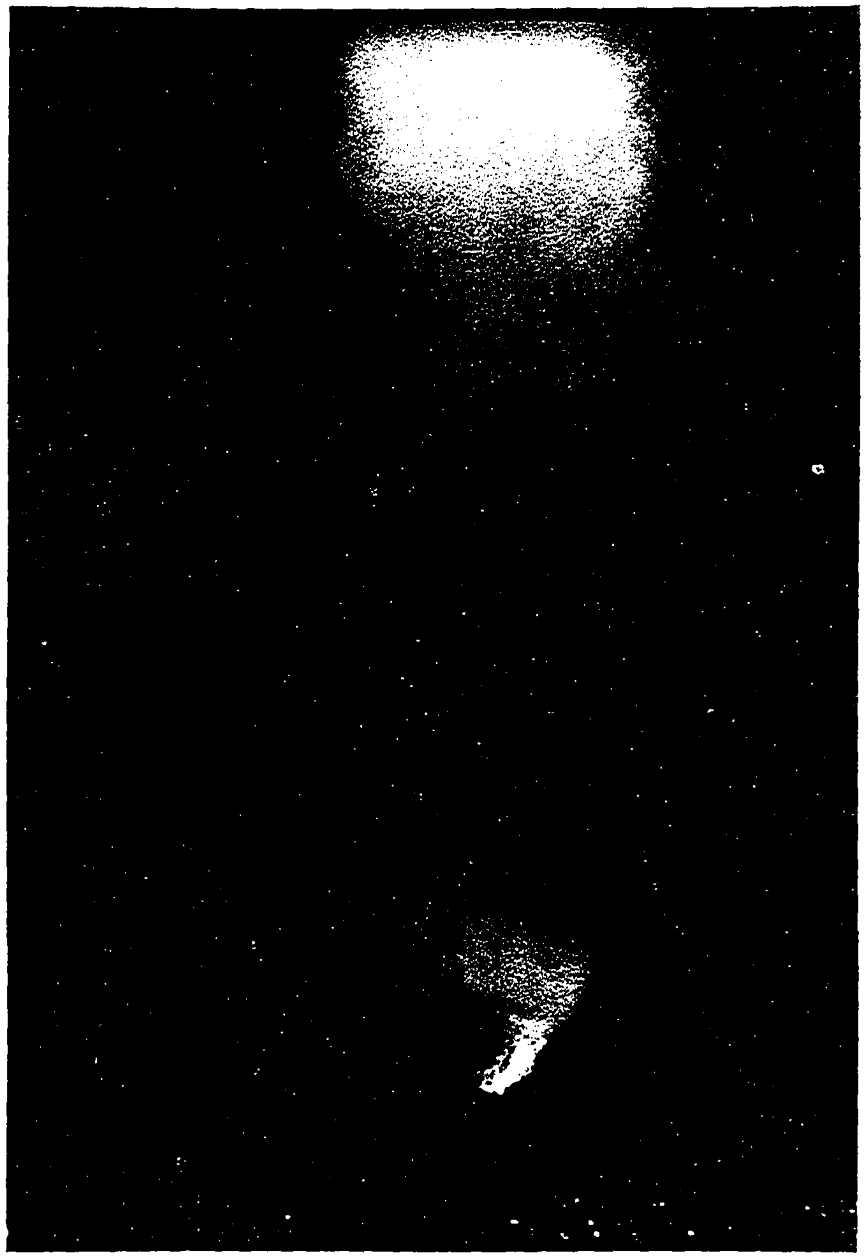

Figure 9. Photograph of a typical turbulent vortex produced in the tornado simulator.

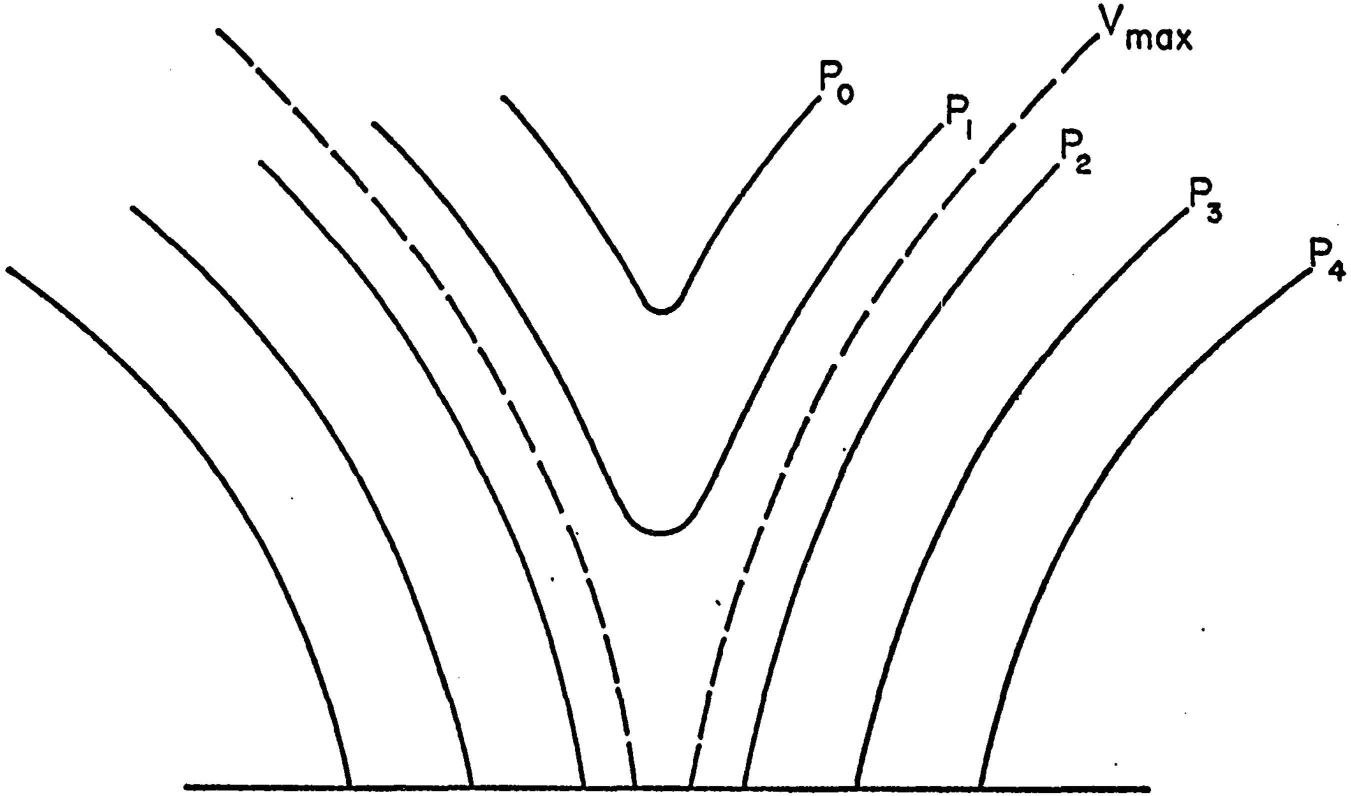

Figure 10. Pressure distribution for a tornado with dashed line indicating the position of a velocity maximum.

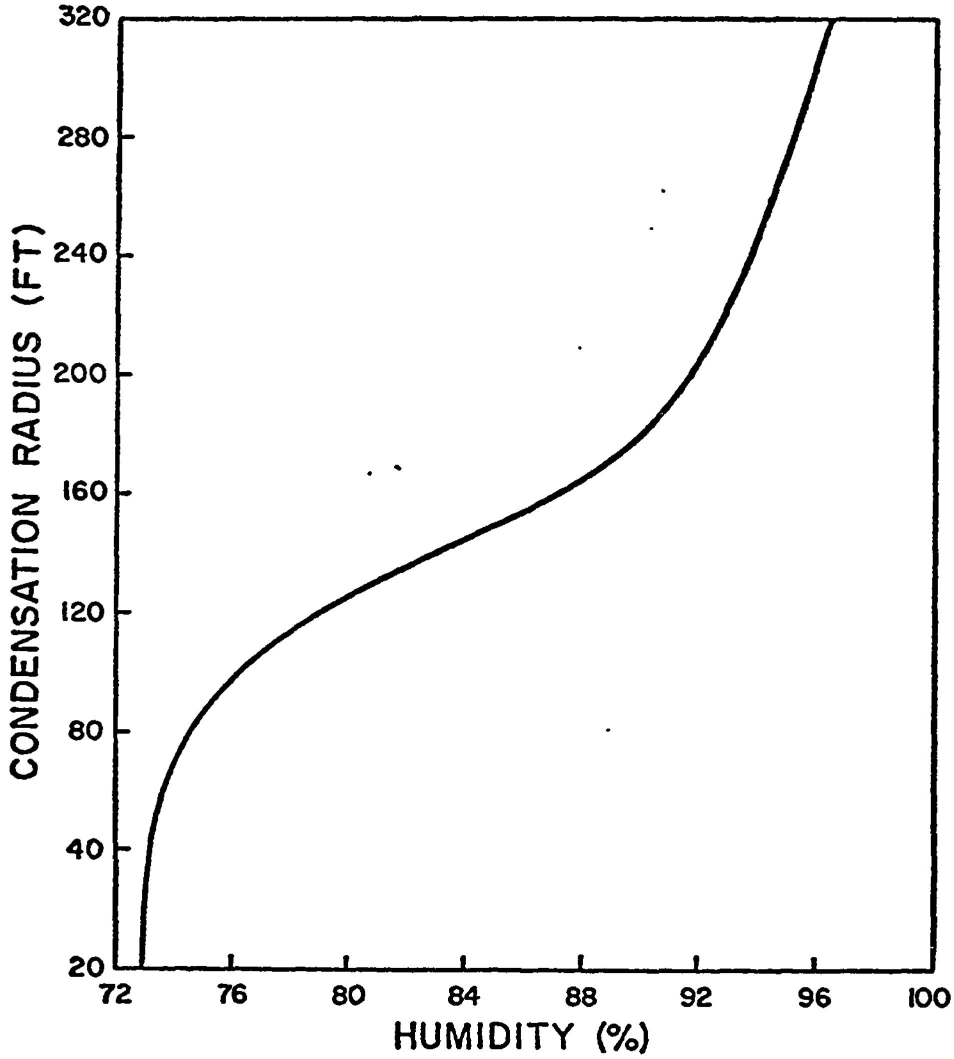

Figure 11. The radius of condensation versus humidity for the Dallas tornado of 1957.

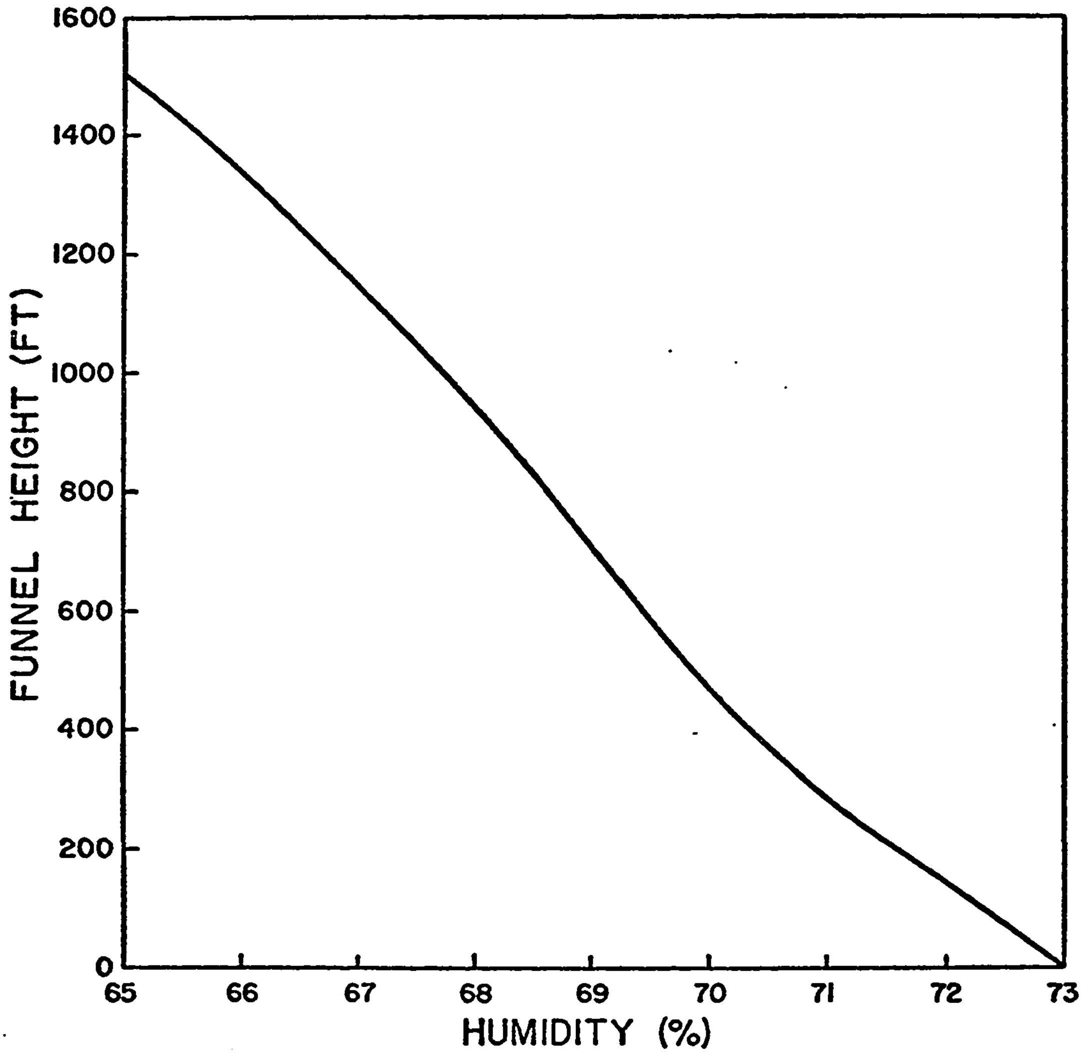

Figure 12. Funnel height versus humidity for the Dallas tornado of 1957.

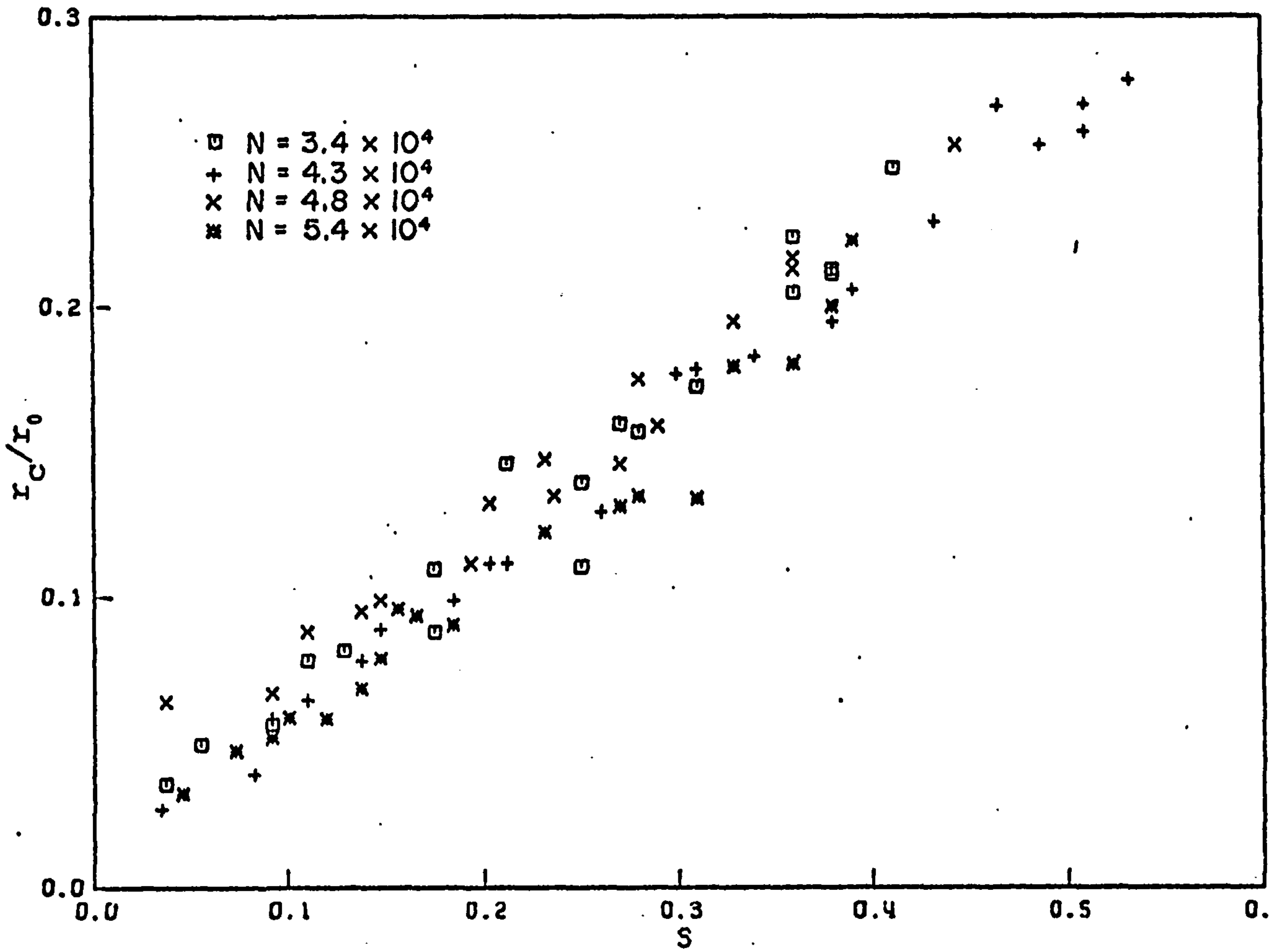

Figure 13. Nondimensionalized core radius versus swirl ratio over a smooth surface with a = 0.479, and r_0/r_s = 1/2.

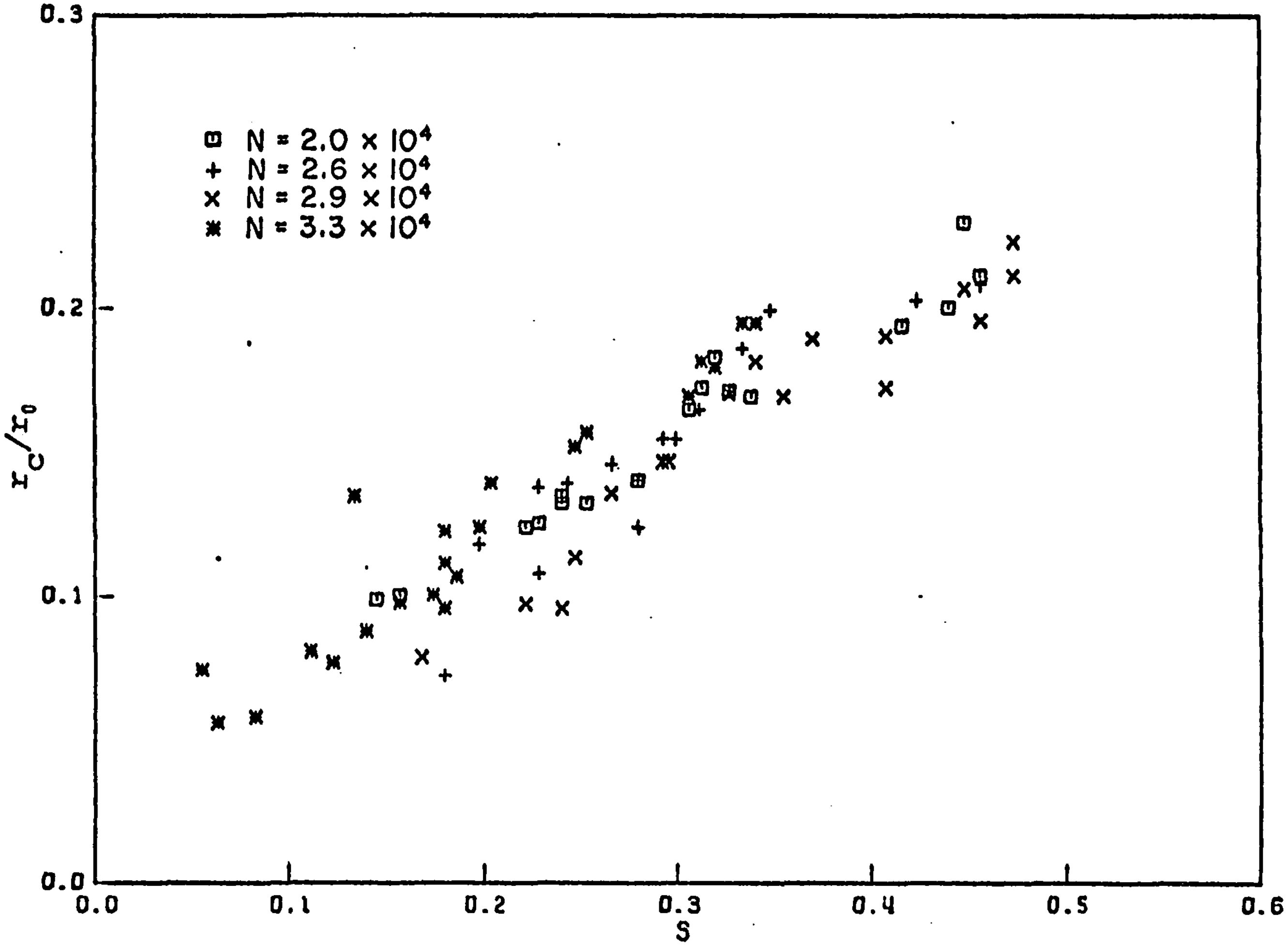

Figure 14. Nondimensionalized core radius versus swirl ratio over a smooth surface with a = 0.797, and r_0/r_s = 1/2.

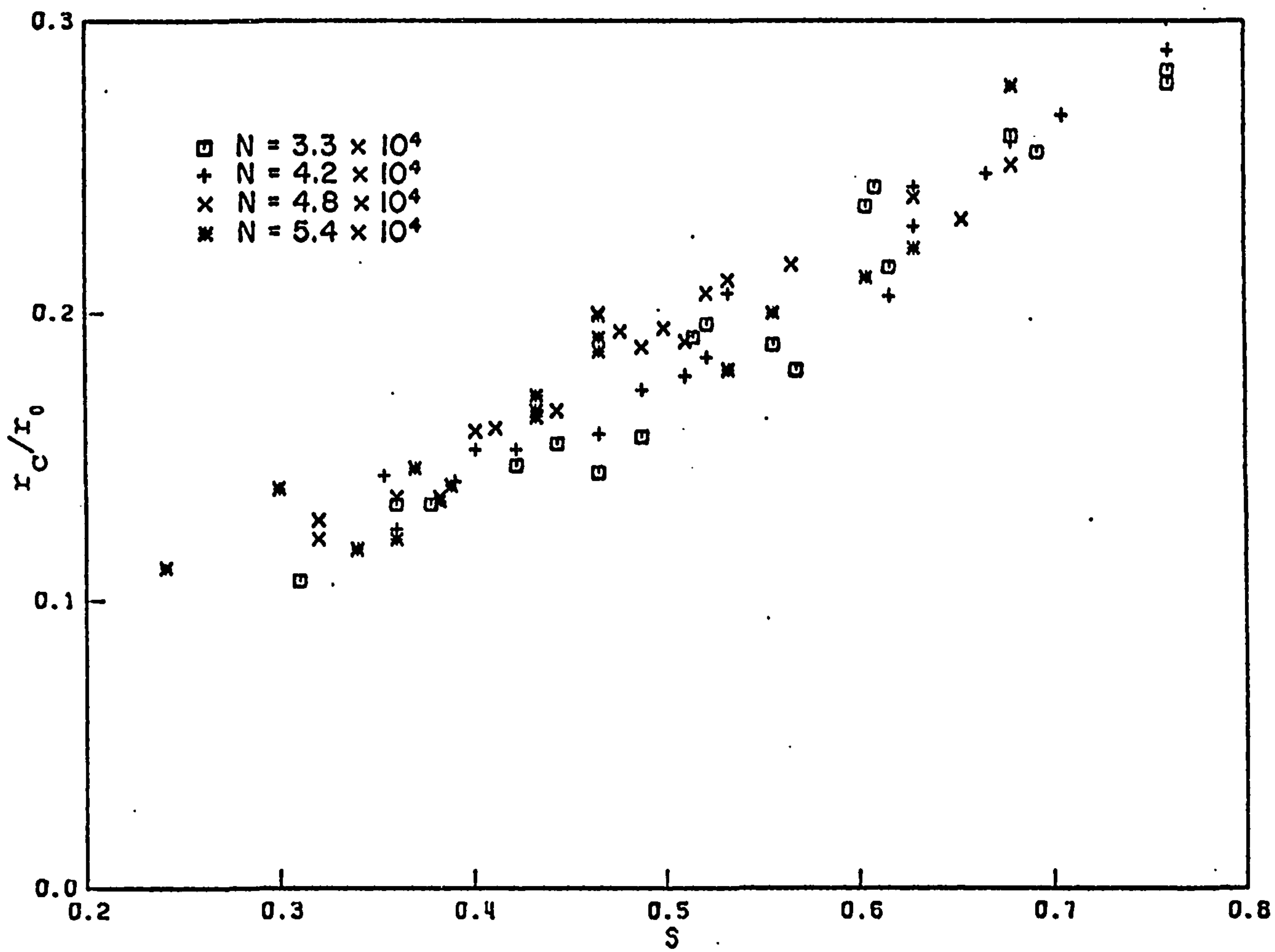

Figure 15. Nondimensionalized core radius versus swirl ratio over a rough surface with a = 0.478, and $r_0/r_s = 1/2$.

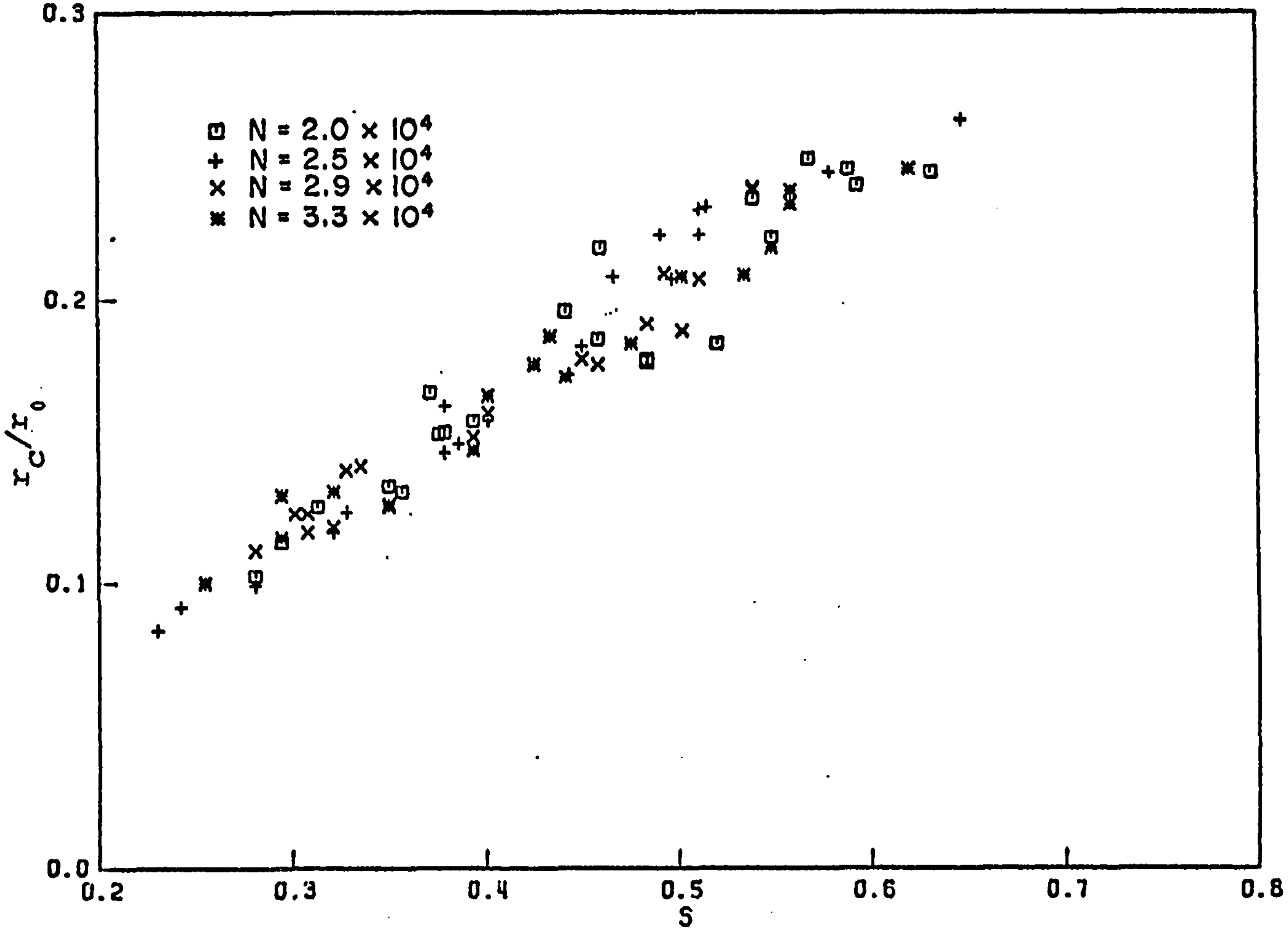

Figure 16. Nondimensionalized core radius versus swirl ratio over a rough surface with a = 0.792, and r /r_s = 1/2.

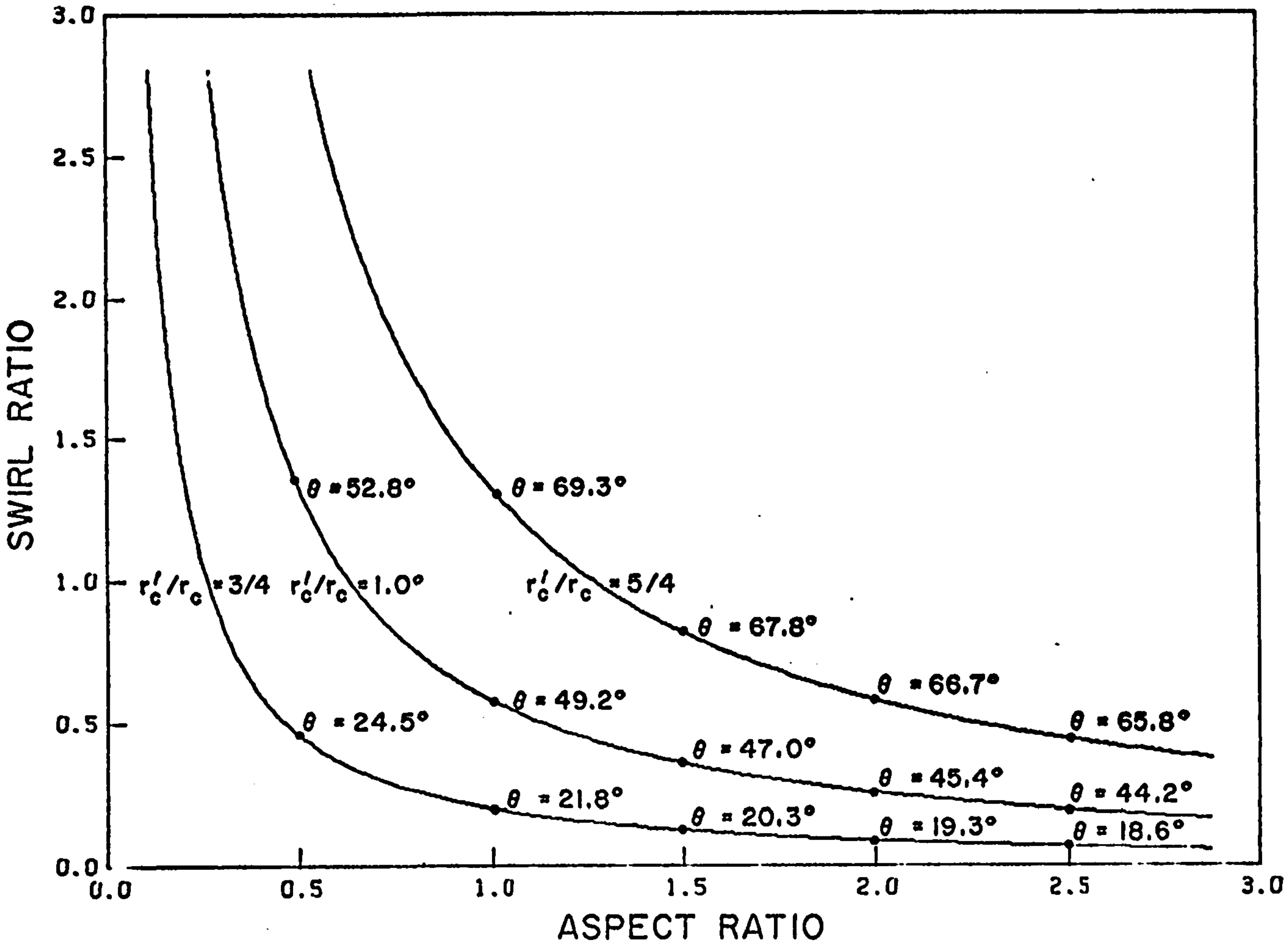

Figure 17. Lines along which the core radius over the rough surface r_c^* is a given fraction of the core radius over the smooth surface r_c.

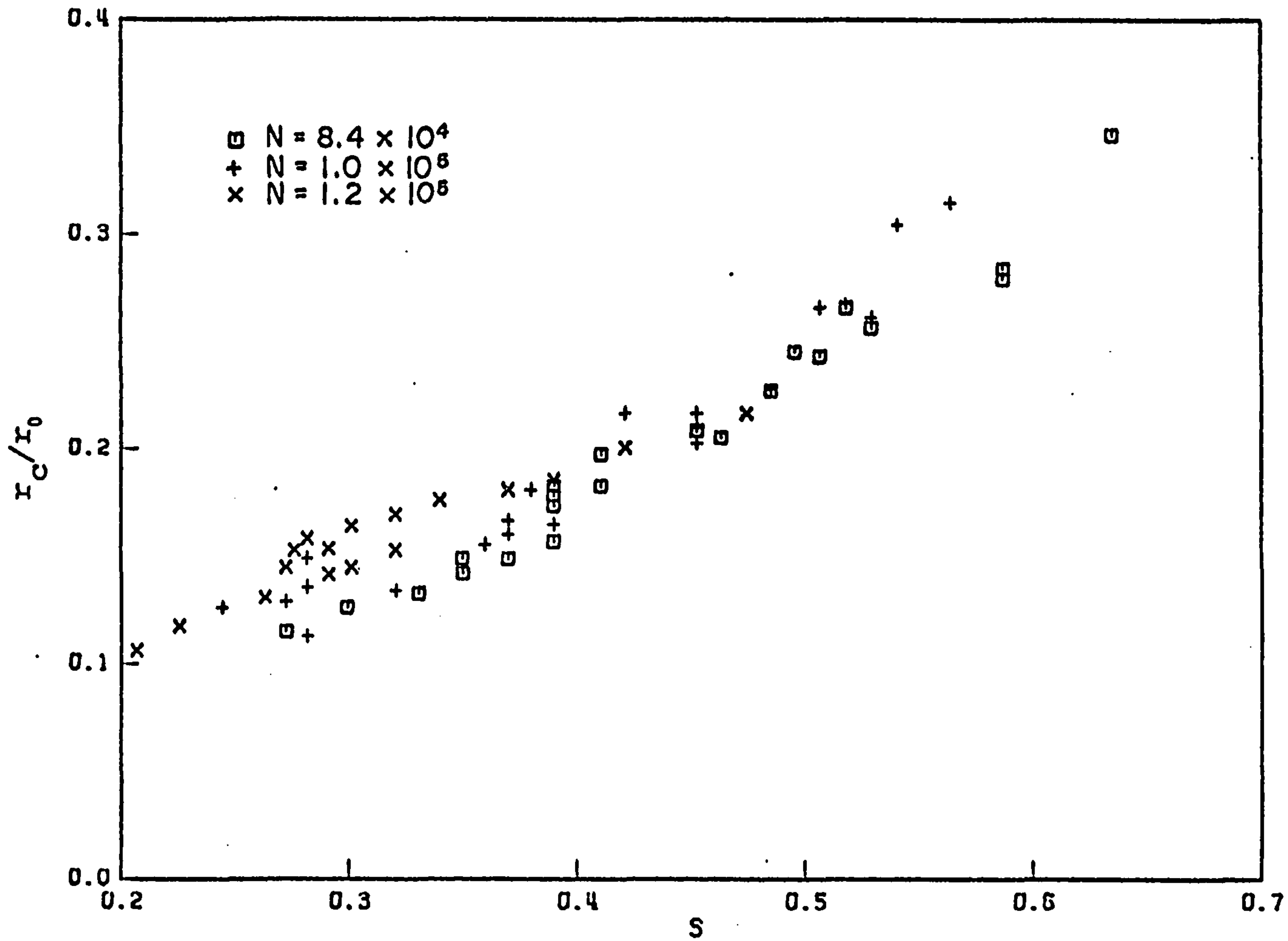

Figure 18. Nondimensionalized core radius data versus swirl ratio over a smooth surface with a = 0.492 and r_0/r_s = 1/4.

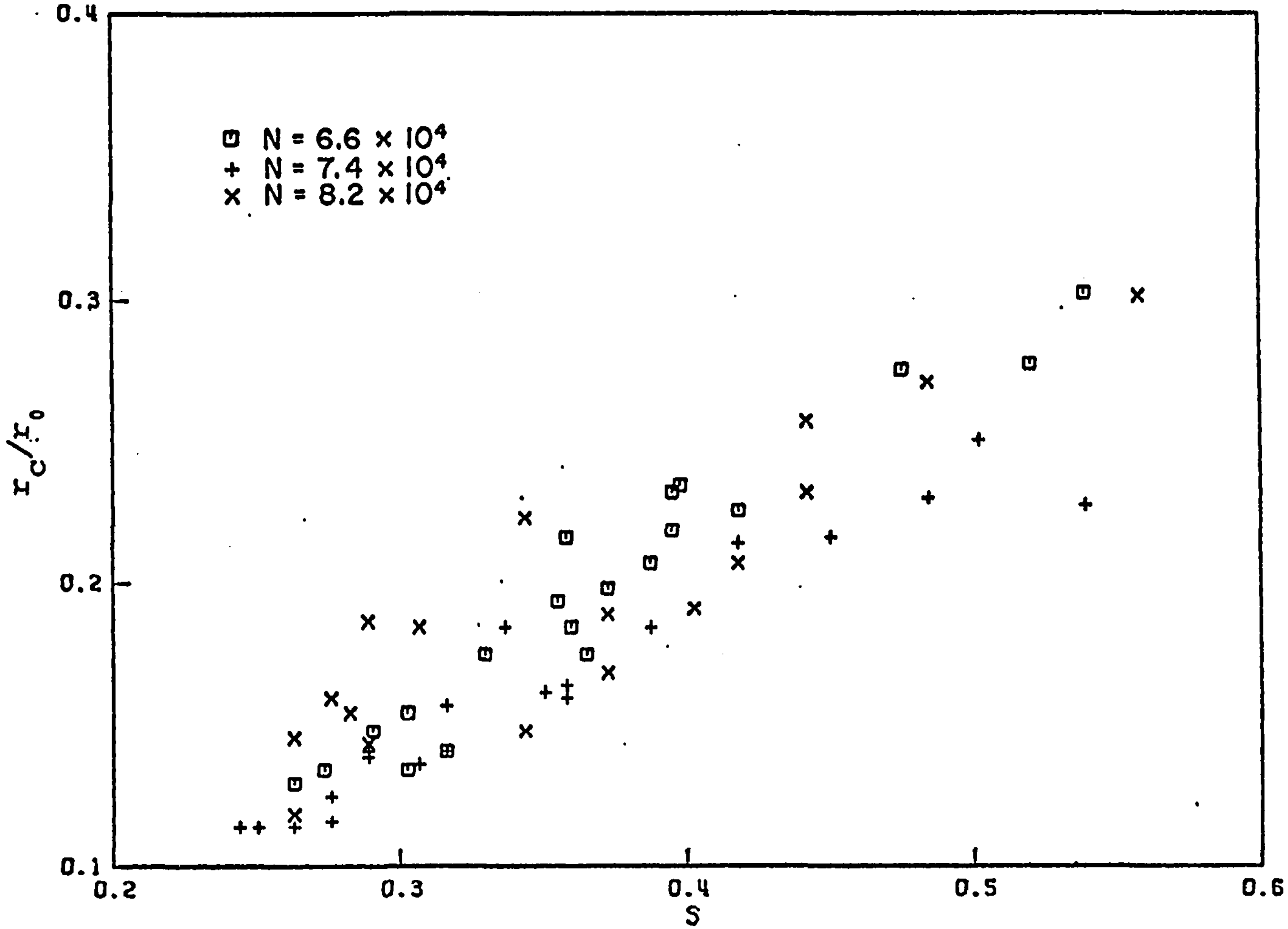

Figure 19. Nondimensionalized core radius data versus swirl ratio over a smooth surface with a = 0.807 and $r_0/r_s = 1/4$.

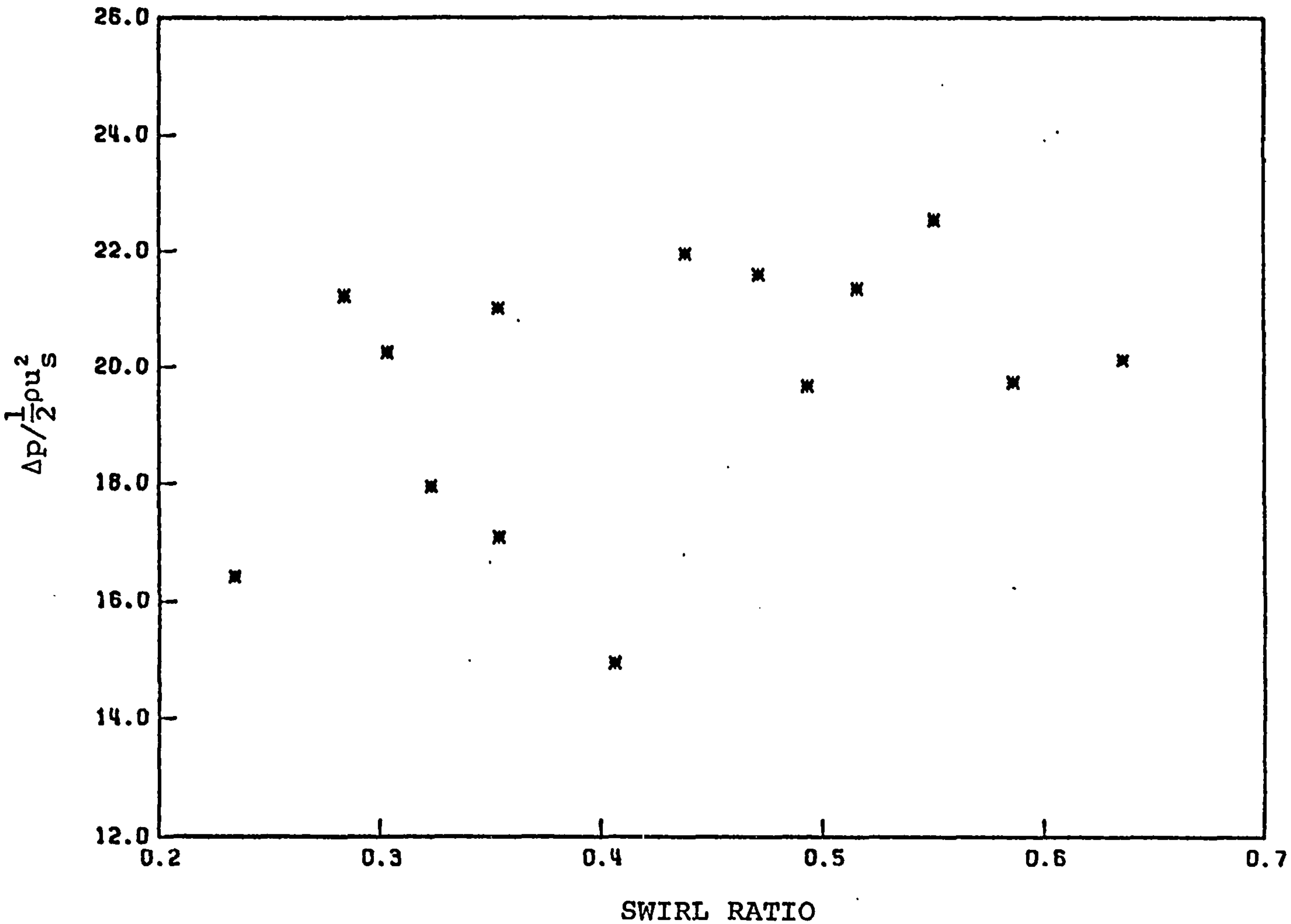

Figure 20. Surface central pressure deficit versus swirl ratio for $a = 0.472$, $N = 5.4 \times 10^4$, and $r_0/r_s = 1/2$.

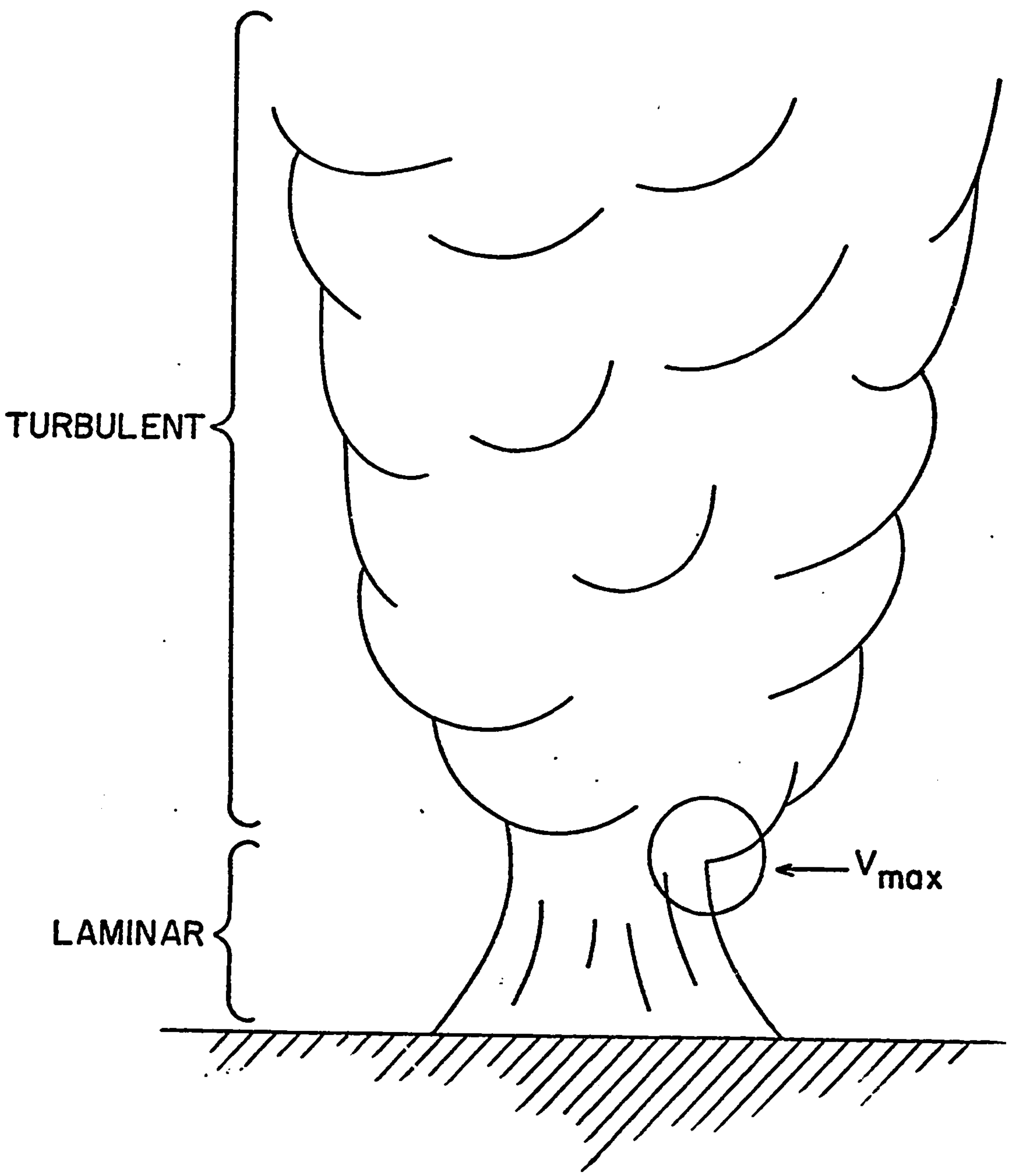

Figure 21. Region of maximum velocity.

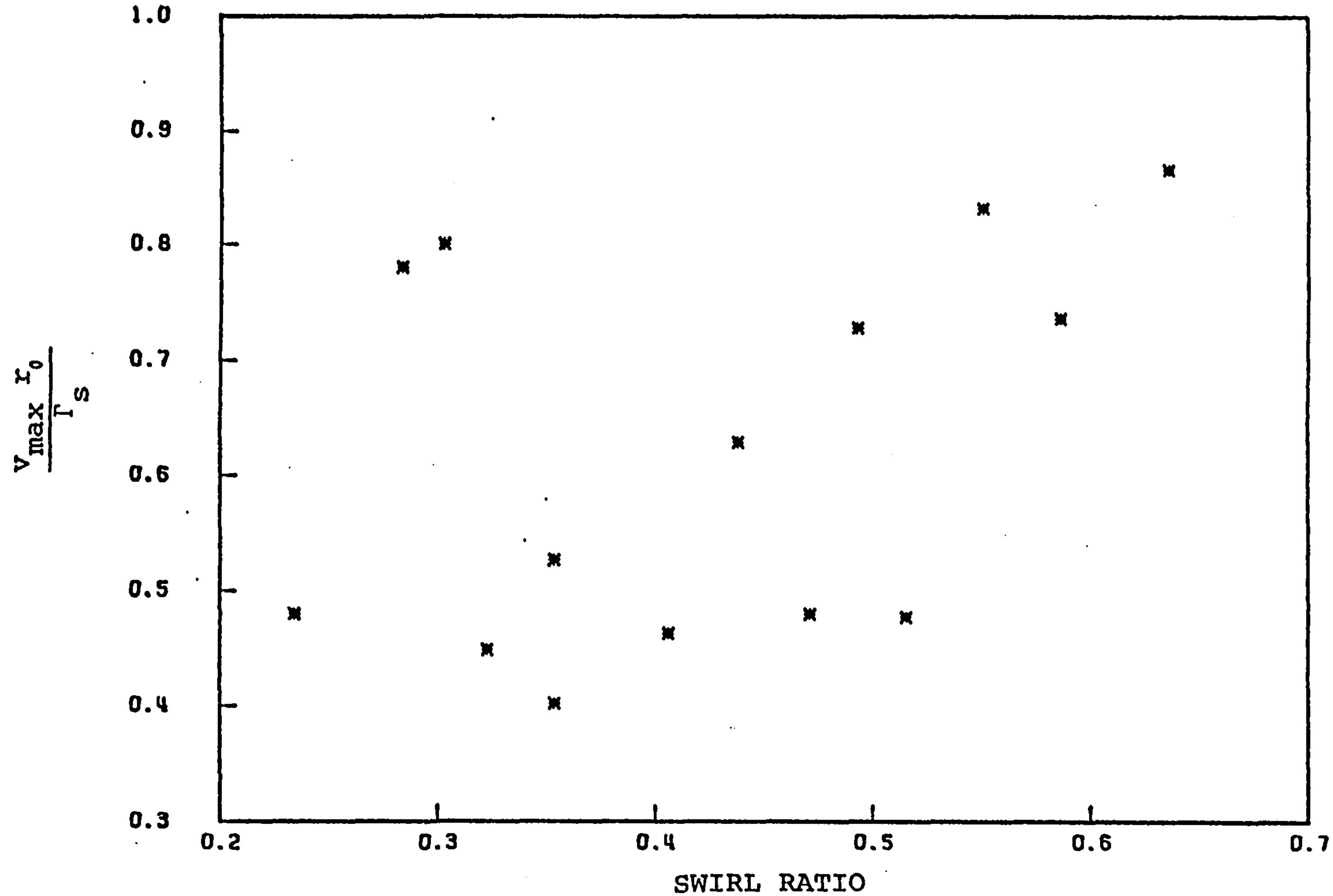

Figure 22. Maximum tangential velocity versus swirl ratio for $a = 0.472$, $N = 5.4 \times 10^4$, and $r_0/r_s = 1/2$.

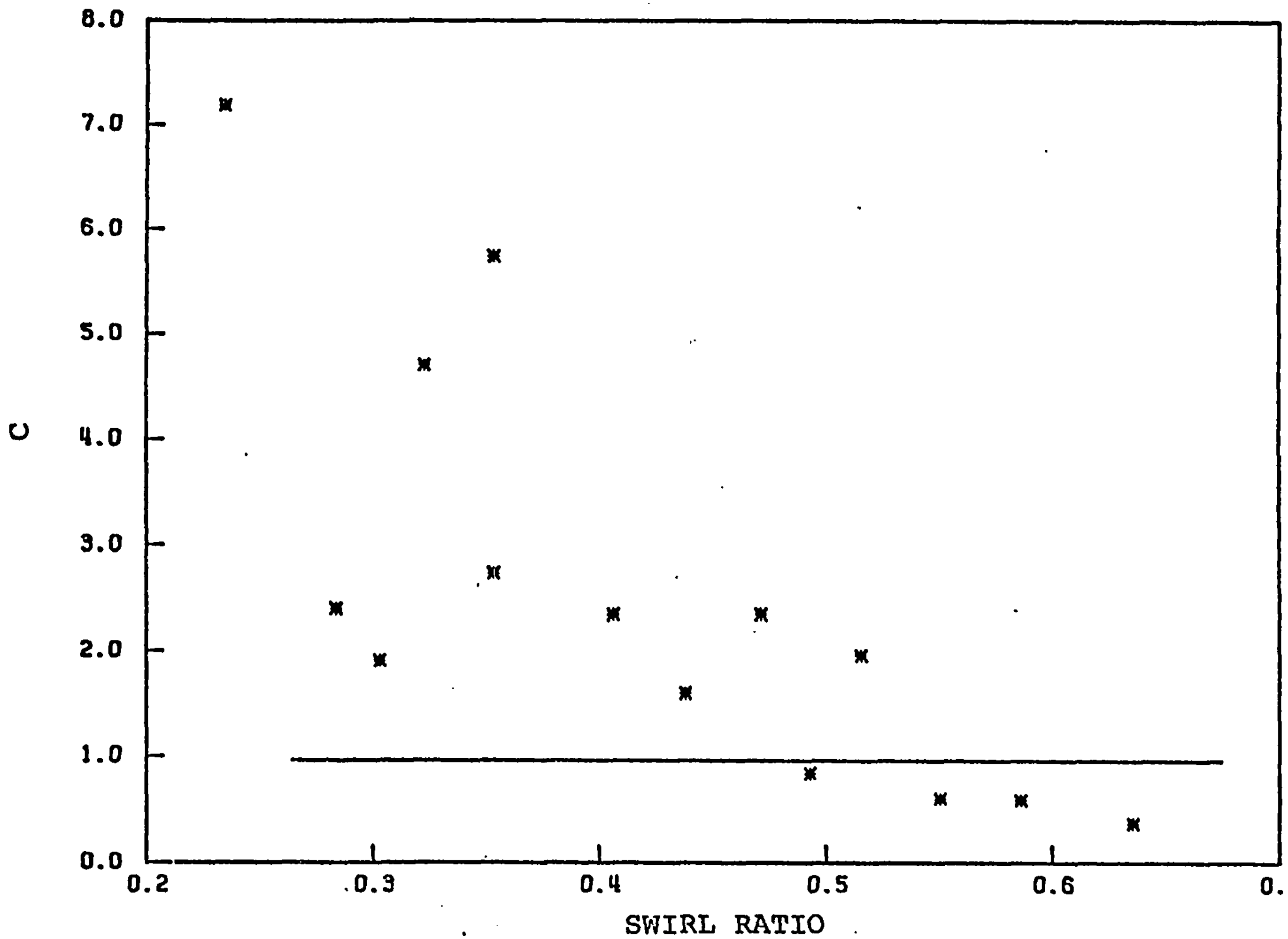

Figure 23. Efficiency factor versus swirl ratio, for a = 0.472, N = 5.4×10^4, and r_0/r_S = 1/2. The asterisks indicate the measurements and the line is a plot of Eqn. (22).

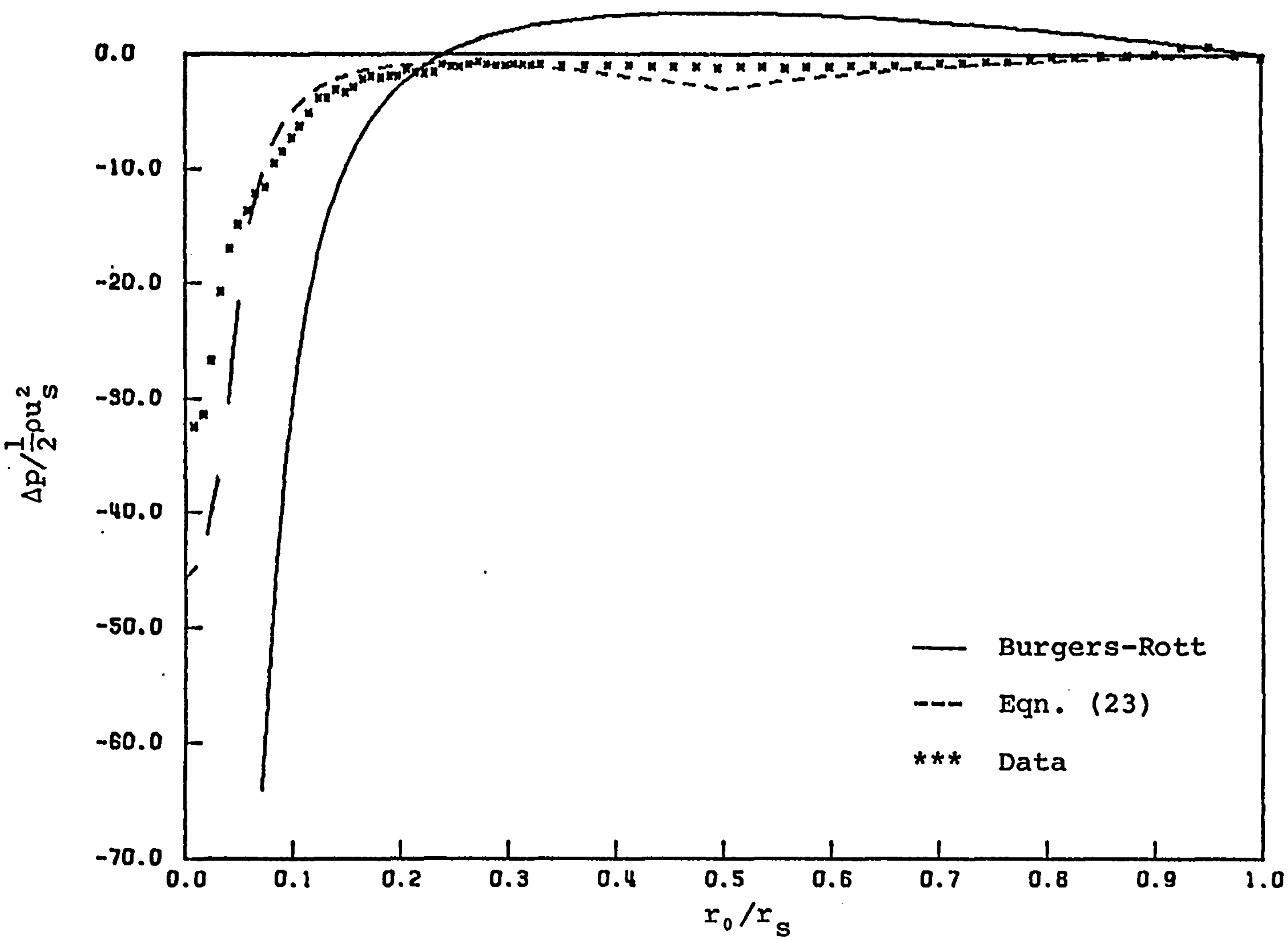

Figure 24. Pressure versus radius for S = 0.25, a = 0.472, Q = 0.413 $m^3\ s^{-1}$, and r_0/r_s = 1/2.

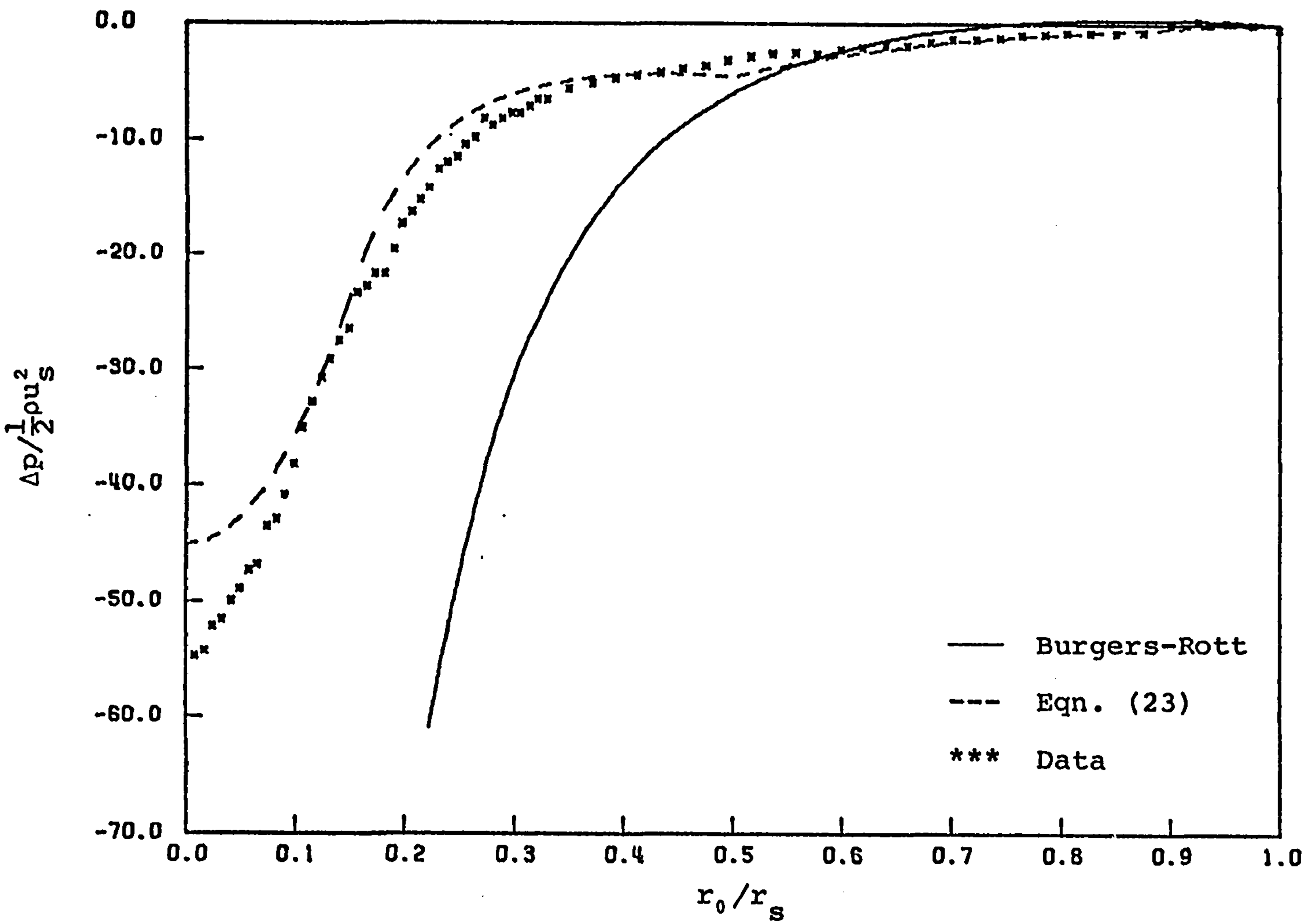

Figure 25. Pressure versus radius for $S = 0.80$, $a = 0.472$, $Q = 0.413\ m^3\ s^{-1}$, and $r_0/r_s = 1/2$.

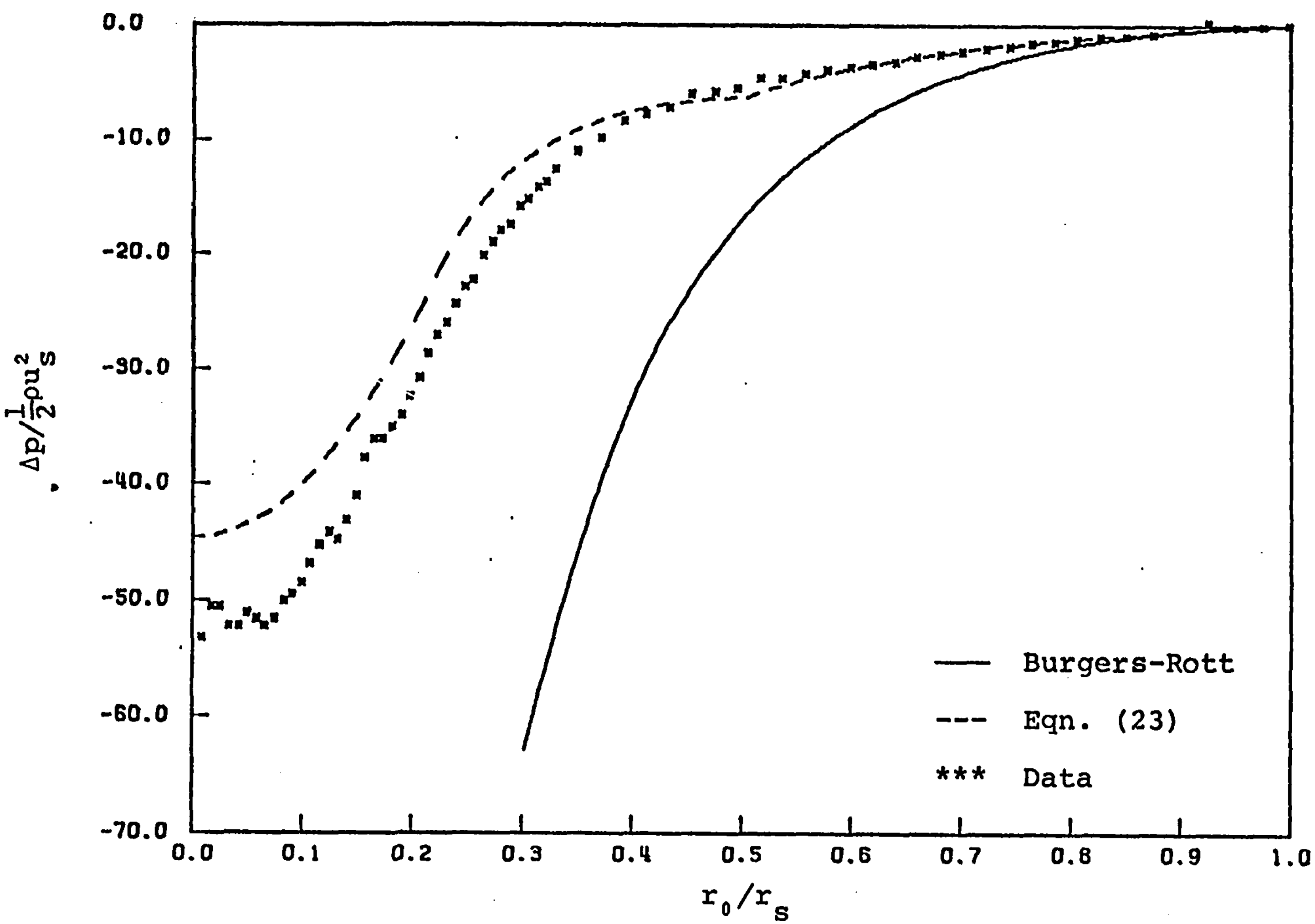

Figure 26. Pressure versus radius for $S = 1.10$, $a = 0.472$, $Q = 0.413\ m^3\ s^{-1}$, and $r_0/r_s = 1/2$.

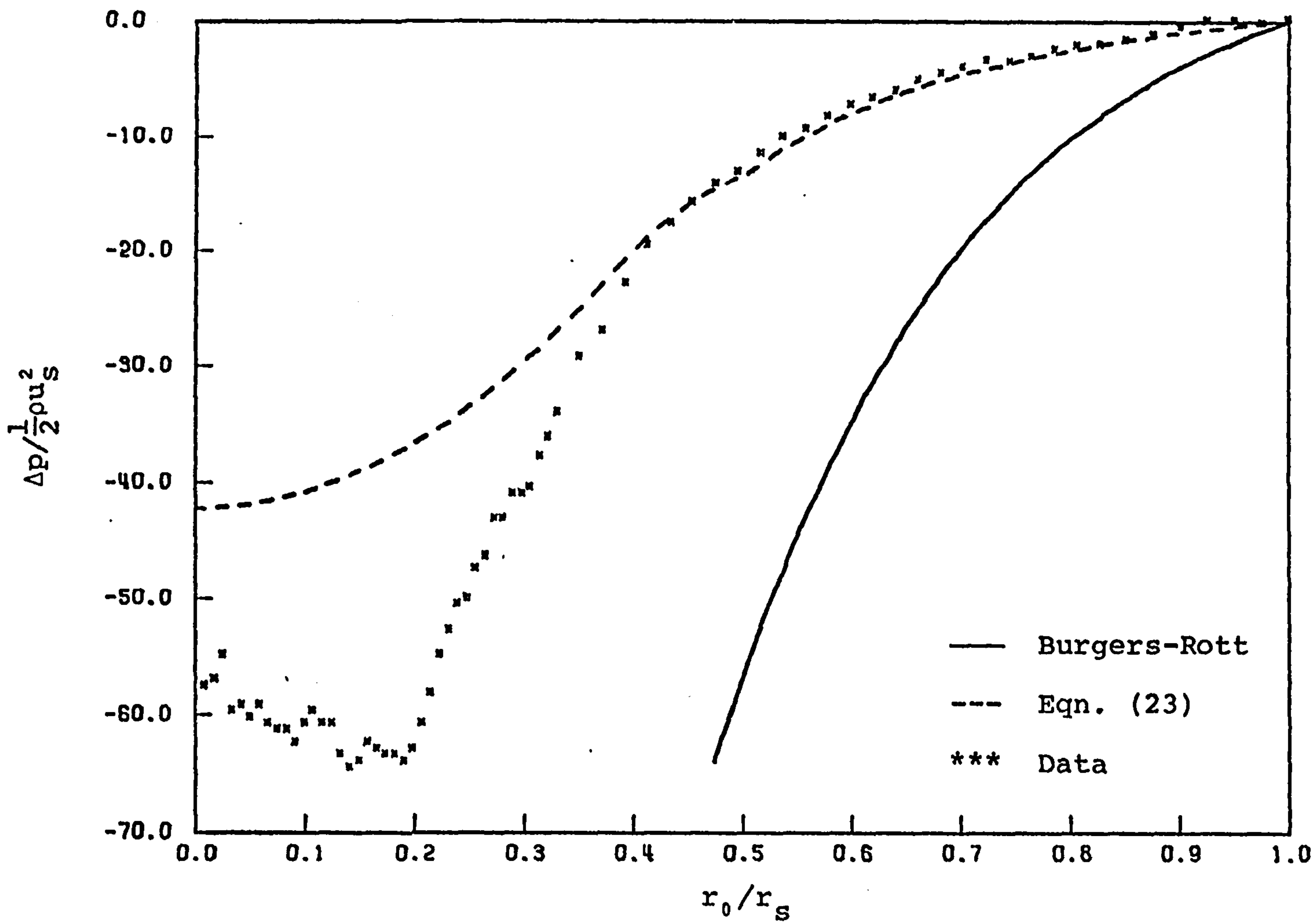

Figure 27. Pressure versus radius for S = 2.00, a = 0.472, Q = 0.413 $m^3\ s^{-1}$, and $r_0/r_s = 1/2$.

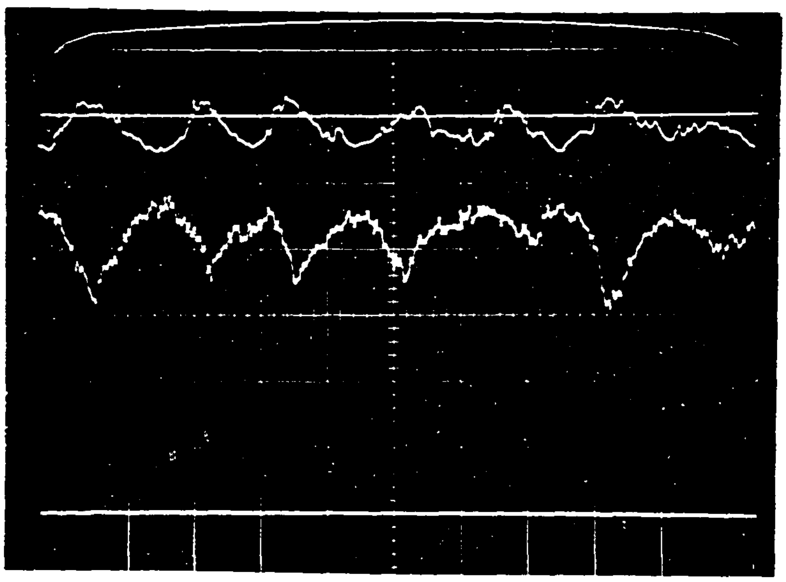

Figure 28. Oscilloscope trace of pressure (bottom trace) and anemometer output (top trace) for multiple vortices with $S = 1.98$, $a = 0.472$, and $Q = 0.413\ m^3\ s^{-1}$.

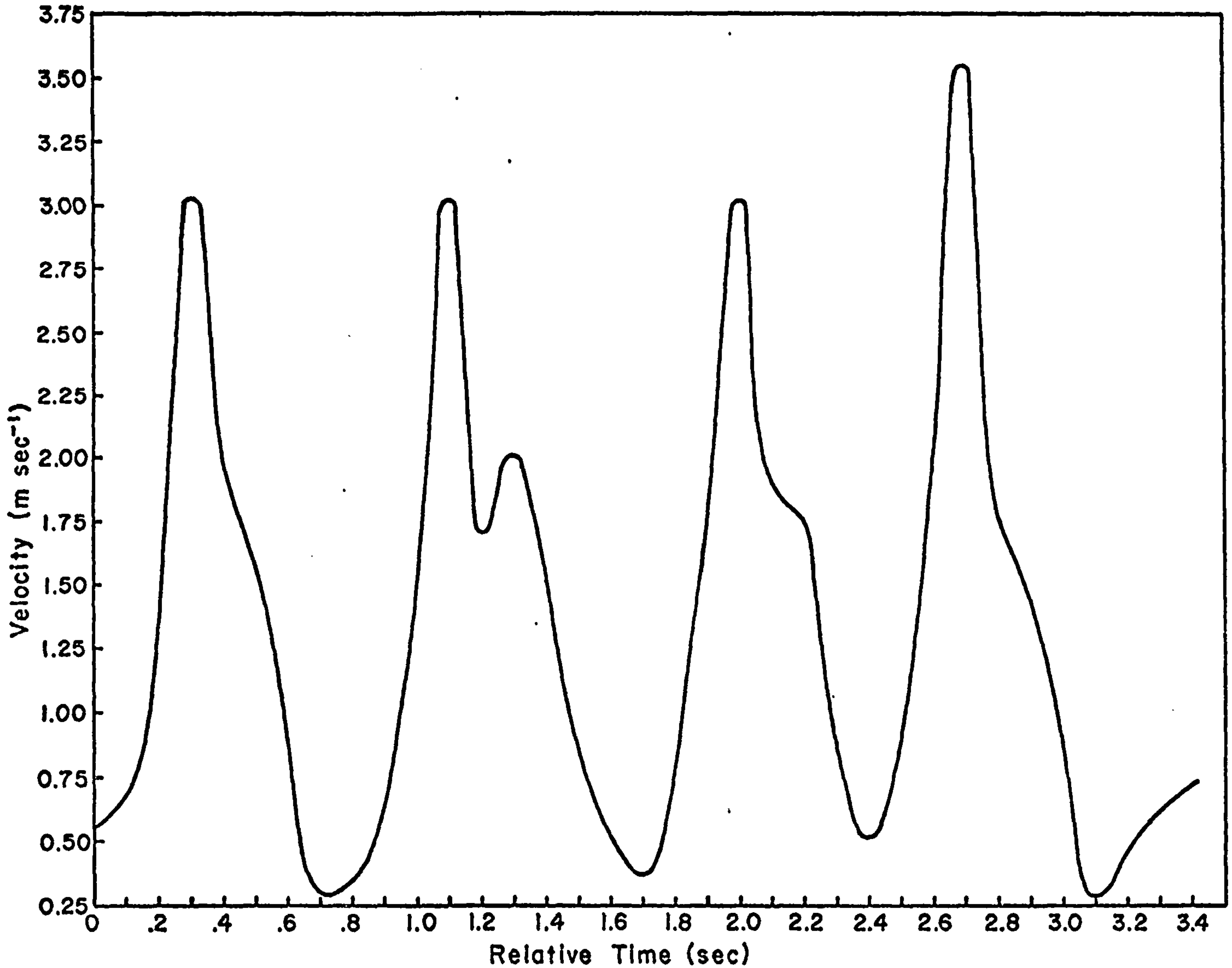

Figure 29. The total velocity of a system of four vortices as they traversed the hot film probe for a = 0.48, Q = 1.23 m^3 s^{-1}, and S = 3.18.

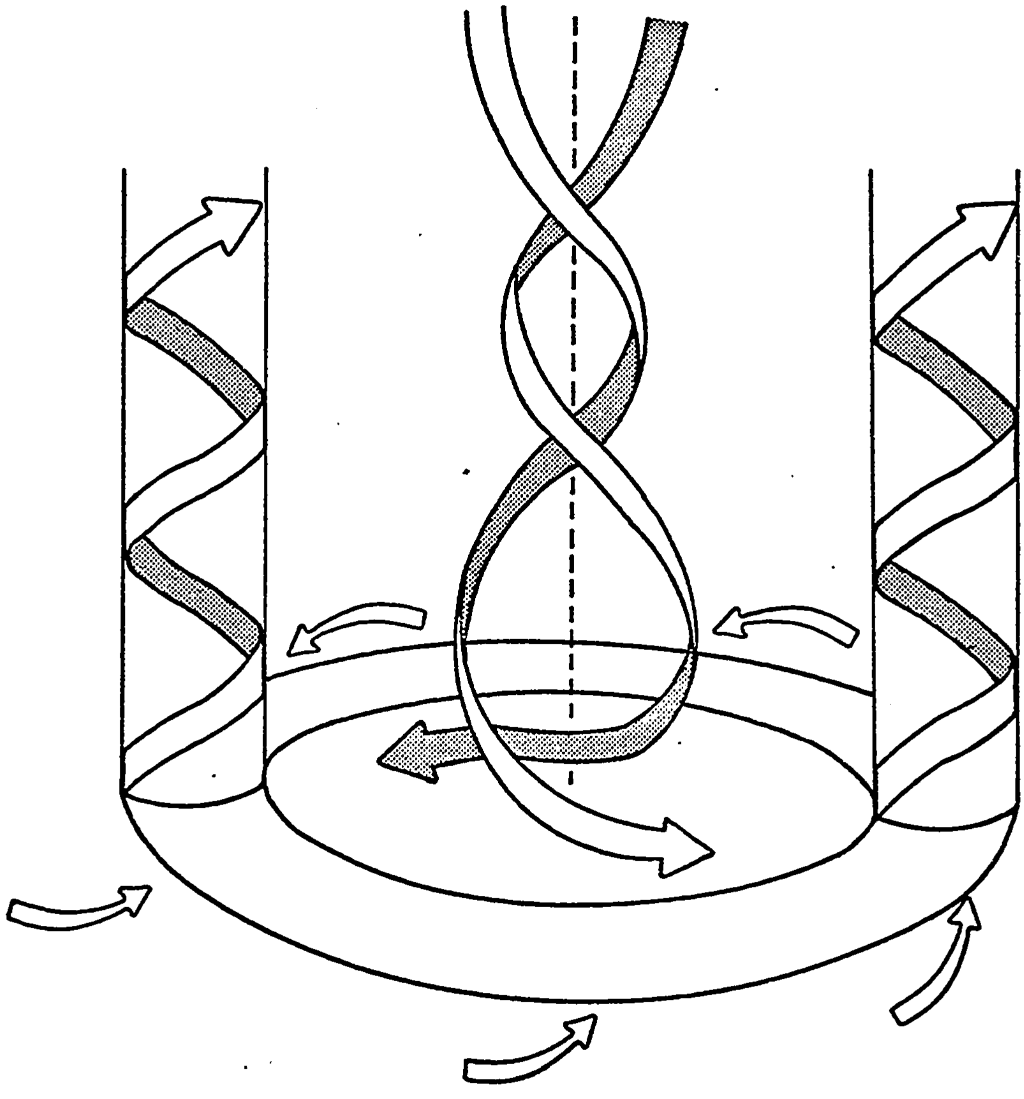

Figure 30. The streamline pattern for a vortex pair as indicated by smoke tracer introduced into the vortex generator.

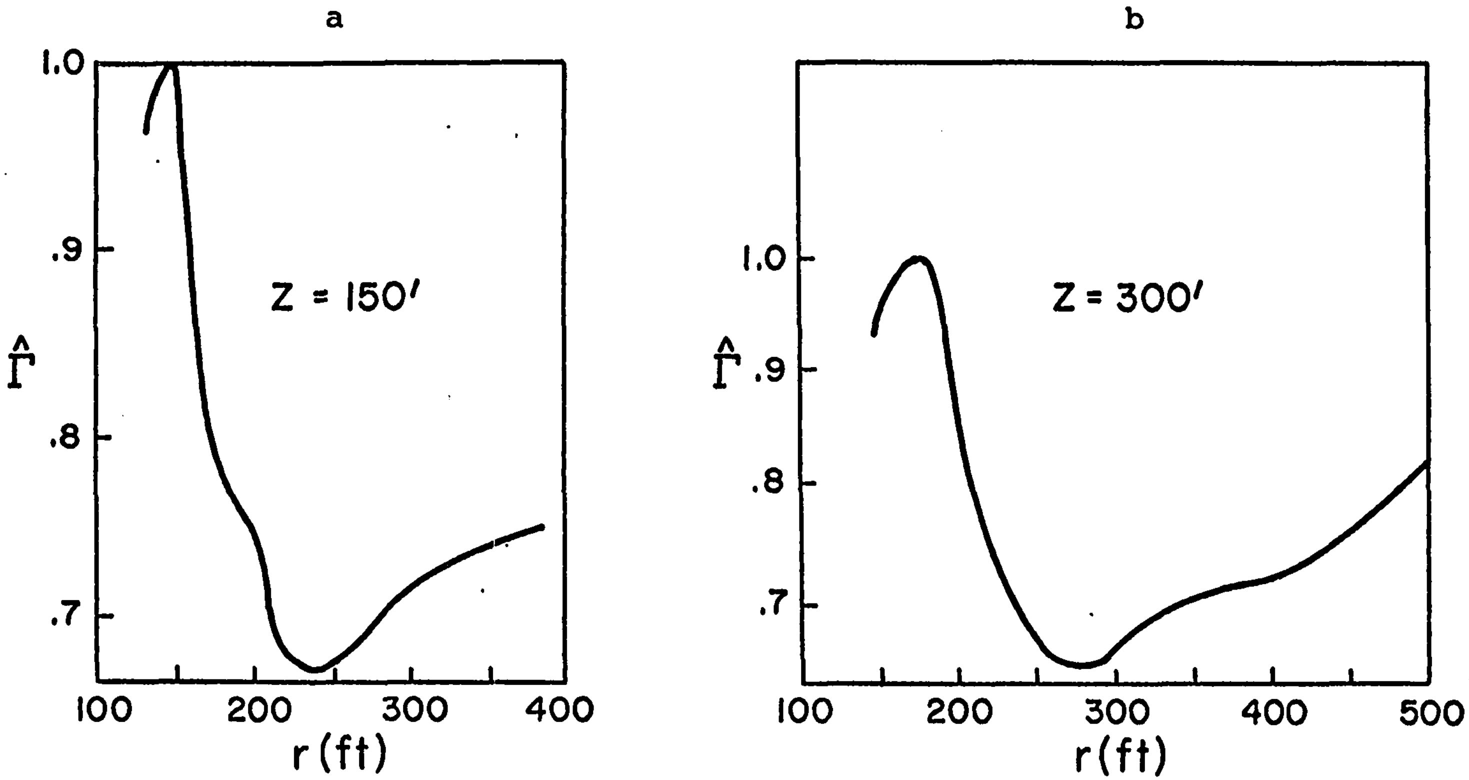

Figure 31. Nondimensionalized circulation profiles for (a) the Dallas tornado of 1957 at z = 150 ft., (b) the Dallas tornado at z = 300 ft.

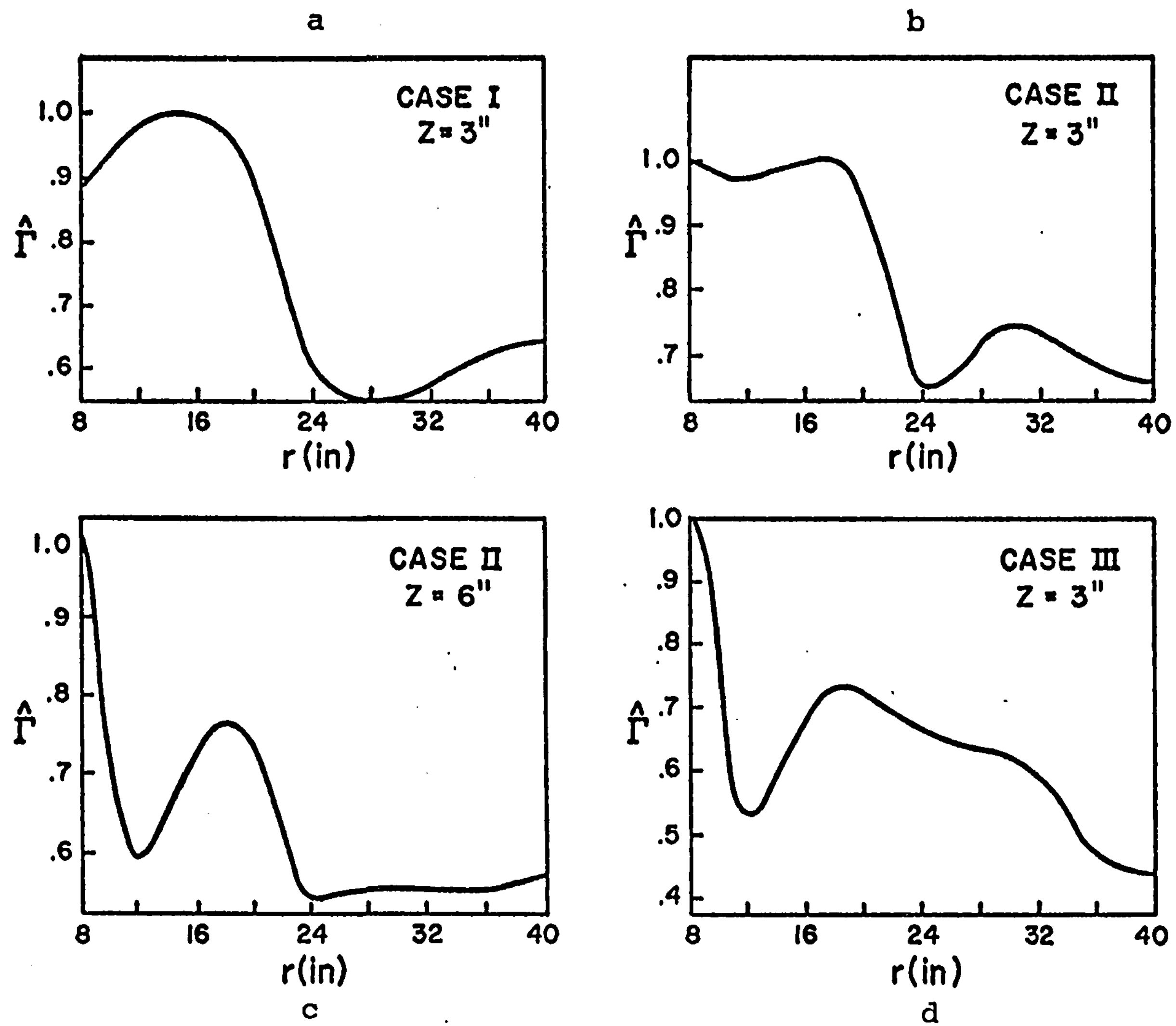

Figure 32. Jischke and Parang's data for (a) case I at z = 3 in.; (b) case II at z = 3 in.; (c) case II at z = 6 in.; and (d) case III at z = 3 in.

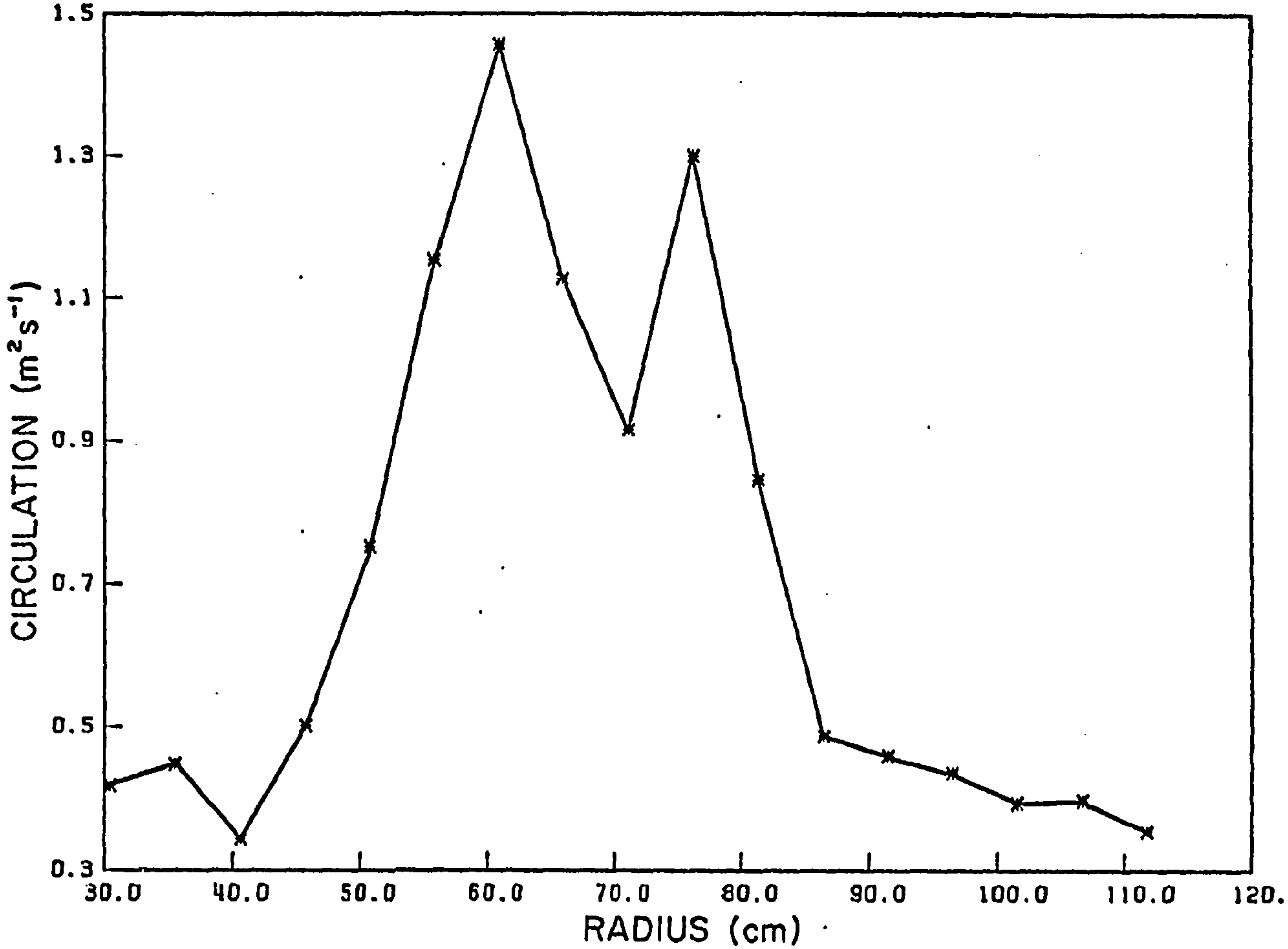

Figure 33. Circulation profile at $z = 1.4$ cm for $S = 0.087$, $a = 0.5$, and $Q = 1.33\ m^3\ s^{-1}$.

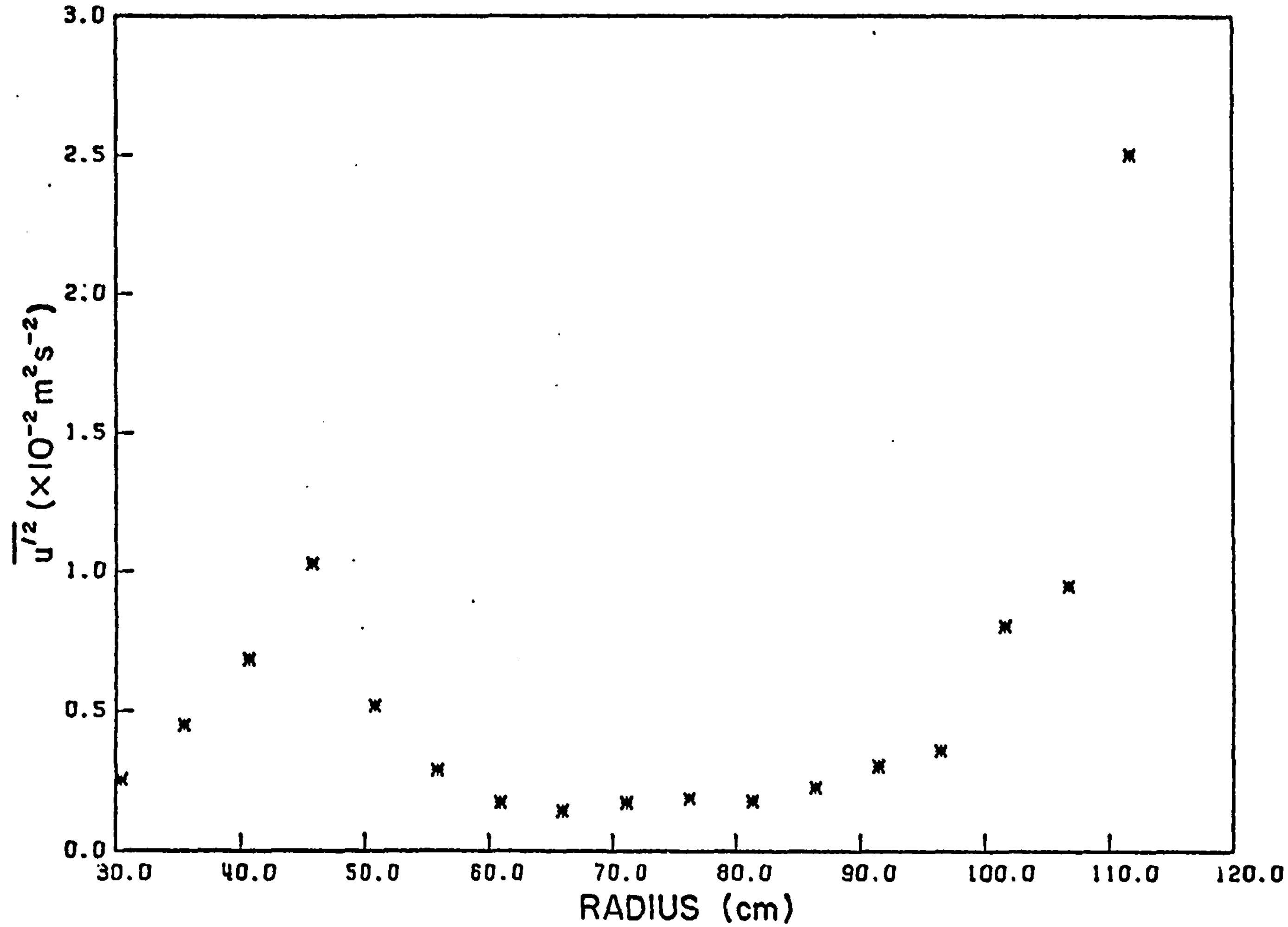

Figure 34. Profile of $\overline{u'^2}$ at $z = 1.4$ cm for $S = 0.087$, $a = 0.5$, and $Q = 1.33\ m^3\ s^{-1}$.

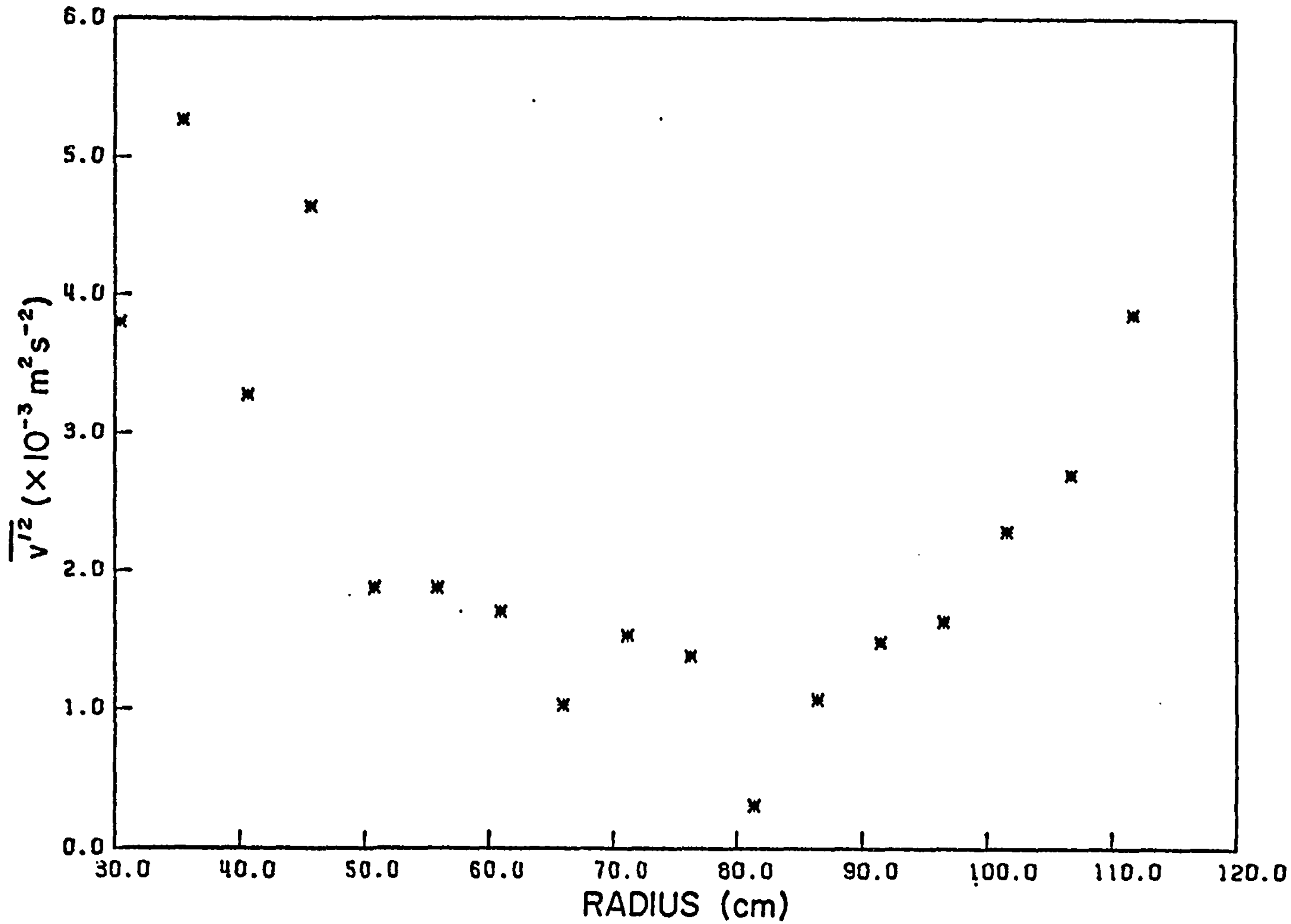

Figure 35. Profile of $\overline{v'^2}$ at z = 1.4 cm for S = 0.087, a = 0.5, and Q = 1.33 m^3 s^{-1}.

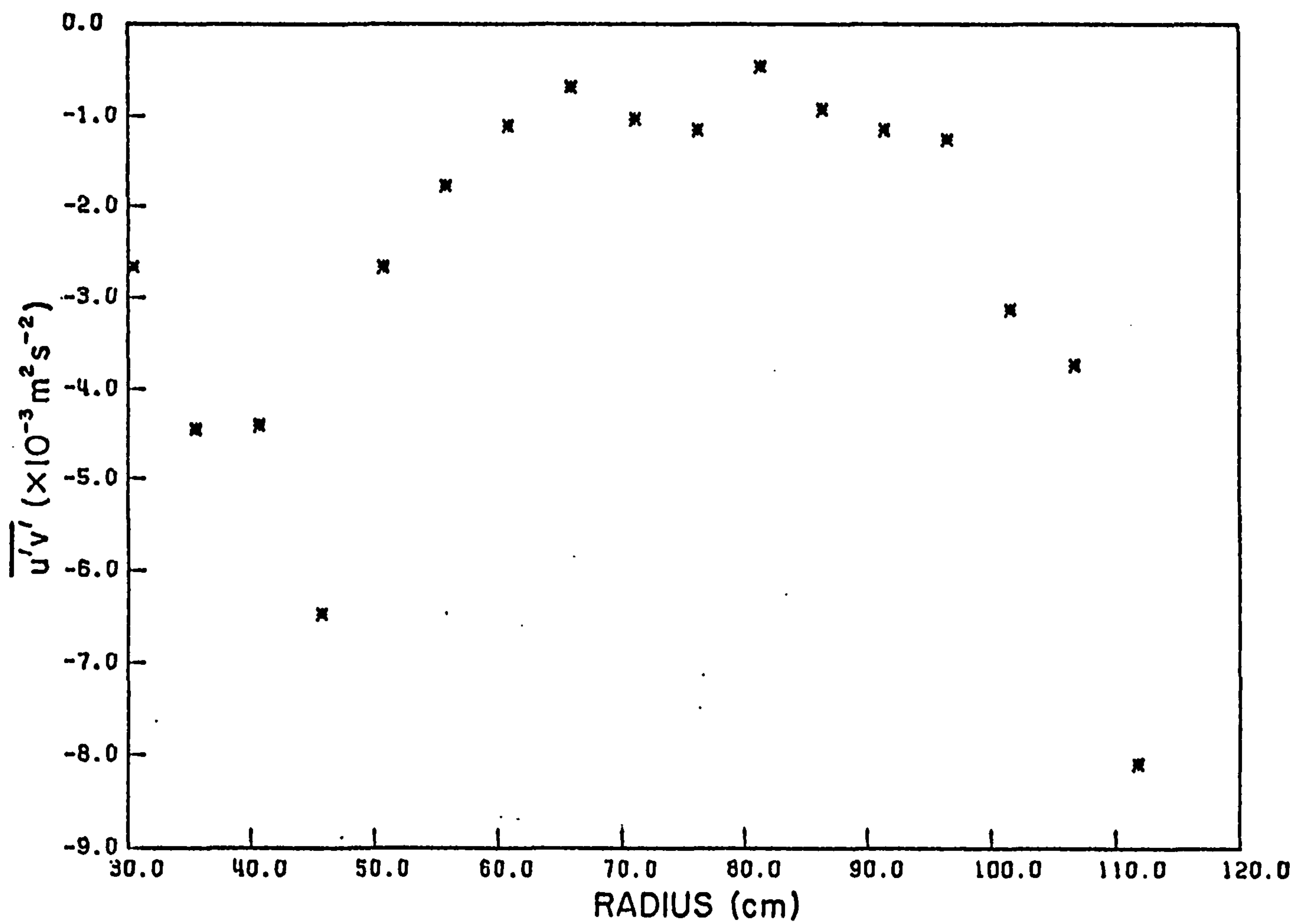

Figure 36. Profile of $\overline{u'v'}$ at $z = 1.4$ cm for $S = 0.087$, $a = 0.5$, and $Q = 1.33\ m^3\ s^{-1}$.

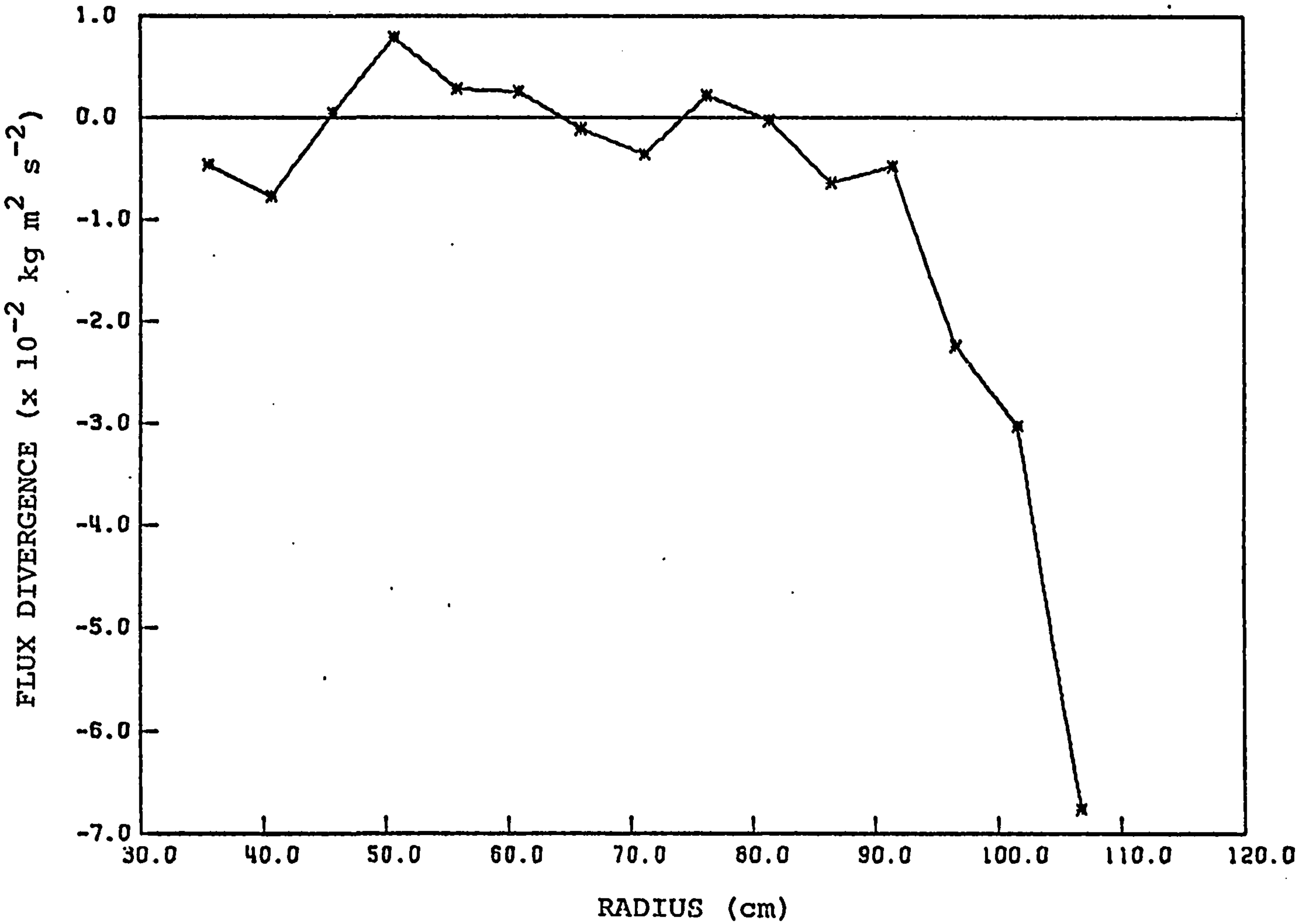

Figure 37. Profile of radial turbulent flux divergence at $z = 1.4$ cm for $S = 0.087$, $a = 0.5$, and $Q = 1.33\ m^3\ s^{-1}$.

TABLE 1

RANGE OF PARAMETERS IN THE TORNADO SIMULATOR

	Minimum	Maximum
$S = \frac{\Gamma_s r_0}{2Q}$	0	10 +
$N = \frac{u_s r_s}{\nu}$	8.5×10^2	1.4×10^5
$a = \frac{h}{r_0}$	0.25	4.0
$\frac{r_0}{r_s}$	0.125	0.5

TABLE II

PARAMETER RANGE FOR CORE RADIUS MEASUREMENTS
OVER A SMOOTH SURFACE

CASE	a	N
I	0.479	3.4×10^4
II	0.479	4.3×10^4
III	0.479	4.8×10^4
IV	0.479	5.4×10^4
V	0.797	2.0×10^4
VI	0.797	2.6×10^4
VII	0.797	2.9×10^4
VIII	0.797	3.3×10^4

TABLE III

PARAMETER RANGE FOR CORE RADIUS MEASUREMENTS OVER A ROUGH SURFACE

CASE	a	N
IX	0.478	3.3×10^4
X	0.478	4.2×10^4
XI	0.478	4.8×10^4
XII	0.478	5.4×10^4
XIII	0.792	2.0×10^4
XIV	0.792	2.5×10^4
XV	0.792	2.9×10^4
XVI	0.792	3.3×10^4

TABLE IV

PARAMETER RANGE FOR CORE RADIUS MEASUREMENTS WITH $r_0 = 0.305$ m

CASE	a	N
XVII	0.492	8.4×10^4
XVIII	0.492	1.0×10^5
XIX	0.492	1.2×10^5
XX	0.807	6.6×10^4
XXI	0.807	7.4×10^4
XXII	0.807	8.2×10^4

TABLE V

CRITICAL SWIRL RATIOS FOR MV TRANSITIONS

	Smooth Surface	Rough Surface
Single Vortex	0.127	0.127
Single to MV_2	0.227	0.313
$MV_2 \rightarrow MV_3$	0.898	1.09
$MV_3 \rightarrow MV_4$	1.79	3.17

TABLE VI

MAXIMUM TANGENTIAL VELOCITIES FOR VARIOUS SWIRL RATIOS AND CENTRAL PRESSURE DEFICITS

Δp \ S	0.2	0.4	0.6
60 mb	25 ms^{-1}	45	101
80 mb	29	52	117
100 mb	33	59	131